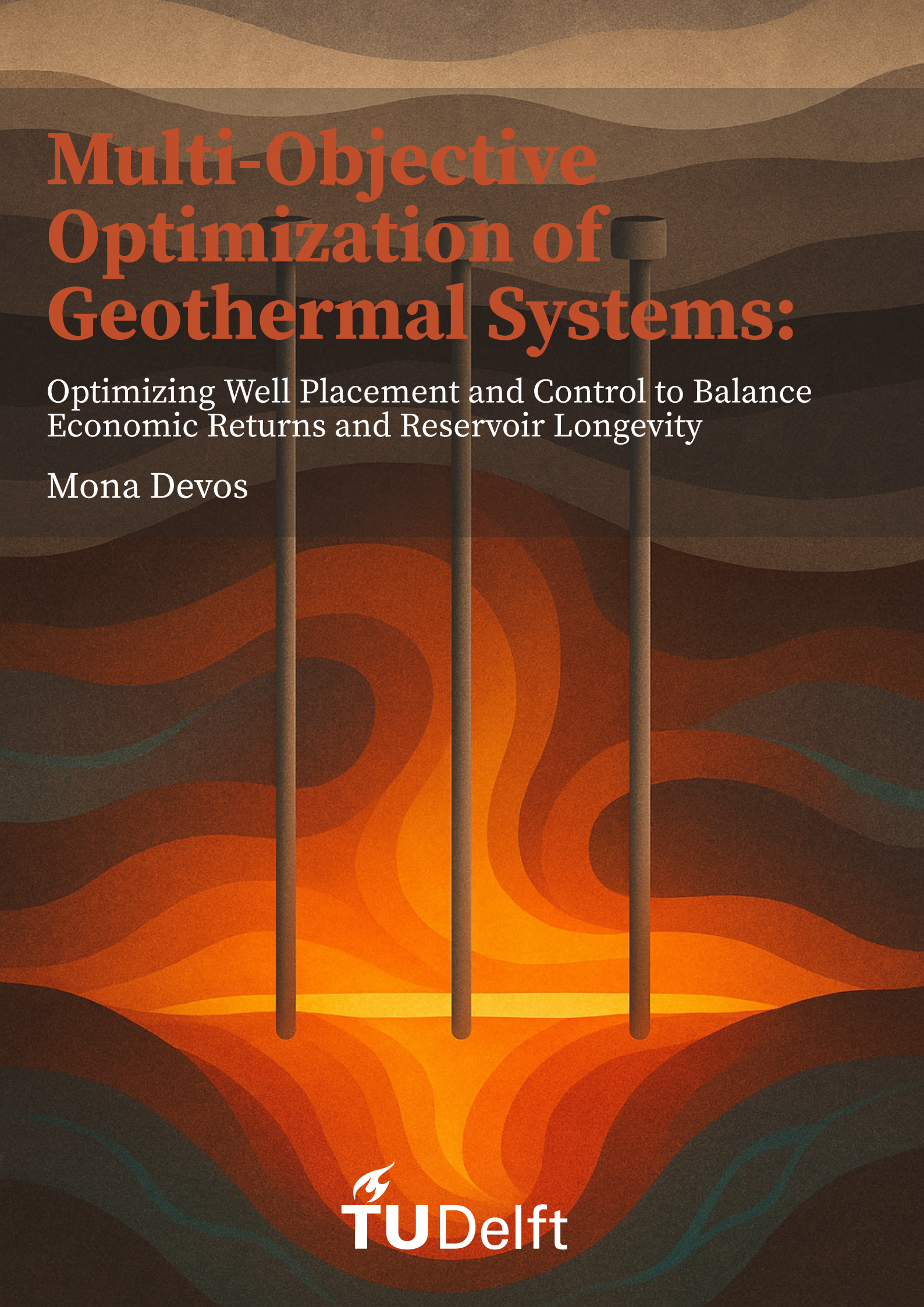


Multi-Objective Optimization of Geothermal Systems:

The background of the cover features a stylized, abstract representation of a geothermal reservoir. It consists of horizontal, wavy bands of varying shades of brown, orange, and yellow, suggesting different geological layers or temperature gradients. Three vertical, dark grey cylindrical shapes, representing wells, are positioned across the center of the image, extending from the top to the bottom. The overall aesthetic is modern and scientific.

Optimizing Well Placement and Control to Balance
Economic Returns and Reservoir Longevity

Mona Devos

Multi-Objective Optimization of Geothermal Systems:

Optimizing Well Placement and Control to Balance
Economic Returns and Reservoir Longevity

by

Mona Devos

in partial fulfillment of the requirements for the degree of

Master of Science in Applied Earth Sciences

at Delft University of Technology, Faculty of Civil Engineering and Geosciences

to be defended publicly on **Tuesday, July 22nd, 2025 at 05:00 PM in CEG Lecture Hall G**

Committee composition:

Chair & Main supervisor:	Dr. A. Daniilidis	TU Delft
Second supervisor:	Dr. D.V. Voskov	TU Delft
Daily supervisor:	C. Wallmeier	TU Delft
External supervisor:	Dr. O. Volkov	Stanford University
Committee member:	Dr. G. Rongier	TU Delft

Cover: Abstract artistic representation of a geothermal system generated by DALL-E.

An electronic version of this thesis is available at <http://repository.tudelft.nl/>.



Abstract

Conduction-dominated geothermal systems are essential for decarbonizing the built environment, particularly in densely populated areas with high heating demand. Geothermal development in the West Netherlands Basin (WNB) has accelerated but still remains largely uncoordinated, following a "first-come, first-served" model which results in suboptimal subsurface resource utilization.

This study presents a multi-objective optimization approach for geothermal field development that simultaneously considers economic performance and reservoir longevity. The framework applies the Non-dominated Sorting Genetic Algorithm II (NSGA-II) to identify Pareto-optimal configurations for well placement and operational control. Objective functions, Net Present Value (NPV) and system lifetime, are evaluated through fully coupled geothermal reservoir simulations using the Delft Advanced Research Terra Simulator (DARTS). The framework incorporates constraint-aware optimization with regulatory compliance, enabling simultaneous optimization of spatial configuration and flow rates through capacity-dependent rate allocation.

The approach is developed and validated on a small-scale synthetic model before application to a realistic corner-point geometry model of the WNB incorporating heterogeneous fluvial architecture. Multiple well configurations (10, 12, and 20 doublets) are systematically evaluated across different geological realizations.

Results demonstrate that NSGA-II effectively identifies diverse Pareto-optimal solutions spanning NPV ranges of 0.8-1.6 billion euros and system lifetimes of 35-100 years. The analysis reveals that total injection capacity directly correlates with economic performance, with higher well-count configurations achieving superior NPV through increased heat extraction capacity. The optimization consistently reveals a distinctive spatial strategy where injection wells are positioned in the thickest reservoir regions with high-permeability zones, while producers balance maximizing distance from injectors with targeting high-temperature, high-permeability areas.

This framework provides quantitative evidence that coordinated planning strategies yield superior performance compared to the current "first-come, first-served" strategies. By applying multi-objective optimization to geothermal planning, the study advocates for the move towards coordinated, regional-scale planning strategies that enable more sustainable and economically superior use of subsurface resources.

Acknowledgments

I would like to sincerely thank my supervisors Alexandros Daniilidis, Carolin Wallmeier, and Denis Voskov for their invaluable guidance throughout my thesis. Alexandros and Carolin consistently provided thoughtful feedback and encouragement, which helped me stay focused and motivated. Denis's insightful suggestions deepened my critical thinking and improved the quality of my work.

I am also grateful to my external supervisor, Oleg Volkov from Stanford University for his helpful advice, especially on the optimization aspects of my project.

Many thanks to Guillaume Rongier for serving as the external member of my committee. His questions and insights were greatly appreciated.

Although not formally part of my supervision team, I want to thank Yuan Chen for his support, especially with DARTS-related questions. Having both Carolin and Yuan nearby during the project was incredibly helpful. Hopefully I wasn't too much of a distraction!

On a personal note, to all the friends who made not only the thesis but the entire Master's experience easier and more enjoyable, thank you. From shared lunches and laughter to venting sessions and coffee breaks, your presence made this journey richer and more memorable. I'm truly grateful.

I want to thank my family for always encouraging me and supporting me in everything I do. And finally, to my boyfriend, Alex, thank you for being by my side through it all. Your support, patience, and encouragement have meant more than I can put into words.

*Mona Devos
Delft, July 2025*

Contents

Abstract	i
Acknowledgments	ii
List of Abbreviations	iv
List of Figures	v
List of Tables	vii
1 Introduction	1
1.1 Motivation and Problem Statement	1
1.2 Research Gap and Opportunity	2
1.3 Research Objectives and Questions	2
1.4 Scope and Approach	3
1.5 Thesis Structure	3
2 Background	4
2.1 West Netherlands Basin Geothermal Context	4
2.1.1 Geological Characteristics	4
2.1.2 Geological Model of the WNB	4
2.1.3 Current Exploitation Status	5
2.1.4 Technical Challenges in Geothermal Development	5
2.2 Reservoir Simulation Fundamentals	5
2.2.1 Governing Principles of Geothermal Reservoir Simulation	6
2.2.2 Delft Advanced Research Terra Simulator	7
2.2.3 Key Performance Indicators	7
2.3 Multi-Objective Optimization Concepts	7
2.3.1 Fundamentals of Multi-Objective Optimization	7
2.3.2 Pareto Optimality	8
2.3.3 Approaches to Multi-Objective Optimization	8
2.4 Evolutionary Algorithms	9
2.4.1 Biological Inspiration and Core Principles	9
2.4.2 Key Advantages	9
2.4.3 Extension to Multi-Objective Problems	9
2.5 The Non-Dominated Sorting Genetic Algorithm II (NSGA-II)	10
2.5.1 Algorithm Structure and Components	10
2.5.2 Advantages and Limitations	10
2.6 Summary	11
3 Methodology	12
3.1 Overall Research Framework	12
3.2 Reservoir Simulation with DARTS	13
3.2.1 Standard Model	13
3.2.2 Enhanced Model	14
3.2.3 Well Implementation	16
3.2.4 Rate Operating Range Determination	17
3.2.5 Simulation Procedure	17
3.2.6 System Lifetime Determination	17

3.2.7	Economic Analysis	18
3.3	Optimization with NSGA-II	19
3.3.1	Problem Formulation	19
3.3.2	Optimization Approach	21
3.3.3	Optimization Loop	22
3.4	Experimental Setup	23
3.4.1	Standard Model Experiments	23
3.4.2	Enhanced Model Experiments	23
3.4.3	Sensitivity and Robustness Analysis	24
3.5	Post-Processing and Analysis	24
3.6	Technical Implementation Details	24
4	Results	26
4.1	Framework Validation and Performance using Standard Model	26
4.1.1	Simulation Results	26
4.1.2	Economic Indicators	27
4.1.3	Optimization Behavior for Standard Model	28
4.2	Enhanced Model Optimization Results	32
4.2.1	Single Configuration Analysis: 20 Doublet System	32
4.2.2	Multi-Configuration Comparison and Optimal Well Placement Strategies	34
4.2.3	Detailed Analysis of Best Lifetime Solution	40
4.2.4	Effect of Temperature Threshold Fraction	41
4.2.5	Sensitivity to Geological Realizations	43
5	Discussion & Limitations	46
5.1	Interpretation of Key Findings	46
5.2	Comparison to Literature and Existing Strategies	48
5.3	Methodological Contributions and Advancements	49
5.4	Limitations and Uncertainties	49
5.4.1	Geological and Model Uncertainties	49
5.4.2	Optimization and Algorithmic Constraints	50
5.4.3	Economic and Operational Assumptions	50
5.5	Future Work Directions	50
5.5.1	Alternative Optimization Formulations	50
5.5.2	Enhanced Optimization Strategies	51
5.5.3	Dynamic and Adaptive Control	51
5.5.4	Uncertainty Quantification and Robustness	51
5.5.5	Systematic Geological Parameter Sensitivity	51
5.5.6	Computational and Algorithmic Improvements	51
5.5.7	Basin-Scale and Multi-Field Applications	52
6	Conclusion & Recommendations	53
6.1	Main Conclusions	53
6.2	Contributions and Impact	53
6.3	Recommendations	54
6.4	Final Remarks	54
	Declaration of Generative AI Use	55
	References	56

List of Abbreviations

BHP Bottom Hole Pressure

CapEx Capital Expenditure

CPG Corner-Point Geometry

DARTS Delft Advanced Research Terra Simulator

EAs Evolutionary Algorithms

HIP Heat In Place

KPIs Key Performance Indicators

MOEA/D Multi-Objective Evolutionary Algorithm based on Decomposition

MOEAs Multi-Objective Evolutionary Algorithms

MOO Multi-Objective Optimization

NPV Net Present Value

NSGA-II Non-Dominated Sorting Genetic Algorithm-II

OBL Operator-Based Linearization

OBM Object-Based Modeling

OpEx Operational Expenditure

SBX Simulated Binary Crossover

SGS Sequential Gaussian Simulation

SodM Staatstoezicht op de Mijnen (Dutch State Supervision of Mines)

SPEA2 Strength Pareto Evolutionary Algorithm 2

TVD True Vertical Depth

WNB West Netherlands Basin

List of Figures

2.1	Key components of the NSGA-II algorithm. From Deb et al. (2002).	10
3.1	Integrated framework for geothermal system optimization. Thicker arrows indicate the main iterative optimization loop, which is repeated until convergence	12
3.2	Visualization of the permeability distribution in the simplified structured grid model.	13
3.3	Spatial distributions and histograms of porosity and permeability in the enhanced CPG grid model.	15
3.4	Structural characterization of the enhanced reservoir model: (a) plan view indicating the location of cross-section through the center of the domain, (b) the corresponding north-south cross-section illustrating increasing reservoir thickness and depth toward the northern sections, and (c) a reservoir thickness map showing the spatial distribution of reservoir thickness across the domain.	16
3.5	Constraint-aware sampling process for initial population generation.	21
4.1	Production well temperature profiles over time. Flow-weighted average temperature, individual well temperatures, breakthrough threshold (dashed line), and system lifetime (dotted line) are shown.	26
4.2	Pressure (a) and flow rate (b) dynamics for injection and production wells over time.	27
4.3	Performance and economic indicators for the geothermal system: (a) pump power consumption, (b) net power output and (c) Net Present Value.	28
4.4	Convergence behavior of the Multi-Objective Optimization (MOO) algorithm showing (a) NPV convergence and (b) system lifetime convergence across multiple independent runs.	29
4.5	Convergence validation experiments demonstrating (a) NPV plateau and (b) system lifetime plateau when continuing optimization from the final populations of Run 1 and Run 9, confirming algorithm convergence.	29
4.6	Visualization of Pareto front results from nine optimization runs: (a) illustrates the consistency of trade-off relationships across runs, and (b) presents the aggregated solution space with the final Pareto-optimal frontier, key solutions, and the influence of injection rate on objective trade-offs.	30
4.7	Spatial optimization analysis showing (a) the underlying geological constraints and (b) preferred well placement patterns identified by the optimization algorithm.	31
4.8	Pareto front analysis showing the trade-off between NPV and system lifetime for the 20-injector, 20-producer optimization run. Gray points represent all evaluations, colored points show feasible solutions meeting water balance constraints (colored by generation), and the black points indicate the final Pareto-optimal solutions.	33
4.9	Well placement frequency heatmaps showing the spatial distribution of (a) injector and (b) producer locations across all optimization evaluations (\log_{10} scale).	34
4.10	Convergence comparison of all optimization runs with different injector configurations. Evolution of the Best (a) NPV and (b) lifetime objectives over generations, comparing 10 optimization runs across three well configurations: 1 run with 10 doublets, 4 runs with 12 doublets, and 5 runs with 20 doublets. Run labels indicate the number of doublets followed by the random seed	35
4.11	Solution space exploration for the 20-doublet restart experiment showing all evaluations and feasible solutions colored by generation, with Pareto fronts for the original run (generations 1-100) and restart continuation (colored from generation 1 to clearly indicate the restart location).	36
4.12	Convergence validation experiments for the 20-doublet configuration demonstrating (a) NPV plateau and (b) system lifetime plateau when continuing optimization from generation 100, confirming algorithm convergence.	36

4.13	Visualization of Pareto front results from 10 enhance model optimization runs: (a) illustrates the impact of well count on trade-off relationships, and (b) presents the aggregated solution space with the final Pareto-optimal frontier, key solutions, and the influence of total injection rate on objective trade-offs.	37
4.14	Optimal well configurations for three key solutions overlaid on the vertically averaged horizontal reservoir permeability field. (i) Best NPV configuration, (ii) Best Lifetime configuration, and (iii) Best Overall configuration. Injectors (blue inverted triangles) and producers (red triangles) are numbered and sized proportionally to their flow rates, showing how well placement and operational strategies vary based on optimization objectives.	38
4.15	Spatial distribution of well placement frequency among final Pareto-optimal solutions for the enhanced model. (a) Injector frequency and (b) producer frequency show preferred optimal locations, with higher frequencies indicating more consistent placement across multiple Pareto solutions.	40
4.16	Temperature evolution of production wells over the 100-year operational period for the Best Lifetime solution. Individual well temperatures (gray), highest-temperature well (red), lowest-temperature well (blue), flow-weighted average temperature (black), and breakthrough threshold (dashed) are shown. The optimal solution maintains the flow-weighted average above the threshold throughout the 100-year period despite some individual wells experiencing breakthrough.	41
4.17	Temporal evolution of reservoir temperature distribution for the Best Lifetime solution, showing cold plume development at (a) 10 years, (b) 50 years, and (c) 100 years. PRD20 and PRD11 are labeled to identify the lowest and highest temperature production wells, respectively. Temperature scale is capped at 345 K to highlight the progression of injection cooling effects through preferential flow paths.	41
4.18	Comparison of Pareto fronts for 15% and 5% temperature threshold fractions. Gray points represent all evaluated solutions, colored points show feasible solutions (colored by generation), and the red and blue points indicate the final Pareto-optimal solutions of both configurations.	42
4.19	Comparison of Pareto fronts for different temperature threshold fractions (15% and 5%), with solutions colored by total injection rate. Key solutions (Best NPV, Best Lifetime, and Best Overall) are highlighted for each threshold configuration.	42
4.20	Comparison of optimal well placement strategies under different temperature threshold criteria.	43
4.21	Comparison of Pareto fronts obtained from optimizations using three different geological realizations. Each realization's Pareto front is shown with a distinct color, with the Best NPV, Best Lifetime, and Best Overall solutions highlighted for each.	43
4.22	Comparison of optimal well placement strategies across different geological realizations, demonstrating how the optimization framework adapts to geological uncertainty while pursuing consistent economic and lifetime objectives.	45

List of Tables

3.1	Standard model: Key simulation parameters	13
3.2	Enhanced model: Grid and geometry configuration	14
3.3	Enhanced model: Reservoir properties	14
3.4	Enhanced model: Initial and boundary conditions	16
3.5	Capital cost components for the geothermal system. Components with a replacement interval of 0 are installed only once at the beginning of the project. Drilling costs are dynamically calculated based on well depths using the formula from Section 3.2.7.	19
3.6	Economic parameters used in Net Present Value (NPV) calculations	19
4.1	Comparison of representative Pareto-optimal solutions from standard model optimization . .	32
4.2	Comparison of representative Pareto-optimal solutions from enhanced model optimization . .	39

1

Introduction

The increasing global demand for sustainable and renewable energy sources has drawn significant attention to geothermal energy as a viable solution to mitigate environmental impacts of fossil fuels. Geothermal energy is heat stored in the subsurface that can be sustainably exploited as a renewable resource (Limberger et al., 2018). This energy source provides commercial base-load electricity generation and has been utilized for over 100 years (Moeck, 2014).

For direct-use applications, geothermal energy offers reliable heating solutions for space heating, district heating (Limberger et al., 2018), and industrial processes. Unlike intermittent renewable energy sources such as solar or wind, geothermal systems provide steady and consistent base-load supply regardless of weather conditions, making them particularly valuable for energy transition strategies (Moeck, 2014).

1.1. Motivation and Problem Statement

Conduction-dominated geothermal systems, which typically operate at reservoir temperatures below 150°C, are particularly suited for direct use in heating applications (Moeck, 2014). These systems are characterized by heat transfer through conduction in sedimentary basins and other passive tectonic settings, where deep aquifers are heated by near-normal geothermal gradients (Moeck, 2014). These systems have gained significant traction in densely populated regions with high heating demands, such as urban and suburban areas. The West Netherlands Basin (WNB) is a notable example, where geothermal heat recovery has been identified as a key contributor to regional energy transition goals, with potential to cover up to 20% of provincial heat demand by 2050 (Willems & M. Nick, 2019). However, optimizing the economic and technical performance of these systems remains challenging due to complex trade-offs between energy production and system lifetime (Daniilidis, Khait, et al., 2020).

The "first-come, first-serve" approach observed in the WNB deployment, where individual operators independently select well locations based on immediate needs and constraints, often neglecting broader optimization opportunities for the reservoir as a whole (Willems & M. Nick, 2019), exemplifies a widespread challenge in geothermal resource exploitation worldwide. This approach results in suboptimal reservoir utilization. Significant inefficiencies arise from:

1. **Poorly coordinated well placement:** In large reservoirs such as the WNB, optimizing the spatial distribution of wells is crucial to maximize overall reservoir performance (Willems & M. Nick, 2019), as poorly coordinated placement can lead to significant interference between doublets (Willems et al., 2017), particularly in fault-affected areas where system lifetime can be reduced by over 40% (Daniilidis, Nick, et al., 2021).
2. **Suboptimal control strategies:** Production and reinjection rates play a critical role in balancing heat recovery efficiency with reservoir sustainability, as thermal recharge processes can extend significantly beyond operational timescales (Wallmeier, 2024). Without coordinated optimization of well placement, these rates may accelerate reservoir depletion (S. Zhang et al., 2021), while suboptimal control strategies can substantially reduce long-term economic returns from geothermal field development (Kane et al., 2025).

The widespread adoption of such uncoordinated approaches across the industry highlights the urgent need for systematic optimization methodologies that can guide more strategic geothermal development.

1.2. Research Gap and Opportunity

Two critical factors influencing the success of conduction-dominated geothermal systems are the *placement of wells* (Y. Wang et al., 2021) and their *control strategies* (Daniilidis, Nick, et al., 2020). These factors directly impact key performance indicators such as the *Net Present Value (NPV)* of projects and the *system lifetime* (Daniilidis, 2024). Despite recent advances in geothermal system optimization, achieving an optimal balance between maximizing economic returns and preserving long-term reservoir performance remains challenging, with several critical issues unresolved:

1. **Thermal Breakthrough and Pressure Decline:** Improper well placement can lead to early thermal breakthrough, where reinjected cooler fluid prematurely reaches production wells (S. Zhang et al., 2021). This thermal interference can significantly reduce energy output and, in severe cases, may cause system shutdown (Kong et al., 2017). Additionally, the injection of cold water triggers strongly coupled thermo-hydro-mechanical processes that can affect both reservoir pressure management and system stability (L. Zhang et al., 2025). These interconnected effects highlight the critical need for optimized well placement and controls.
2. **Economic Viability vs. Reservoir Longevity:** Current optimization studies typically focus on single objectives, making it challenging to balance short-term economic returns with long-term reservoir performance, especially in conduction-dominated systems with narrow profit margins (Daniilidis, Khait, et al., 2020). Without coordinated optimization, operational strategies may accelerate reservoir depletion or reduce economic returns (Kane et al., 2025). Advanced optimization frameworks are needed to strike a balance between these competing objectives.

Addressing these interconnected challenges requires moving beyond conventional approaches that optimize well placement and operational controls separately. While recent research has demonstrated effectiveness in optimizing either spatial configurations with fixed operational parameters (Kane et al., 2025) or operational controls for predetermined well layouts (Daniilidis, Khait, et al., 2020), integrated optimization of both elements remains largely unexplored. Multi-objective optimization approaches, particularly Non-Dominated Sorting Genetic Algorithm-II (NSGA-II), offer a framework for simultaneously addressing well placement and operational strategies while balancing competing objectives such as economic performance and system longevity (Deb et al., 2002).

This study aims to address this gap by developing a comprehensive optimization framework that integrates well placement and control strategies using NSGA-II, applied to a model incorporating geological features representative of the WNB.

1.3. Research Objectives and Questions

The primary goal of this research is to develop a comprehensive optimization framework for conduction-dominated geothermal systems, using the WNB as a case study. The research will address the following main question:

How can Multi-Objective Optimization (MOO) with NSGA-II be applied to determine the optimal placement and control of multi-well geothermal systems to maximize both NPV and system lifetime?

To address this question comprehensively, the following sub-questions are defined:

1. What makes well placement and operational controls critical decision variables in optimizing multi-well geothermal systems in the WNB?
2. What constraints are necessary for balancing economic and operational performance in geothermal system optimization?
3. How can NSGA-II be applied to balance the competing objectives of maximizing NPV and system lifetime in geothermal systems?
4. How can trade-offs between NPV and system lifetime be quantified and analyzed using the Pareto front generated by NSGA-II?

5. What practical design and operational insights can be derived from the optimized solutions, and how can these insights inform improvements to the current "first-come, first-served" deployment strategies in large reservoirs like the WNB?

1.4. Scope and Approach

This thesis develops a generalizable optimization framework for conduction-dominated geothermal systems, using the WNB as a case study with a representative geological model of the Delft Sandstone formation. The research develops a MOO framework using NSGA-II, targeting well placement and control strategies to maximize NPV and system lifetime.

During the development phase, a smaller, computationally efficient model with heterogeneous fluvial characteristics was used for initial testing and debugging. The final optimization results are based on a larger, geologically detailed model that better captures the regional characteristics of the WNB. The framework integrates reservoir simulation with economic modeling, enabling a systematic evaluation of trade-offs between economic and operational performance through Pareto-optimal solutions. These results provide actionable insights to support more strategic geothermal deployment.

1.5. Thesis Structure

The remainder of this thesis is organized as follows:

- Chapter 2: Provides theoretical background on geothermal systems in the WNB, reservoir simulation fundamentals, MOO concepts, and the NSGA-II algorithm.
- Chapter 3: Describes the methodology, including the development of the optimization framework, the reservoir simulation approach, economic modeling, and the application of the NSGA-II algorithm.
- Chapter 4: Presents the validation of the optimization framework and the resulting outcomes, including Pareto fronts and optimal well configurations.
- Chapter 5: Interprets key findings by answering the research questions, compares results to literature, and discusses methodological contributions and limitations.
- Chapter 6: Summarizes the key findings, conclusions, and recommendations for future work.

This research contributes to the sustainable development of geothermal energy systems by providing a systematic approach to enhancing economic performance while ensuring long-term reservoir sustainability. The findings can inform more effective resource management policies and support the broader adoption of geothermal energy as part of the energy transition.

2

Background

This chapter provides the foundational knowledge necessary to understand the research context, methods, and significance of this study. It begins with an overview of the WNB's geothermal characteristics, followed by the fundamentals of reservoir simulation as applied to geothermal systems. The chapter then introduces multi-objective optimization concepts and explores NSGA-II, which serves as the primary optimization method in this research.

2.1. West Netherlands Basin Geothermal Context

The WNB represents one of the most promising areas for geothermal energy development in the Netherlands, characterized by its favorable geological conditions and proximity to population centers with high heat demand (Mijnlieff, 2020). This section examines the geological characteristics of the region, introduces the geological model used in this study, and reviews the current exploitation status.

2.1.1. Geological Characteristics

The WNB is a Mesozoic rift basin characterized by thick sedimentary sequences formed during Jurassic and Early Cretaceous extensional phases. The primary geothermal targets lie within the Lower Cretaceous Nieuwerkerk Formation, with the Delft Sandstone Member representing the most prolific target (Mijnlieff, 2020). Detailed reservoir architecture studies reveal that the Delft Sandstone Member consists of stacked fluvial sandstones deposited by meandering rivers, interbedded with claystone, lignite, and coal layers (Donselaar, 2016).

These formations offer favorable porosity and permeability conditions for geothermal energy production. The Delft Sandstone, in particular, features laterally amalgamated, vertically stacked channel bodies that enhance reservoir connectivity (Donselaar, 2016). Reservoir depths typically range from 1.7 to 2.5 km, with production temperatures between 60°C and 95°C, suitable for direct-use heating applications (Willems & M. Nick, 2019).

However, the subsurface is structurally complex, with faults that can act as flow barriers or conduits. These features, along with heterogeneity in reservoir architecture, introduce uncertainties in flow behavior and thermal breakthrough, necessitating detailed geological characterization in development planning (Daniilidis, Nick, et al., 2021).

2.1.2. Geological Model of the WNB

Subsurface data from the geothermal doublet on the campus of Delft University of Technology and the surrounding area served as the foundation for the geological model of the WNB employed in this study (Chen et al., 2025). An Object-Based Modeling (OBM) approach was applied to represent the fluvial depositional architecture, specifically to simulate channel structures and associated facies. OBM makes use of parameterized geometric objects—such as sinuous channels and related levee and crevasse features—that are stochastically positioned within the simulation grid (Deutsch & Wang, 1996). The shape and spatial organization of these structures are controlled by statistical distributions of parameters such as channel width, thickness, sinuosity, and orientation.

The placement and geometry of these objects were refined through an iterative optimization procedure to produce realizations that respect global facies proportions and well data. This approach enables the model to reproduce realistic sedimentary structures which are consistent with conceptual geological understanding and observed data. The target aquifer, the Delft Sandstone Member, has been interpreted as meandering river

deposits (Chen et al., 2025) with a reservoir thickness of approximately 120 m.

Subsequent to the facies modeling, porosity was simulated using Sequential Gaussian Simulation (SGS), conditioned on the facies realizations. SGS generates spatially correlated continuous properties by drawing values from a Gaussian random field that honors the statistical distribution and spatial continuity inferred from data (Deutsch & Journel, 1997). To guarantee consistency between the petrophysical characteristics and depositional architecture, each simulation is limited by the geological structure specified by the facies model as well as the known porosity values at well locations. Permeability was subsequently distributed using the porosity-permeability relationship derived from Willems et al. (2020).

This study employs the enhanced geological model developed by Chen et al. (2025), which uses Corner-Point Geometry (CPG) to discretize the spatial domain and incorporates data from the Delft campus geothermal wells (DEL-GT-01 and DEL-GT-02-S2) and eight additional wells from the WNB region. The CPG approach enables better alignment with geological structures compared to conventional Cartesian grids, particularly for the heterogeneous fluvial architecture of the Delft Sandstone Member. For computational efficiency, this study uses a slightly smaller and coarser version of Chen et al.'s original model, while maintaining essential geological characteristics. The model was generated with a net-to-gross ratio of 50%, and a total of three realizations were created using identical parameters to account for stochastic variability while maintaining consistent geological properties.

2.1.3. Current Exploitation Status

Geothermal development in the WNB has progressed steadily since 2007, making the region a focal point for Dutch geothermal activity. By 2018, over a dozen geothermal doublets were operational, predominantly targeting the Lower Cretaceous Nieuwerkerk Formation for direct-use heating applications, with heat production capacities between 7 and 21 MW_{th} per doublet (Willems & M. Nick, 2019).

Operational data reveal increasing trends in production rates and injection capacities. Older doublets typically produced at 150–200 m³/h, while more recent installations have reached flow rates up to 360 m³/h (Vardon et al., 2024). The producer-injector spacing varies from 1.0 to 2.1 km, and the thermal recovery areas range from approximately 2 to 7.2 km² (Willems & M. Nick, 2019).

This study contributes to ongoing efforts to develop more coordinated, optimization-based approaches to geothermal development in the WNB.

2.1.4. Technical Challenges in Geothermal Development

Geothermal development in the WNB faces several technical challenges relevant to this optimization study:

1. **Geological uncertainties:** Subsurface uncertainty regarding reservoir properties presents challenges for accurate prediction of system performance and optimal development planning. Y. Wang et al. (2023) highlighted how heterogeneity in fluvial sandstone reservoirs affects geothermal performance, while Compennolle et al. (2023) and Schulte et al. (2020) emphasized the need for integrated optimization approaches under geological uncertainty.
2. **Thermal and hydraulic interference:** The proximity of geothermal installations creates risks of thermal breakthrough and pressure interference. Daniilidis, Nick, et al. (2021) demonstrated that interference effects can significantly impact system performance, particularly near geological structures such as faults.
3. **Economic-technical trade-offs:** The high upfront investment costs for geothermal projects, combined with relatively long payback periods, create economic pressures that must be balanced against long-term reservoir sustainability (Kane et al., 2025).

These technical challenges highlight the need for integrated optimization frameworks that can balance competing objectives while accounting for geological uncertainty.

2.2. Reservoir Simulation Fundamentals

Accurate modeling of subsurface processes is critical for optimizing geothermal energy production, particularly in systems where heat is extracted via fluid circulation and cold water reinjection. Numerical reservoir

simulation provides a predictive tool to analyze heat transport, optimize well operations, and assess the long-term sustainability of geothermal fields. This section provides an overview of the governing principles of geothermal reservoir simulation and introduces the Delft Advanced Research Terra Simulator (DARTS), the numerical simulator employed in this study.

2.2.1. Governing Principles of Geothermal Reservoir Simulation

Geothermal reservoir simulation involves solving the conservation equations for mass and energy to describe fluid flow and heat transport in porous media. The primary physical processes include convective flow of multiphase fluids, conductive heat transfer between fluids and the rock matrix, and gravitational effects on fluid flow. These processes are coupled through the thermodynamic properties of the fluid-rock system, with fluid properties varying significantly with pressure and temperature.

The conservation equations, as implemented in DARTS, are formulated for fully coupled multiphase systems and typically solved using a fully-implicit finite volume method (Voskov et al., 2024):

- **Mass conservation** over all fluid phases:

$$\frac{\partial}{\partial t} \left(\phi \sum_{j=1}^{n_p} \rho_j s_j \right) - \nabla \cdot \sum_{j=1}^{n_p} \rho_j v_j + \sum_{j=1}^{n_p} \rho_j \tilde{q}_j = 0 \quad (2.1)$$

- **Energy conservation** for the fluid-rock system:

$$\frac{\partial}{\partial t} \left(\phi \sum_{j=1}^{n_p} \rho_j s_j U_j + (1 - \phi) U_r \right) - \nabla \cdot \sum_{j=1}^{n_p} h_j \rho_j v_j + \nabla \cdot (\kappa \nabla T) + \sum_{j=1}^{n_p} h_j \rho_j \tilde{q}_j = 0 \quad (2.2)$$

In these equations, ϕ is porosity, n_p is the total number of phases existing in the geothermal system, ρ_j is the density of phase j , s_j the saturation, v_j the Darcy velocity, U_j and U_r the specific internal energies of phase j and the rock matrix, h_j the specific enthalpy of phase j , T the temperature, and κ the thermal conduction coefficient. The source/sink term \tilde{q}_j represents mass injection or production per unit volume.

The thermal conduction coefficient κ is defined as a volume-weighted average of fluid and rock contributions:

$$\kappa = \phi \sum_{j=1}^{n_p} s_j \kappa_j + (1 - \phi) \kappa_r \quad (2.3)$$

where κ_j is the conduction coefficient of phase j , and κ_r is the conduction coefficient of the rock matrix.

Fluid motion is governed by Darcy's law, accounting for gravity:

$$v_j = K \frac{k_{rj}}{\mu_j} (\nabla p - \gamma_p \nabla D) \quad (2.4)$$

where K is the permeability of the porous media, k_{rj} the phase relative permeability, μ_j the viscosity of phase j , p pressure, γ_p the specific weight, and D depth.

For compressible rock, porosity can be updated based on:

$$\phi = \phi_0 (1 + c_r (p - p_{\text{ref}})) \quad (2.5)$$

where ϕ_0 is the initial porosity of the rock, c_r is rock compressibility, and p_{ref} is the reference pressure.

Similarly, fluid compressibility is accounted for through pressure and temperature-dependent fluid properties. The fluid is compressible, and its properties (density, viscosity, enthalpy) are evaluated using thermodynamic correlations such as IAPWS-97 (Y. Wang et al., 2020).

Due to the nonlinear coupling of pressure, temperature, and fluid properties, geothermal simulators typically employ fully implicit numerical schemes with Newton-Raphson solvers to ensure numerical stability and convergence across time steps.

2.2.2. Delft Advanced Research Terra Simulator

DARTS is a high-performance geothermal reservoir simulator developed to accurately and efficiently model coupled mass and energy transport in porous media (Y. Wang et al., 2020). It uses a molar formulation with pressure and enthalpy as primary variables which makes it particularly suitable for multi-phase, non-isothermal geothermal systems.

By using a fully-implicit finite-volume discretization on unstructured grids, DARTS enables detailed representation of geological heterogeneity, including faults and fractures. Its core innovation lies in the Operator-Based Linearization (OBL) approach, which reformulates nonlinear terms—such as fluxes and accumulations—into state-dependent operators. These operators are pre-tabulated in physical space and interpolated during simulation. This reduces the need for frequent recomputation of thermodynamic derivatives.

This strategy improves computational performance and convergence robustness, particularly in large-scale or uncertainty quantification studies. Benchmark comparisons show that DARTS matches the accuracy of established simulators such as TOUGH2 and AD-GPRS while offering substantial gains in efficiency (Y. Wang et al., 2020).

2.2.3. Key Performance Indicators

Reservoir simulation enables the evaluation of Key Performance Indicators (KPIs) that serve as objective functions in the optimization process:

1. **System Lifetime:** This is defined as the period during which a geothermal system can maintain production temperature above a specified threshold (e.g., initial production temperature minus 15% of the difference between initial temperature and injection temperature) (Daniilidis, Saeid, et al., 2021). It is a critical indicator of long-term system sustainability.
2. **Net Present Value (NPV):** NPV is a key economic performance indicator that accounts for the time value of money by discounting future cash flows to their present value (Daniilidis, Khait, et al., 2020). It incorporates Capital Expenditure (CapEx), Operational Expenditure (OpEx), and revenue from heat production:

$$\text{NPV} = \sum_{t=0}^T \frac{R_t - C_t}{(1+r)^t} \quad (2.6)$$

where R_t denotes the revenue at time t , C_t the corresponding costs, r the discount rate, and T the total project duration (Daniilidis, Khait, et al., 2020).

These KPIs provide a basis for evaluating and comparing different design and operational strategies in the MOO framework.

2.3. Multi-Objective Optimization Concepts

MOO forms the methodological foundation of this research. This section introduces the key concepts, principles, and approaches in MOO, with particular emphasis on their relevance to geothermal system design and operation.

2.3.1. Fundamentals of Multi-Objective Optimization

Unlike single-objective optimization, which seeks to find a solution that maximizes or minimizes a single objective function, MOO addresses problems with multiple, often conflicting, objectives (Emmerich & Deutz, 2018). These problems can be formally expressed as:

$$\begin{aligned} &\text{Minimize (or Maximize)} && F(\mathbf{x}) = [f_1(\mathbf{x}), f_2(\mathbf{x}), \dots, f_m(\mathbf{x})]^T \\ &\text{subject to} && g_i(\mathbf{x}) \leq 0, \quad i = 1, 2, \dots, p \\ & && h_j(\mathbf{x}) = 0, \quad j = 1, 2, \dots, q \\ & && \mathbf{x}_L \leq \mathbf{x} \leq \mathbf{x}_U \end{aligned} \quad (2.7)$$

Where:

- $\mathbf{x} = [x_1, x_2, \dots, x_n]^T$ is the vector of decision variables
- $f_k(\mathbf{x})$ are the objective functions to be optimized
- $g_i(\mathbf{x})$ and $h_j(\mathbf{x})$ represent inequality and equality constraints, respectively
- \mathbf{x}_L and \mathbf{x}_U are the lower and upper bounds of the decision variables

In the context of geothermal system optimization, typical objectives include maximizing NPV (Daniilidis, Khait, et al., 2020; Kane et al., 2025), maximizing energy generation (Daniilidis, Khait, et al., 2020), maximizing system lifetime, or maximizing heat recovery factor. Decision variables commonly include well locations, well spacing, production and injection rates, and operational controls over time.

2.3.2. Pareto Optimality

A central concept in MOO is Pareto optimality. A solution is considered Pareto optimal if no other solution can improve at least one objective without degrading at least one other objective (Emmerich & Deutz, 2018). Mathematically, a solution \mathbf{x}^* is Pareto optimal if there exists no other feasible solution \mathbf{x} such that:

$$\begin{aligned} f_i(\mathbf{x}) &\leq f_i(\mathbf{x}^*) \quad \forall i \in \{1, 2, \dots, m\} \\ f_j(\mathbf{x}) &< f_j(\mathbf{x}^*) \quad \text{for at least one } j \in \{1, 2, \dots, m\} \end{aligned} \quad (2.8)$$

The set of all Pareto optimal solutions forms the Pareto front, which represents the trade-off surface between competing objectives (Coello Coello et al., 2007). In geothermal applications, the Pareto front can provide valuable insights into the trade-offs between economic performance (e.g., NPV) and sustainability indicators (e.g., system lifetime or resource depletion rate).

2.3.3. Approaches to Multi-Objective Optimization

Several approaches have been developed to solve MOO problems:

1. **Weighted sum method:** This classical approach converts the multi-objective problem into a single-objective problem by assigning weights to each objective and summing them:

$$F(\mathbf{x}) = \sum_{i=1}^m w_i f_i(\mathbf{x}) \quad (2.9)$$

While straightforward, this method is sensitive to the choice of weights (Deb et al., 2002) and may not capture non-convex portions of the Pareto front (Coello Coello et al., 2007).

2. **ϵ -constraint method:** This approach optimizes one primary objective while converting other objectives into constraints:

$$\begin{aligned} &\text{Minimize} \quad f_1(\mathbf{x}) \\ &\text{subject to} \quad f_i(\mathbf{x}) \leq \epsilon_i, \quad i = 2, \dots, m \end{aligned} \quad (2.10)$$

By systematically varying the values of ϵ_i , different Pareto optimal solutions can be obtained.

3. **Evolutionary algorithms:** These population-based stochastic optimization methods maintain multiple candidate solutions simultaneously and use selection, crossover, and mutation operators to evolve the population toward the Pareto front (Coello Coello et al., 2007). Unlike single-objective methods, Multi-Objective Evolutionary Algorithms (MOEAs) employ specialized selection mechanisms that consider multiple objectives simultaneously, often using dominance-based ranking and diversity preservation strategies to generate multiple Pareto optimal solutions in a single run (Deb et al., 2002). Examples include NSGA-II, Strength Pareto Evolutionary Algorithm 2 (SPEA2), which uses strength-based fitness assignment and an external archive (Zitzler et al., 2001), and Multi-Objective Evolutionary Algorithm based on Decomposition (MOEA/D), which decomposes the multi-objective problem into multiple single-objective subproblems (Q. Zhang & Li, 2007).

For geothermal system optimization, evolutionary algorithms offer several advantages, including their ability to handle high-dimensional, discontinuous, and multi-modal optimization problems with complex constraints (Islam et al., 2020), and their capacity to provide diverse solution sets for decision-makers (Deb et al., 2002).

These characteristics make them well-suited for addressing the complex interplay between well placement, operational parameters, and heterogeneous reservoir conditions encountered in geothermal applications (Song et al., 2021; Wallmeier, 2024).

2.4. Evolutionary Algorithms

Evolutionary Algorithms (EAs) represent a class of nature-inspired optimization techniques that simulate the process of biological evolution to search for optimal solutions within complex solution spaces (Bäck, 1996; Coello Coello et al., 2007). These population-based stochastic methods have emerged as particularly effective tools for problems that are difficult to solve using traditional optimization approaches.

2.4.1. Biological Inspiration and Core Principles

EAs draw inspiration from natural evolutionary processes, where populations of organisms evolve over time through selection, reproduction, and genetic variation. Fitter individuals have higher chances of survival and reproduction, passing advantageous traits to their offspring (Emmerich & Deutz, 2018).

In computational terms, EAs translate these biological concepts into optimization frameworks where:

- **Individuals** represent candidate solutions to the optimization problem
- **Population** maintains multiple candidate solutions simultaneously
- **Fitness** measures solution quality through objective function evaluation
- **Selection** determines which individuals contribute to reproduction
- **Genetic operators** create new candidate solutions:
 - **Crossover:** Combines information from two parent solutions to create offspring. For continuous variables, Simulated Binary Crossover (SBX) creates offspring following a probability distribution around parents (Deb & Agrawal, 1995).
 - **Mutation:** Introduces random variations to maintain diversity and explore new search regions. Polynomial mutation perturbs continuous variables using controlled probability distributions (Deb et al., 2002).
- **Repair operators** ensure solution feasibility by correcting constraint violations after genetic operations.

2.4.2. Key Advantages

Evolutionary algorithms offer several distinctive characteristics that make them suitable for complex optimization problems (Deb et al., 2002; Luke, 2013):

Population-based search: EAs maintain multiple candidate solutions simultaneously, enabling parallel exploration of the solution space and reducing the risk of premature convergence to local optima.

Derivative-free operation: No gradient information is required, making EAs applicable to problems with discontinuous, non-differentiable, or computationally expensive objective functions.

Flexibility: EAs can handle various problem types, including discrete, continuous, mixed-variable, and constrained optimization problems without requiring significant algorithmic modifications.

2.4.3. Extension to Multi-Objective Problems

The population-based nature of evolutionary algorithms makes them particularly well-suited for multi-objective optimization, where the goal is to find a set of trade-off solutions rather than a single optimum (Emmerich & Deutz, 2018). Multi-Objective Evolutionary Algorithms (MOEAs) can generate approximations of the entire Pareto front in a single run, providing decision-makers with comprehensive insights into available trade-offs.

This capability has led to the development of sophisticated MOEAs that employ specialized selection mechanisms and diversity preservation strategies to simultaneously achieve convergence toward the Pareto front while maintaining solution diversity—principles exemplified in algorithms such as NSGA-II.

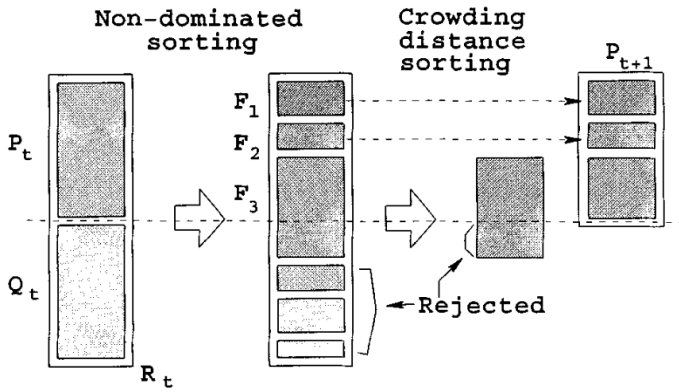
2.5. The Non-Dominated Sorting Genetic Algorithm II (NSGA-II)

NSGA-II, introduced by Deb et al. (2002), is one of the most established and widely adopted evolutionary algorithms in MOO and serves as the primary optimization method in this research. This section explores its structure, key components, and relevance to geothermal system optimization.

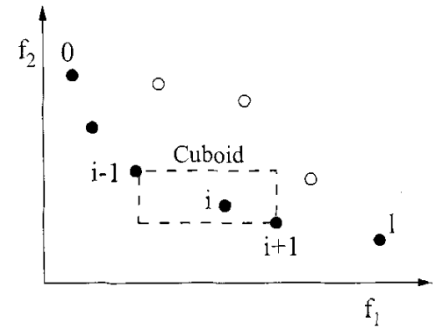
2.5.1. Algorithm Structure and Components

NSGA-II addresses three critical limitations of earlier evolutionary multi-objective algorithms: high computational complexity and lack of elitism. The algorithm follows a structured process (Fig. 2.1a):

1. **Initialization:** A population of candidate solutions is randomly generated within the feasible decision space.
2. **Non-dominated sorting:** Solutions are ranked based on non-domination levels. Solutions not dominated by any other solution are assigned rank 1 (forming the first Pareto front). Solutions dominated only by rank 1 solutions are assigned rank 2, and so on.
3. **Crowding distance calculation:** Within each non-domination level, solutions are assigned a crowding distance value, which measures the density of solutions surrounding a particular point (Fig. figure 2.1b).
4. **Selection:** A binary tournament selection is used, preferring solutions of lower rank or higher crowding distance. This promotes quality and diversity in the Pareto front.
5. **Genetic operators:** Crossover and mutation operators are applied to create a new offspring population.
6. **Elitism and replacement:** Parents and offspring are combined, and the best solutions based on rank and crowding distance are selected for the next generation.
7. **Termination:** Steps 2-6 are repeated until a termination criterion (e.g., maximum number of generations) is met.



(a) Procedure of NSGA-II, including sorting, selection, and elitism.



(b) Crowding distance calculation within a nondominated front.

Figure 2.1: Key components of the NSGA-II algorithm. From Deb et al. (2002).

The key innovations of NSGA-II include a fast non-dominated sorting approach with $O(MN^2)$ computational complexity (where M is the number of objectives and N is the population size), an elitist strategy that preserves the best solutions across generations, and a parameter-less crowding distance approach to maintain diversity (Deb et al., 2002).

2.5.2. Advantages and Limitations

NSGA-II offers several advantages that make it suitable for geothermal system optimization:

- **Efficient handling of multiple objectives:** The algorithm can effectively handle two or more competing objectives simultaneously, making it suitable for balancing economic and sustainability goals in geothermal applications (Schulte et al., 2020).

- **Diverse solution set:** The crowding distance mechanism helps maintain diversity in the solution set, providing decision-makers with a wide range of options on the Pareto front (Coello Coello et al., 2007).
- **Constraint handling:** NSGA-II incorporates constraint handling through a modified dominance principle that prioritizes feasible solutions over infeasible ones and ranks infeasible solutions by their constraint violation levels, eliminating the need for penalty parameters (Deb et al., 2002). These mechanisms are important for addressing the physical and operational constraints inherent in geothermal systems.
- **No derivative information required:** Unlike gradient-based methods, NSGA-II does not require derivative information, making it suitable for problems where the objective functions are complex, non-linear, or computationally expensive to evaluate (Dey, 2024).

However, NSGA-II also has limitations that must be considered:

- **Computational intensity:** For problems requiring expensive function evaluations (e.g., reservoir simulations), the large number of evaluations required by NSGA-II can be computationally prohibitive (J. Wang et al., 2022).
- **Parameter tuning:** While NSGA-II eliminates the need for a sharing parameter, it still requires tuning of several parameters, including population size, crossover and mutation rates, and termination criteria (Luke, 2013).
- **Convergence rate:** For complex problems, the algorithm may require many generations to converge to the true Pareto front (Dey, 2024).

2.6. Summary

This chapter established the foundation for the research by first outlining the geothermal potential and development challenges in the WNB. It then introduced the principles of geothermal reservoir simulation and DARTS as the modeling tool used to evaluate system performance.

Key concepts in MOO were presented, including Pareto optimality and solution methods, followed by an introduction to EAs as a powerful approach for multi-objective problems. Particular focus was given to NSGA-II, which is employed in this study to balance economic and sustainability objectives in geothermal system design.

Together, these elements—geological context, simulation framework, and optimization methodology—form the basis for the integrated research approach presented in the following chapter.

3

Methodology

This chapter presents the methodology developed for MOO of geothermal systems in the WNB. The approach integrates reservoir simulation, economic analysis, and MOO to determine optimal well placement and operational strategies that balance economic returns with system longevity.

3.1. Overall Research Framework

The research framework consists of three main components integrated into a unified optimization workflow (Figure 3.1). The workflow begins with the definition of optimization parameters, which feed into the NSGA-II multi-objective genetic algorithm. For each candidate solution, the framework executes a complete geothermal reservoir simulation using DARTS, followed by an economic evaluation. These simulation results inform both objective functions: NPV and system lifetime. The process iterates until the optimization algorithm terminates on a set of Pareto-optimal solutions that represent the trade-off between economic performance and reservoir longevity.

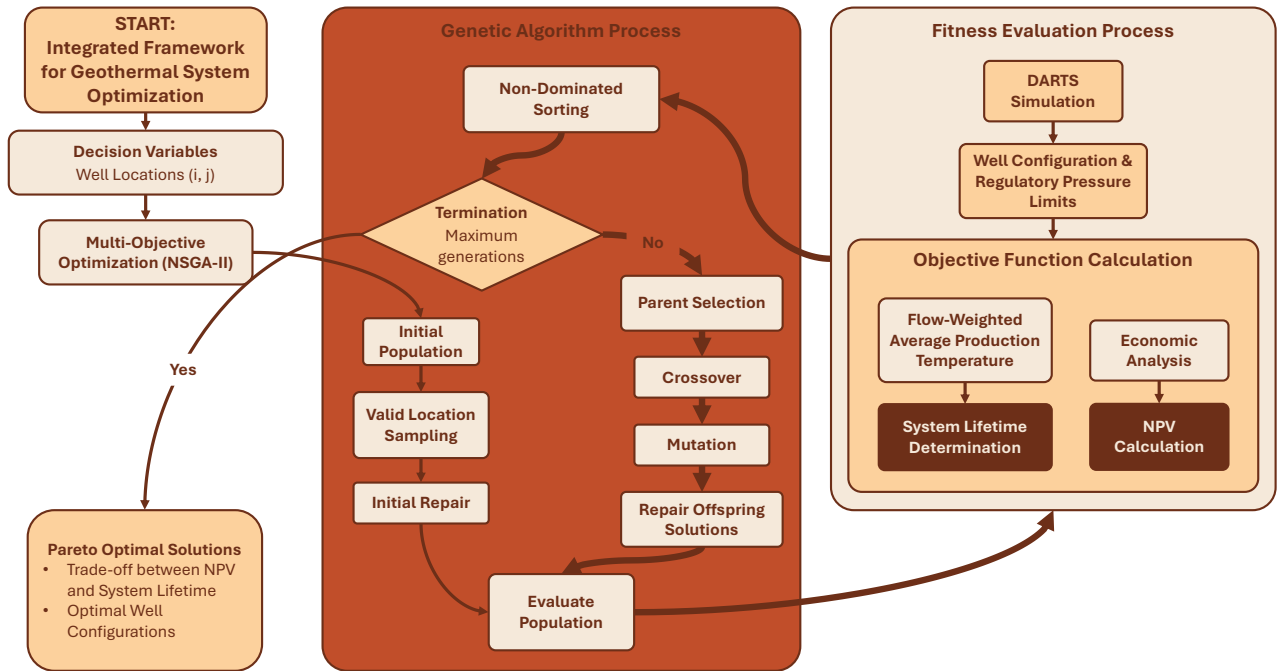


Figure 3.1: Integrated framework for geothermal system optimization. Thicker arrows indicate the main iterative optimization loop, which is repeated until convergence

The methodology outlined above directly addresses the research questions posed in Section 1.3. The integrated simulation-optimization framework operationalizes the main research question by implementing NSGA-II to determine optimal well placement and controls that maximize both NPV and system lifetime. The detailed reservoir simulation components, with both standard and enhanced models, enable exploration of why well placement and operational controls are critical variables (RQ 1). The implementation of geological, physical, and regulatory constraints (RQ 2) ensures realistic solutions. Our custom NSGA-II operators and objective

function formulations facilitate balancing competing objectives (RQ 3), while the post-processing analysis provides quantitative methods to analyze trade-offs through the Pareto front (RQ 4). Finally, the comprehensive approach yields practical design insights that can inform improvements to current deployment strategies in the WNB (RQ 5). Each subsequent section elaborates on specific methodological components that contribute to answering these research questions.

3.2. Reservoir Simulation with DARTS

We implemented the geothermal reservoir simulation using DARTS, a high-performance geothermal simulator. We developed two model implementations: a simplified structured grid model (standard model) for development and testing, and an enhanced CPG model for the main optimization studies. The enhanced model more accurately represents the complex geological characteristics of the WNB. Each simulation initializes the reservoir with specified pressure and temperature gradients, applies operational constraints on injection and production wells, and runs over a defined period. We determine system lifetime based on thermal breakthrough criteria and evaluate economic performance by computing NPV from the resulting production and cost profiles.

3.2.1. Standard Model

To facilitate development and algorithmic testing, we implemented a simplified structured grid model with the following configuration:

Category	Parameter	Value / Description
Grid Configuration	Grid size	$60 \times 60 \times 3$
	Cell dimensions	$30 \text{ m} \times 30 \text{ m} \times 30 \text{ m}$
Geological Properties	Permeability distribution	Heterogeneous (Fig. 3.2)
	Porosity	Uniform, 0.2
	Top layer	$\phi = k = 1 \cdot 10^{-6}$ (acts as barrier)
	$k_z/k_{x,y}$ ratio	$k_z = 0.1 \cdot k_{x,y}$
Thermal Properties	Heat capacity (rock)	$2200 \text{ kJ/m}^3/\text{K}$
	Heat conductivity (rock)	500 kJ/m/day/K
Initial & Boundary Conditions	Temperature	350 K
	Pressure	200 bar
	Lateral boundaries	10^{12} m^3 (infinite-acting aquifer)

Table 3.1: Standard model: Key simulation parameters

Figure 3.2 illustrates the permeability distribution and histogram of the standard model.

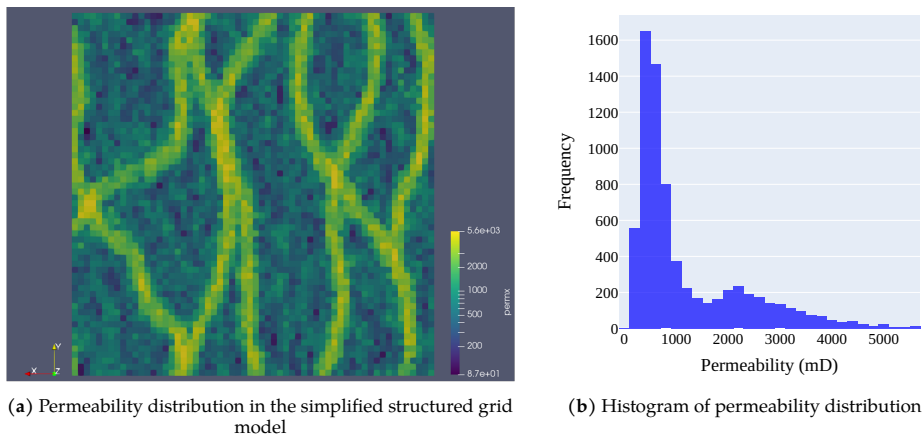


Figure 3.2: Visualization of the permeability distribution in the simplified structured grid model.

This standard model offers computational efficiency and a simplified geometry that enables faster convergence. We used this model as the primary testbed for adapting the MOO algorithm before applying it to more complex geological scenarios.

3.2.2. Enhanced Model

The model setup and geological characterization are detailed in Section 2.1.2, incorporating data from the Delft campus geothermal doublet and regional wells.

Grid and Geometry

The enhanced model leverages industry-standard GRDECL files to define the reservoir geometry:

Parameter	Value / Description
Grid dimensions	$102 \times 102 \times 20$ cells
Grid size	$55 \times 55 \times (0.25 - 22.55)$ m
Active cells	205834 cells
Burden layers	4 layers added above and below the reservoir (8 total)

Table 3.2: Enhanced model: Grid and geometry configuration

Reservoir Properties

The enhanced model reservoir properties for the first realization are defined as follows:

Category	Parameter	Value / Description
Porosity	Source	Loaded from GRDECL
	Threshold	Minimum 0.001
	Value range	0.001 - 0.354
Permeability	Source	Calculation based on Willems et al. (2020) correlation (Eq. 3.1)
	Vertical to horizontal ratio	$k_z = 0.1 \cdot k_{x,y}$
	Threshold	Minimum 0.001 mD
	Value range	0.001 - 3067 mD
Thermal Properties	Shale heat capacity	2300 kJ/m ³ /K
	Shale heat conductivity	190.8 kJ/m/day/K
	Sandstone heat capacity	2450 kJ/m ³ /K
	Sandstone heat conductivity	259.2 kJ/m/day/K

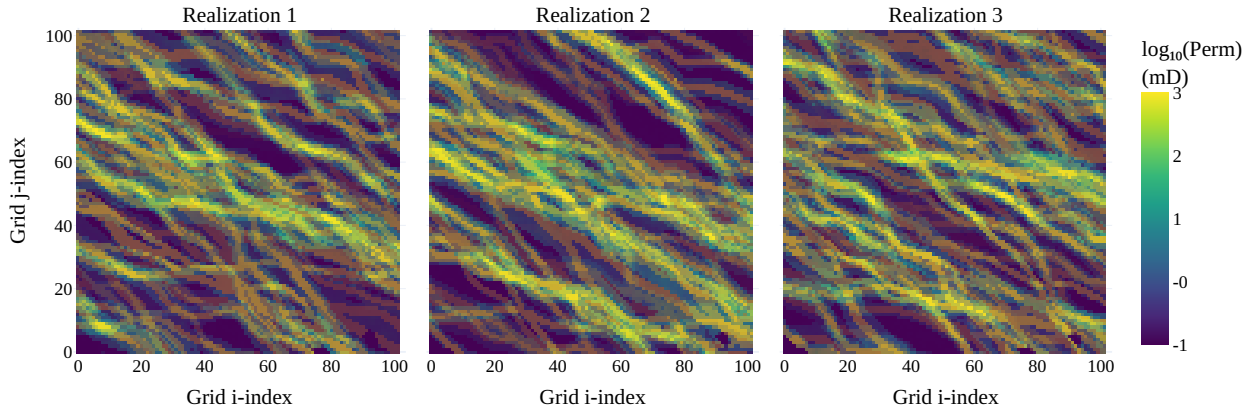
Table 3.3: Enhanced model: Reservoir properties

Permeability k is computed from porosity ϕ using the empirical relationship:

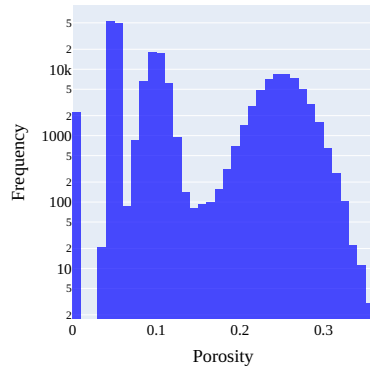
$$\log_{10}(k) = (-3.523 \cdot 10^{-7}) \cdot \phi^5 + 4.278 \cdot 10^{-5} \cdot \phi^4 - 1.723 \cdot 10^{-3} \cdot \phi^3 + 1.896 \cdot 10^{-2} \cdot \phi^2 + 0.333 \cdot \phi - 3.222 \quad (3.1)$$

where k is permeability in mD and ϕ is porosity in percent.

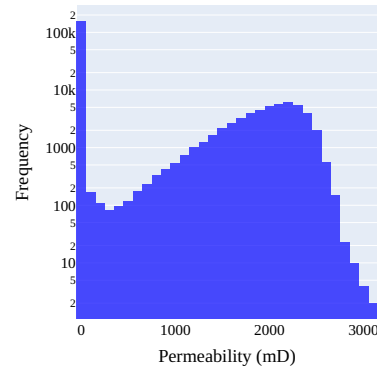
Figure 3.3 shows the permeability distributions for three different geological realizations, highlighting the fluvial channel structures within the enhanced model. The permeability visualization uses partial transparency for the top five layers to reveal vertical distribution patterns, while the histograms show porosity and permeability statistics for the first realization (other realizations exhibit similar characteristics).



(a) 3D visualization of permeability (\log_{10} scale) for three different realizations of the enhanced model. The top five layers are shown with partial transparency to reveal the heterogeneous channel structures throughout the reservoir layers.



(b) Histogram of Porosity for the first realization of the enhanced model.



(c) Histogram of Permeability for the first realization of the enhanced model.

Figure 3.3: Spatial distributions and histograms of porosity and permeability in the enhanced CPG grid model.

Figure 3.4 illustrates the structural characteristics of the enhanced reservoir model, showing both the spatial context and vertical structure of the reservoir. The plan view (Figure 3.4a) displays the cross-section location overlaid on the depth field, while the north-south cross-section (Figure 3.4b) demonstrates the variable reservoir thickness and depth distribution across the domain. The thickness map (Figure 3.4c) provides a detailed visualization of how reservoir thickness varies spatially across the entire model domain. It is clear from this map that the reservoir is thicker in the northern sections.

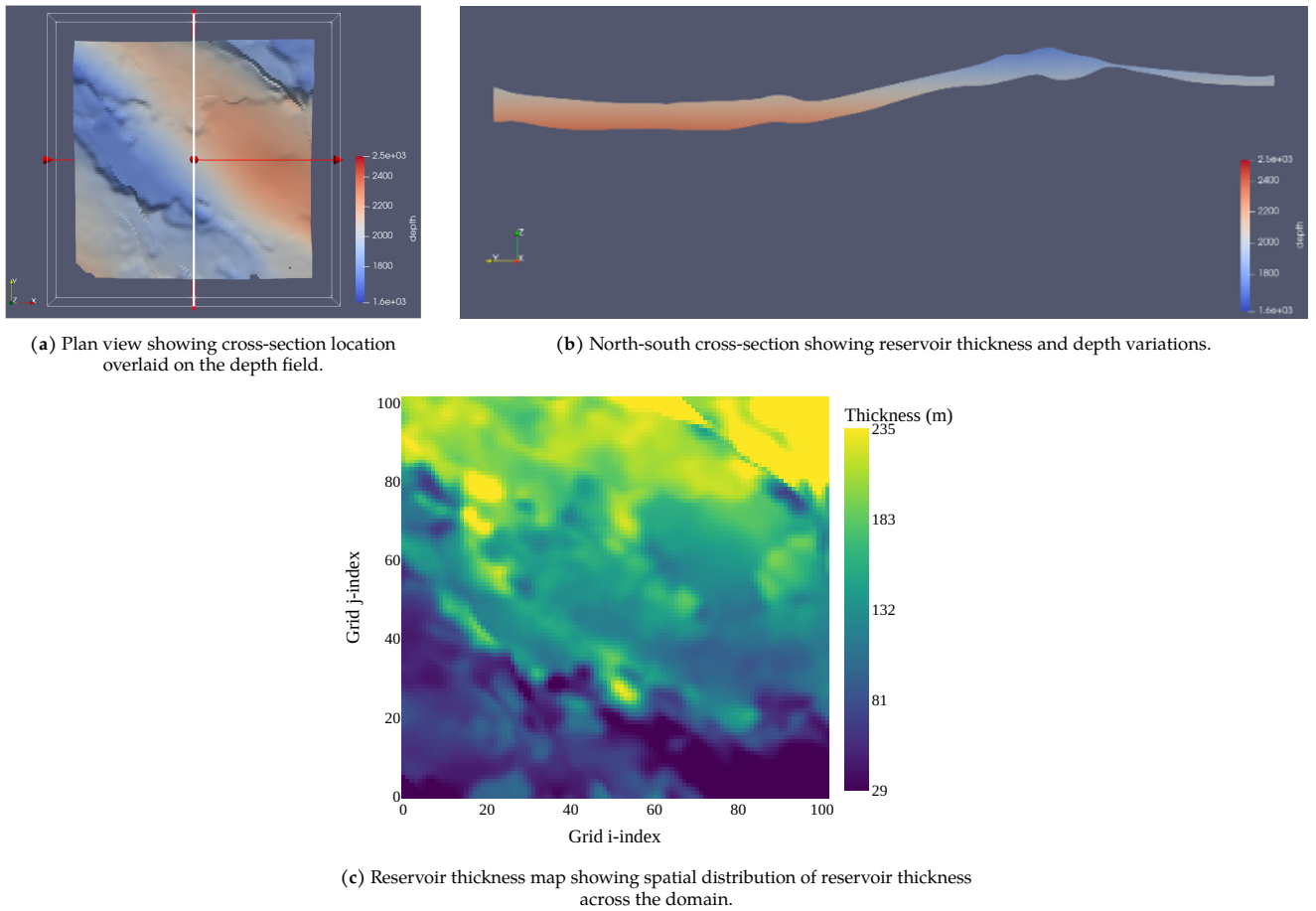


Figure 3.4: Structural characterization of the enhanced reservoir model: (a) plan view indicating the location of cross-section through the center of the domain, (b) the corresponding north-south cross-section illustrating increasing reservoir thickness and depth toward the northern sections, and (c) a reservoir thickness map showing the spatial distribution of reservoir thickness across the domain.

Initial and Boundary Conditions

Non-uniform initial conditions are applied to better represent in-situ reservoir conditions:

Parameter	Value / Description
Pressure gradient	100 bar/km (hydrostatic)
Temperature gradient	30 K/km (geothermal)
Lateral boundaries	10^{18} m^3 (infinite-acting aquifer)
Vertical boundaries	Heat exchange with overburden and underburden

Table 3.4: Enhanced model: Initial and boundary conditions

3.2.3. Well Implementation

Well Configuration

The framework supports flexible configuration of injection and production wells:

- Well locations are specified as (i, j) coordinates within the grid
- Wells are perforated vertically across all reservoir layers, excluding confining layers
- Well radius is set to 0.16m for all wells

Well Operation Controls

Two primary well control modes are implemented:

- Rate control: Wells operate at a specified flow rate (m^3/day) with Bottom Hole Pressure (BHP) constraints
- BHP control: Wells operate at a specified BHP (bar)

For injection wells operating under rate control, a maximum BHP constraint is applied based on the Staatstoezicht op de Mijnen (Dutch State Supervision of Mines) (SodM) regulations (SodM, 2024), calculated as:

$$BHP_{max} = P_{reservoir} + 0.0135 \cdot TVD_{reservoir} \cdot 10 \quad (3.2)$$

where BHP_{max} is the maximum allowed BHP in bar, $TVD_{reservoir}$ is the True Vertical Depth (TVD) in meters at the top of the reservoir at the well location, and 0.0135 MPa/m is the SodM pressure gradient limit, and 10 is the conversion factor from MPa to bar.

For production wells, a minimum BHP constraint is implemented to prevent excessively low pressures:

$$BHP_{min} = 0.7 \cdot BHP_{hydrostatic} \quad (3.3)$$

where $BHP_{hydrostatic}$ is the initial hydrostatic pressure at the well head depth.

3.2.4. Rate Operating Range Determination

A key feature of the framework is the ability to determine sustainable flow rates that respect BHP constraints:

- Individual capacity assessment through a single BHP-controlled pre-simulation
- Injectors operated at SodM limits and producers at minimum BHP simultaneously
- Measurement of resulting flow rates to determine individual well capacities
- Application of safety factor of 0.65 to account for rate stabilization uncertainty

The safety factor of 0.65 compensates for the limited one-year duration of the BHP pre-simulation, during which flow rates have not reached steady-state equilibrium. This safety factor of 0.65 was selected based on preliminary testing to ensure water balance constraints ($<2\%$ imbalance) are maintained when rates are applied to full-duration simulations, preventing overestimation of sustainable well capacity.

3.2.5. Simulation Procedure

The simulation follows these steps:

1. Initialize the reservoir with pressure and temperature gradients
2. Configure injection and production wells at specified locations
3. Apply operational constraints (flow rates and BHP limits)
4. Run time-stepping simulation for the specified duration (typically 100 years)
5. Monitor flow-weighted production temperature at each timestep; when thermal breakthrough is detected (flow-weighted production temperature drops below threshold), continue for 5 additional timesteps and terminate simulation
6. Extract system lifetime as the time when thermal breakthrough occurred, or assign maximum simulation time if no breakthrough detected
7. Verify injection-production fluid balance by comparing total injected and produced volumes

3.2.6. System Lifetime Determination

System lifetime is defined as the time until thermal breakthrough occurs, based on a flow-weighted production temperature:

$$T_{weighted} = \frac{\sum_{i=1}^n Q_i \cdot T_i}{\sum_{i=1}^n Q_i} \quad (3.4)$$

where T_i is the production temperature at producer i , and Q_i is the production flow rate at producer i .

Thermal breakthrough is detected when:

$$T_{weighted} \leq T_{initial} - \alpha \cdot (T_{initial} - T_{injection}) \quad (3.5)$$

where $T_{initial}$ is the initial flow-weighted production temperature at year 1 of the simulation, $T_{injection}$ is the injection temperature, $T_{weighted}$ is the flow-weighted production temperature at the current timestep, and α is the temperature threshold fraction (typically 0.15 or 15%).

System lifetime is calculated as the time until thermal breakthrough occurs. If thermal breakthrough is not reached within the simulation duration, the system lifetime is set to the maximum simulation time (e.g., 100 years).

3.2.7. Economic Analysis

The economic evaluation of geothermal systems is performed using GTEcon (Akin, 2025), an open-source economic analysis module developed within the PUSH-IT project (Scholten et al., 2023) that calculates financial performance metrics of each simulated geothermal system.

Power Calculations

The economic analysis relies on accurate determination of thermal power production and electrical power consumption, which form the basis for revenue and operational cost calculations.

Heat Power Calculation: Thermal power is computed using the IAPWS97 industrial formulation for water and steam properties (Wagner & Kretzschmar, 2008). For each well, the heat power is calculated as:

$$P_{heat} = \dot{Q} \cdot \rho(T, P) \cdot h(T, P) \quad (3.6)$$

where \dot{Q} is the volumetric flow rate (m^3/s), $\rho(T, P)$ is the water density (kg/m^3), and $h(T, P)$ is the specific enthalpy (kJ/kg), both evaluated at the well temperature T and pressure P using IAPWS97 correlations. The calculation yields power in MW, with positive flow rates corresponding to heat injection (injection wells) and negative flow rates corresponding to heat production (production wells). The total system heat production is determined by summing contributions from all wells.

Pumping Power Calculation: Electrical power consumption for pumping operations accounts for pressure differentials between reservoir conditions and surface requirements:

$$P_{pump} = \frac{|\Delta p| \cdot |\dot{Q}|}{\eta_{pump}} \quad (3.7)$$

where Δp is the absolute pressure differential (MPa), \dot{Q} is the volumetric flow rate (m^3/s), and η_{pump} is the pump efficiency. The pressure differential is calculated as the absolute difference between reservoir pressure and the required pressure, which includes the hydrostatic head (based on well depth) and surface pipeline pressure requirements.

Well Drilling Cost

A key contribution is the implementation of depth-based drilling cost calculations in the economic analysis framework. The model uses the formula from TNO (n.d.) to accurately account for the nonlinear relationship between well depth and drilling costs:

$$Cost_{drilling} = 375,000 + 1,150 \cdot depth + 0.3 \cdot depth^2 \quad (3.8)$$

where depth is the reservoir depth in meters. The implementation dynamically extracts well depths from the reservoir model and calculates appropriate drilling costs for each configuration being evaluated.

Cash Flow Model

The economic model implements a simplified cash flow structure focusing on the core trade-off between capital investment and operational pumping costs:

$$CF_t = -CapEx_t - OpEx_{pump,t} + Revenue_t \quad (3.9)$$

where:

- CapEx_t includes initial drilling costs, equipment purchases, and periodic pump replacements
- $\text{OpEx}_{\text{pump},t} = P_{\text{pump}} \cdot \text{Hours} \cdot \text{Electricity Price}$ represents pumping electricity costs
- $\text{Revenue}_t = P_{\text{heat}} \cdot \text{Hours} \cdot \text{Heat Price}$ from thermal energy sales

NPV Calculation

NPV is calculated by discounting future cash flows to present value:

$$\text{NPV} = \sum_{t=0}^T \frac{\text{CF}_t}{(1+r)^t} \quad (3.10)$$

where CF_t is the cash flow at time t , r is the discount rate, and T is the project lifetime.

Economic Input Parameters

The economic evaluation incorporates several key parameters that influence NPV calculations. Table 3.5 details the capital cost components, while Table 3.6 presents the financial parameters.

Component	Unit Cost (€)	Quantity	Replacement Interval (years)
VSD	150,000	1	0
Christmas tree	12,500	1	0
Degasser	500,000	1	0
Filter (candle + bag)	2,250	1	0
Heat exchanger	1,000,000	1	0
CHP	800,000	1	0
Pump	350,000	1	1
Drilling	Depth-based formula	1	0

Table 3.5: Capital cost components for the geothermal system. Components with a replacement interval of 0 are installed only once at the beginning of the project. Drilling costs are dynamically calculated based on well depths using the formula from Section 3.2.7.

Parameter	Value
Annual discount rate	7%
Heat price	40 €/MWh
Electricity price	125 €/MWh
Pump efficiency	65%

Table 3.6: Economic parameters used in NPV calculations

These parameters were selected based on typical values for geothermal projects in the Netherlands and represent the baseline economic scenario.

Economic calculations account for the full project lifetime, with the evaluation period dynamically determined as either the time of thermal breakthrough or the maximum simulation duration (100 years), whichever occurs first. This approach ensures that NPV calculations realistically reflect system performance by truncating economic analysis when production temperatures drop below effective thresholds.

3.3. Optimization with NSGA-II

The optimization framework employs NSGA-II to handle the multi-objective nature of the problem.

3.3.1. Problem Formulation

Decision Variables

The optimization problem includes the following decision variables:

- Injection well locations: (i_a, j_a) for each injector a
- Production well locations: (i_b, j_b) for each producer b
- Flow rates (conditional): Q_a for each injector a when using preserve mode

The variables are encoded as integers for grid coordinates and discrete flow rate values. The problem dimensionality depends on the rate optimization mode:

- **Preserve mode:** $2(n_{inj} + n_{prod}) + n_{inj}$ variables, where:
 - $2(n_{inj} + n_{prod})$ represents spatial location variables (2 grid coordinates per well)
 - n_{inj} represents flow rate variables (1 rate per injection well)
- **Maximize mode:** $2(n_{inj} + n_{prod})$ location variables only (rates determined through constraint-aware presimulation)

The problem dimensionality scales with the number of wells, with a total of $2(n_{inj} + n_{prod})$ location variables, and an additional n_{inj} rate variables when rate optimization is in preserve mode.

Objective Functions

Two competing objectives are simultaneously optimized:

$$\max f_1(x) = NPV(x) \quad (3.11)$$

$$\max f_2(x) = Lifetime(x) \quad (3.12)$$

where x represents the decision vector containing well locations and flow rates (if applicable).

As described in Section 3.2, the objective functions are evaluated through reservoir simulations, which provide the necessary data for calculating NPV and system lifetime.

Constraints

The optimization problem includes several constraints:

- Minimum well distance: $d(w_{inj}, w_{prod}) \geq d_{min}$ for any injector-producer pair
- Boundary distance: $d(w_i, \text{boundary}) \geq d_{boundary}$ for any well w_i ; note that different minimum distances can be applied for injectors and producers.
- Valid location: Wells must be placed in active cells in the enhanced model
- BHP constraints: Well pressures must respect SodM limits
- Flow rate bounds: $Q_{min} \leq Q \leq Q_{max}$ for all flow rates

The implementation enforces constraints hierarchically, with well distance constraints evaluated first to avoid running simulations for infeasible configurations. BHP constraints are handled through pressure-controlled pre-simulations to determine maximum allowable rates.

Rate Optimization Strategy

The framework implements two distinct rate optimization modes:

1. **Preserve Mode:** Flow rates are explicit decision variables within bounds $[Q_{min}, Q_{max}]$, but these optimizer-controlled rates are adjusted through configuration-aware presimulation to ensure feasibility and well interference effects are accounted for.
2. **Maximize Mode:** Flow rates are determined entirely through constraint-aware presimulation that runs BHP-controlled simulations to find maximum sustainable rates respecting SodM pressure limits and well interference effects.

Both modes use configuration-aware presimulation to account for well interference effects, with results cached to avoid redundant calculations. Producer rates in both modes use capacity-based distribution, where individual well capacities are determined via BHP-controlled presimulations and rates are distributed proportionally to maintain exact water balance.

Experimental Implementation: This study primarily employed maximize mode due to reduced search space dimensionality compared to preserve mode and automatic constraint satisfaction.

3.3.2. Optimization Approach

Custom Operators

Several custom genetic operators were implemented to handle the specific characteristics of geothermal optimization:

Constraint-Aware Sampling Process This operator ensures the initial population contains only feasible well locations by:

- Enforcing boundary distance constraints
- In the enhanced model, ensuring wells are only placed in active cells
- Creating exclusion zones around injectors when placing producers
- Supporting initial guess inclusion and checkpoint resumption: the framework can initialize the population from a previous optimization run's final generation, enabling convergence assessment and extended optimization without restarting from random solutions

The process is illustrated in Figure 3.5, which demonstrates the steps involved in generating a constraint-aware initial population.

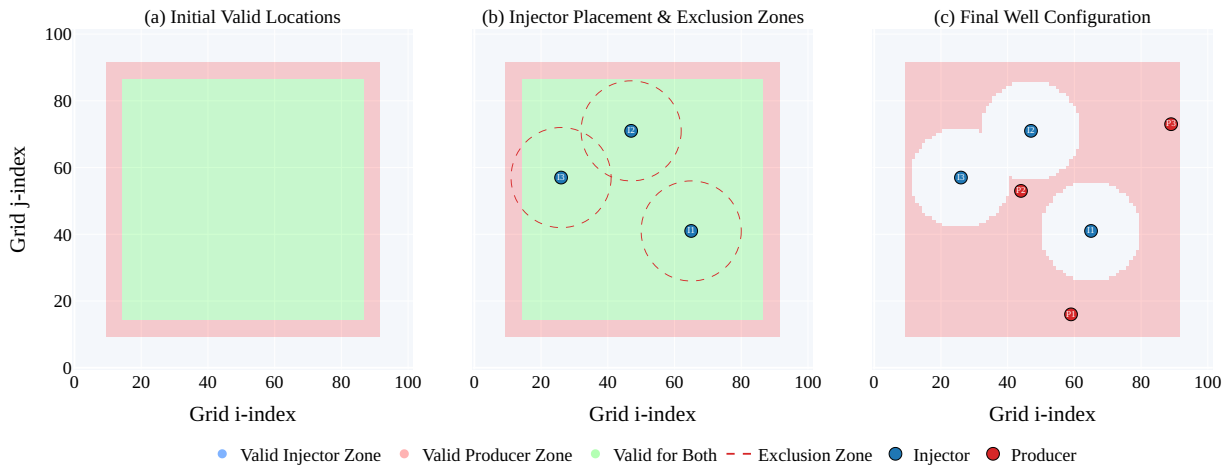


Figure 3.5: Constraint-aware sampling process for initial population generation.

Repair Process This repair operator replaces infeasible solutions with feasible alternatives that are then evaluated by the algorithm. This creates a feedback loop that guides the evolutionary search toward naturally feasible regions while maintaining the optimization intent. The operator maintains solution feasibility through:

- Projecting invalid well locations to the nearest valid position using combined constraint masks
- Enforcing well ordering to eliminate permutation symmetry (injectors sorted by i-coordinate, producers by j-coordinate)
- **Rate Adjustment:**
 - Executes configuration-aware presimulations to determine optimal rates for each well placement
 - Operates injectors at SodM pressure limits and producers at minimum BHP constraints
 - Applies capacity-based rate distribution ensuring exact water balance
 - Implements shared caching system to avoid redundant presimulations for identical configurations
 - Supports both 'preserve' and 'maximize' rate modes

NSGA-II Configuration

The NSGA-II algorithm is configured with the following parameters:

- Population size and maximum generations: scaled based on the number of wells
- Offspring size: $N_{offspring} = N_{pop}/2$
- Crossover probability: $p_c = 0.9$ with distribution index $\eta_c = 10$
- Mutation probability: $p_m = 1/n_{var}$, where n_{var} is the number of decision variables; mutation distribution index: $\eta_m = 10$
- Termination: occurs upon reaching the maximum number of generations. Preliminary experiments with function tolerance-based convergence criteria ($ftol = 0.001$) resulted in premature termination due to the varying scales and normalization of objectives, therefore all subsequent optimization runs rely solely on generation limits.

The distribution index η_c controls the spread of offspring around the parents—lower values produce offspring farther from parents (more exploratory), while higher values keep offspring closer to parents (more exploitative). Similarly, the mutation distribution index η_m controls the mutation strength—lower values produce larger perturbations, while higher values result in smaller, localized changes. The mutation probability follows standard practice (Deb et al., 2002) of $1/n_{var}$ to ensure that, on average, one variable per solution undergoes mutation. The specific values $\eta_c = 10$ and $\eta_m = 10$ represent a balanced approach between exploration and exploitation, commonly used in engineering optimization problems.

Objective Normalization

To ensure a balanced contribution of both objectives—NPV and system lifetime—in the optimization process, normalization is applied. This step is essential because the two objectives operate on different scales: NPV typically ranges in millions to billions of euros, while lifetime is measured in years.

The normalization uses the following formulation:

$$f'_i(x) = \frac{f_i(x) - \text{nadir}_i}{\text{ideal}_i - \text{nadir}_i} \quad (3.13)$$

where $f_i(x)$ is the raw value of the i -th objective, and ideal_i and nadir_i represent the best and worst values respectively.

The ideal and nadir points are predetermined based on conservative estimates and preliminary optimization studies. For NPV, the nadir point is set to 0€ as a conservative worst-case bound (representing scenarios with no economic viability), while the ideal point is estimated based on maximum NPV values observed in previous runs with similar well configurations, typically with some overestimation to ensure adequate range coverage. For lifetime, the nadir is set to 1 year as a conservative minimum, and the ideal corresponds to the simulation time horizon (100 years).

Parallelization

To handle the computational demands of reservoir simulation, the optimization framework implements parallel evaluation of individuals:

- Multiprocessing with a process pool for simulation runs
- Shared memory for efficient data exchange between processes
- Thread-safe rate caching to avoid redundant pre-simulations

3.3.3. Optimization Loop

The optimization process follows a structured loop, iterating through the following steps until termination criteria are met:

1. **Initial Population Generation:** Create candidate solutions with valid well locations using the custom constraint-aware sampling operator.
2. **Solution Repair:** Apply the custom repair operator to ensure solutions meet spatial constraints and determine optimal flow rates for each well configuration.

3. **Full Simulation Evaluation:** Evaluate the repaired solutions using complete DARTS reservoir simulations to calculate NPV and system lifetime.
4. **Selection and Genetic Operations:** Apply NSGA-II's selection, crossover, and mutation operations to generate the next population.
5. **Repair of New Solutions:** Apply the repair operator again to the new population.
6. **Evaluation of New Solutions:** Run full simulations for the repaired solutions.
7. **Repeat:** Continue steps 4-6 until convergence criteria are met.

3.4. Experimental Setup

This section describes the comprehensive experimental campaign designed to evaluate the proposed optimization framework. The experiments systematically test optimization performance across different model complexities and assess result reliability through multiple independent runs with varying random seeds.

3.4.1. Standard Model Experiments

The standard reservoir model experiments established baseline optimization performance and algorithm validation. Each configuration was executed with nine independent optimization runs using different random seeds (42, 12, 13, 14, 15, 16, 17, 18, 19) to ensure statistical reliability and assess algorithm stability.

Configuration:

- Well configuration: 2 injection wells, 2 production wells
- Minimum well distance: 10 grid cells (300 m)
- Boundary distances: 15 grid cells (450 m) for injectors, 10 grid cells (300 m) for producers
- Population size: 30 individuals, maximum generations: 60
- NPV normalization: €300M ideal point, €0 nadir point
- Lifetime normalization: 100 years ideal point, 1 year nadir point

3.4.2. Enhanced Model Experiments

The enhanced model experiments utilized the higher-resolution geological model to evaluate optimization performance under realistic subsurface conditions and assess framework scalability across different well configurations.

10-Doublet Configuration (seed 42):

- Well configuration: 10 injection wells, 10 production wells
- Minimum well distance: 10 grid cells (550 m)
- Boundary distances: 15 grid cells (825 m) for both injectors and producers
- Population size: 80, maximum generations: 80
- NPV normalization: €1.25B ideal point, €0 nadir point
- Lifetime normalization: 100 years ideal point, 1 year nadir point

12-Doublet Configuration (seeds 0, 1, 2, 3):

- Well configuration: 12 injection wells, 12 production wells
- Minimum well distance: 10 grid cells (550 m)
- Boundary distances: 15 grid cells (825 m) for both injectors and producers
- Population size: 96, maximum generations: 80
- NPV normalization: €1.4B ideal point, €0 nadir point
- Lifetime normalization: 100 years ideal point, 1 year nadir point

20-Doublet Configuration (seeds 42, 0, 1, 2, 3):

- Well configuration: 20 injection wells, 20 production wells
- Minimum well distance: 10 grid cells (550 m)
- Boundary distances: 15 grid cells (825 m) for both injectors and producers
- Population size: 160, maximum generations: 150
- NPV normalization: €1.8B ideal point, €0 nadir point
- Lifetime normalization: 100 years ideal point, 1 year nadir point

All enhanced model experiments employed 20 parallel processes and used geological realization 1.

3.4.3. Sensitivity and Robustness Analysis

Additional experiments were conducted to assess parameter sensitivity and geological uncertainty:

Temperature Threshold Sensitivity: The 20-doublet configuration (seed 0) was re-executed with a reduced temperature threshold of 5% to evaluate the impact of stricter lifetime criteria on optimization outcomes.

Geological Realization Analysis: To assess robustness across geological uncertainty, the 20-doublet configuration (seed 0) was executed using alternative geological realizations (realization 2 and realization 3), complementing the base experiments conducted with realization 1.

3.5. Post-Processing and Analysis

Optimization results underwent comprehensive post-processing to extract insights and evaluate framework performance through several analytical approaches.

Feasibility Assessment: Solutions were classified as feasible based on water balance maintenance (zero imbalance) and BHP constraint compliance. Pareto-optimal solutions were identified using dominance-based filtering to find non-dominated points maximizing both NPV and system lifetime.

Key Solution Identification: From the Pareto front, three representative solutions were identified: (1) the *Best NPV solution* with the highest economic performance, (2) the *Best Lifetime solution* with the maximum system longevity, and (3) the *Best Overall solution* determined by normalizing both objectives to $[0, 1]$ scales and selecting the solution with the highest combined score, representing an optimal compromise between competing objectives.

Convergence Analysis: Algorithm performance was tracked through cumulative maximum objective values across generations. Multi-run experiments employed colormap visualization grouped by doublet count to assess consistency and optimization trends.

Solution Visualization: Scatter plots displayed all solutions colored by generation or injection rate, with Pareto fronts and best solutions highlighted to reveal trade-off characteristics and optimization space coverage.

Spatial Analysis: Well placement patterns were analyzed using \log_{10} -scaled frequency heatmaps across the reservoir grid. Key solutions were visualized with well configurations overlaid on permeability fields, using flow rate-proportional marker sizing.

3.6. Technical Implementation Details

The optimization and simulation workflow was implemented in Python. NSGA-II was executed using the pymoo library, version 0.6.1.3, and geothermal reservoir simulations were carried out using DARTS, version 1.2.1.

To track optimization progress, log hyperparameters, and monitor system performance across runs, the Weights & Biases platform was integrated into the workflow. This enabled real-time visualization of convergence behavior, population evolution, and constraint satisfaction.

Data visualization was performed using both matplotlib and plotly, with the latter used for interactive exploration of Pareto fronts and well configurations. Paraview was used for advanced 3D visualization of reservoir models and simulation results. Pre- and post-processing relied on standard Python libraries including NumPy and Pandas.

Development and testing were conducted on a Dell Precision Tower 5810 running Ubuntu 22.04.4 LTS, equipped with an Intel Xeon E5-1620 v3 CPU (8 threads), 32 GB of RAM, and an NVIDIA Quadro K620 GPU. Large-scale optimization and simulation runs were executed on the DelftBlue supercomputer at TU Delft to handle the computational intensity of running multiple NSGA-II generations with full reservoir simulations. These runs primarily utilized compute-p2 nodes, each equipped with 2× Intel Xeon E5-6448Y CPUs (64 cores per node) and 250 GB RAM. Job scheduling and resource allocation were managed through the SLURM workload manager.

This setup provided the necessary computational efficiency and scalability to explore the optimization space and support detailed analysis of results.

4

Results

This chapter presents the results from applying the MOO framework to geothermal well placement in the WNB. First, the framework is validated using a simplified standard model to demonstrate convergence and constraint satisfaction. The main findings are then presented using the enhanced WNB model, revealing optimal trade-offs between economic returns and system longevity.

The results directly address how MOO can balance short-term economic objectives with long-term sustainability goals in geothermal development.

4.1. Framework Validation and Performance using Standard Model

To validate the proposed MOO framework, we applied it to the standard model described in 3.2.1. This section presents results across geothermal simulation, economic performance, and optimization behavior, illustrating the framework's capability to ensure feasible, convergent solutions while balancing competing objectives.

4.1.1. Simulation Results

Here we present the simulation results of a representative run using the standard model with maximize rate mode.

Figure 4.1 illustrates the temperature profiles of production wells over time, showing individual well temperatures, the flow-weighted average temperature, breakthrough threshold, and system lifetime. The system lifetime is defined as the time until the flow-weighted average temperature drops below the breakthrough threshold, indicating a significant loss in thermal energy production. The gradual temperature decline and eventual breakthrough at 89 years demonstrates the finite nature of geothermal resources and validates the importance of lifetime optimization in system design.

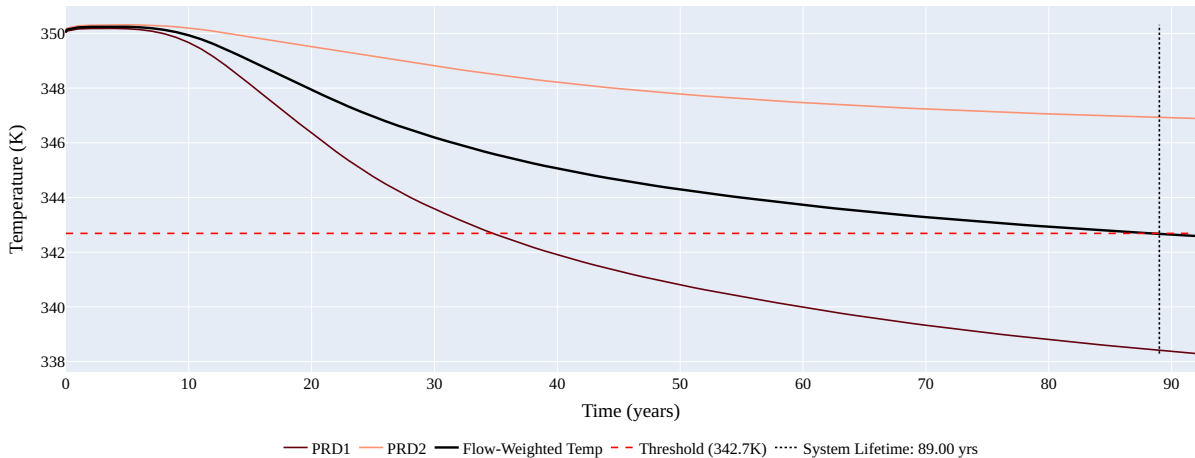


Figure 4.1: Production well temperature profiles over time. Flow-weighted average temperature, individual well temperatures, breakthrough threshold (dashed line), and system lifetime (dotted line) are shown.

Figure 4.2 shows the pressure and flow rate dynamics for both injection and production wells. The pressure

profiles remain within operational limits throughout the simulation, as shown by the pressure limits in the plot. The injection flow rates are lower than the maximum 15,000 m³/day because pre-simulation determined the maximum sustainable rates at these well locations based on pressure constraints. The equal production flow rates indicate that both production wells have sufficient capacity to handle the maximum allowable flow rate under the given conditions, resulting in an even distribution of the total injection flow rate between the two production wells. While the wells may have different pressure-based capacities (as shown in the pressure profiles), both exceed the operational limit of 15,000 m³/day, so they are effectively capped at the same level. This balanced flow distribution, combined with stable pressure profiles, confirms that the constraint-aware optimization successfully identifies operationally feasible configurations that respect regulatory limits while maximizing sustainable extraction rates.

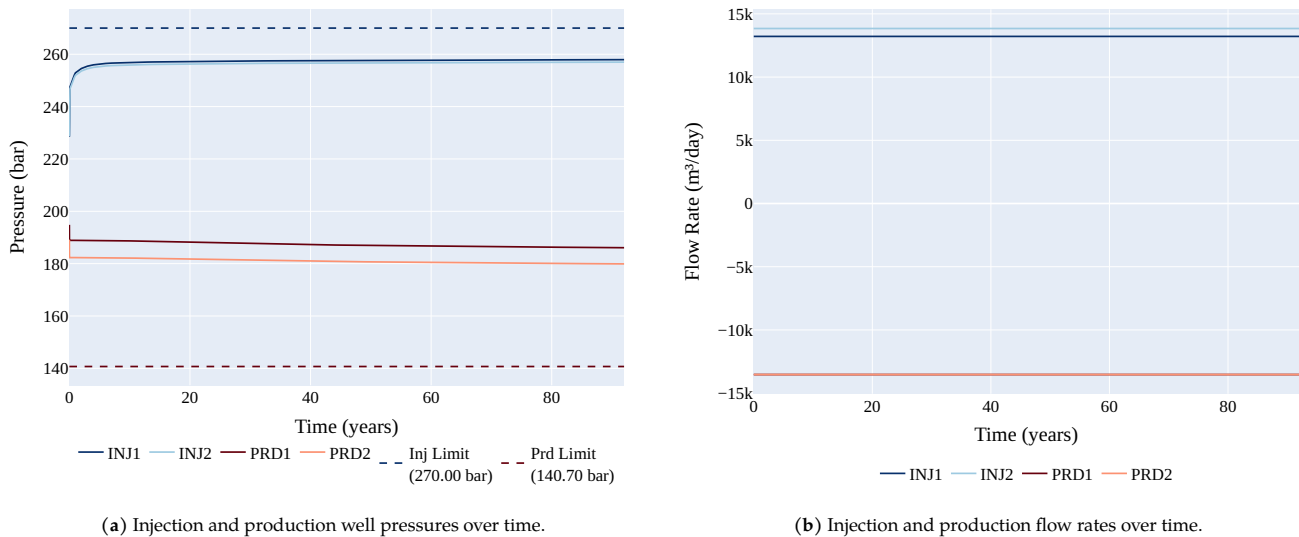
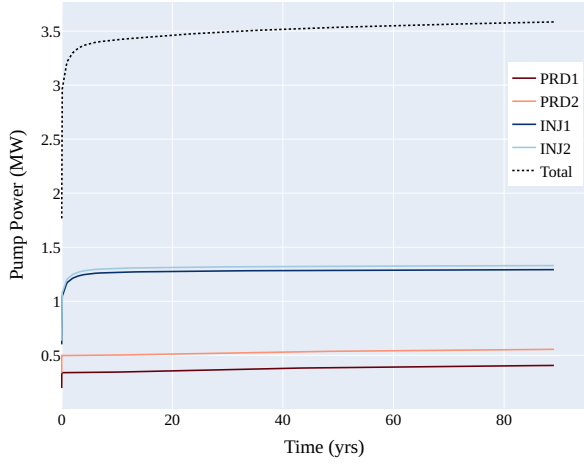


Figure 4.2: Pressure (a) and flow rate (b) dynamics for injection and production wells over time.

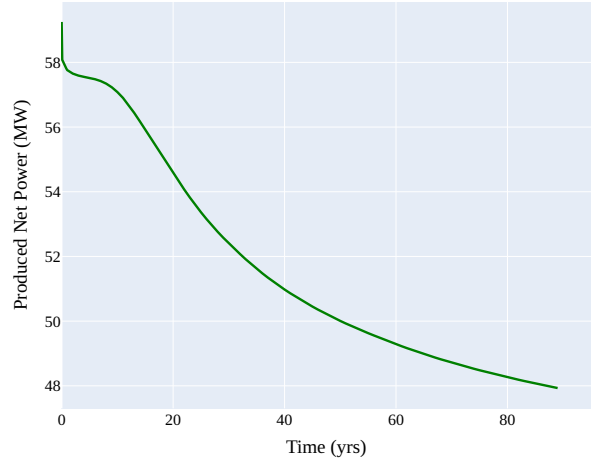
4.1.2. Economic Indicators

Figure 4.3 presents the key economic performance indicators that shows the financial viability of the geothermal system over its operational lifetime.

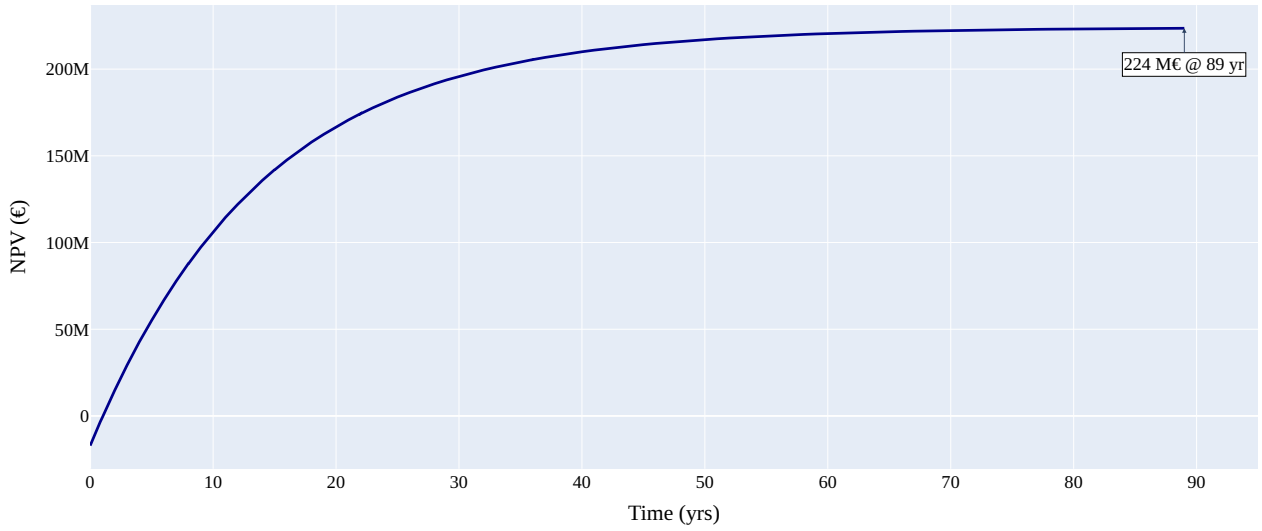
Figure 4.3a shows the evolution of pumping power consumption for both injection and production operations. The net power output, presented in Figure 4.3b, represents the useful energy available after accounting for pumping power consumption. The declining trend depicts both the temperature reduction shown in Figure 4.1 and the increasing power consumption. Figure 4.3c illustrates the cumulative NPV over the project lifetime, incorporating all capital expenditures, operational costs, and revenue streams. The NPV trajectory shows the point at which the project becomes profitable and the total financial return at the end of the operational period. The analysis accounts for the depth-based drilling costs and realistic operational expenses specific to the well configuration.



(a) Pumping power consumption for injection and production wells.



(b) Net power output.



(c) Net Present Value (NPV).

Figure 4.3: Performance and economic indicators for the geothermal system: (a) pump power consumption, (b) net power output and (c) Net Present Value.

4.1.3. Optimization Behavior for Standard Model

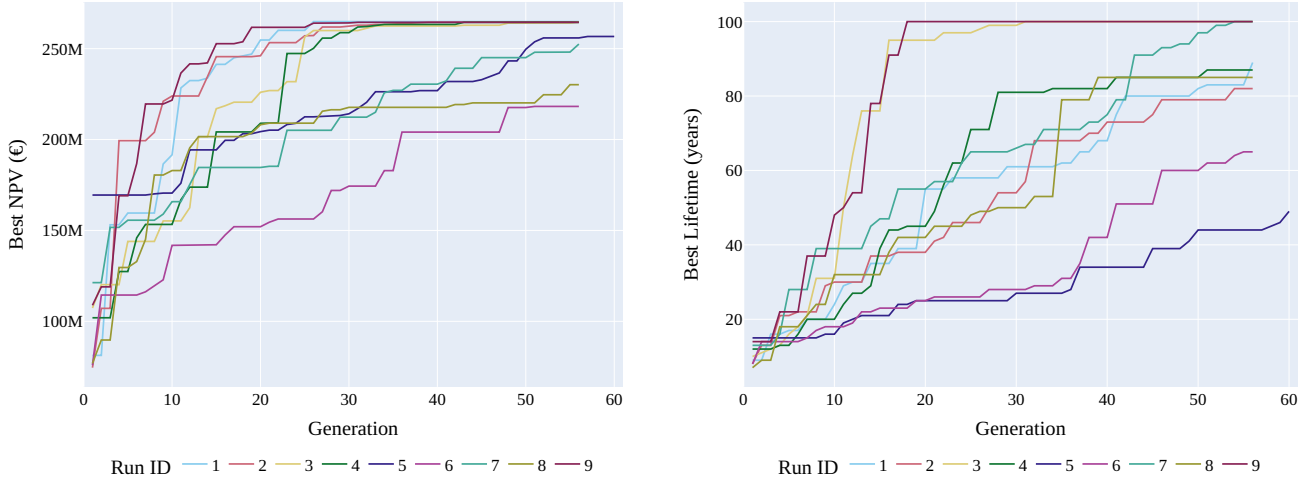
The optimization framework is applied to a 2-doublet well configuration. This well count was determined through preliminary optimization studies that evaluated different doublet configurations, with the 2-doublet configuration demonstrating superior performance for both NPV and system lifetime objectives under the given reservoir conditions and constraints.

To validate the robustness and convergence behavior of the MOO framework, we conducted nine independent optimization runs using different random seeds for the initialization. Figure 4.4 demonstrates the convergence characteristics of both objective functions across generations.

Figure 4.4a shows the evolution of the best NPV values across generations for all runs. In many runs, the algorithm identifies solutions with NPV values exceeding 200 M€, often converging within 20–30 generations. However, some runs exhibit slower convergence and achieve lower objective values, reflecting variability in algorithm performance across different initializations.

Similarly, Figure 4.4b illustrates the progression of the best system lifetime values. While several runs achieve lifetimes of 80–100 years, others show more gradual improvement. This variation highlights the stochastic

nature of NSGA-II but also demonstrates its capacity to consistently explore high-performing regions of the solution space. Overall, the results support the algorithm's robustness, albeit with some variability across runs.

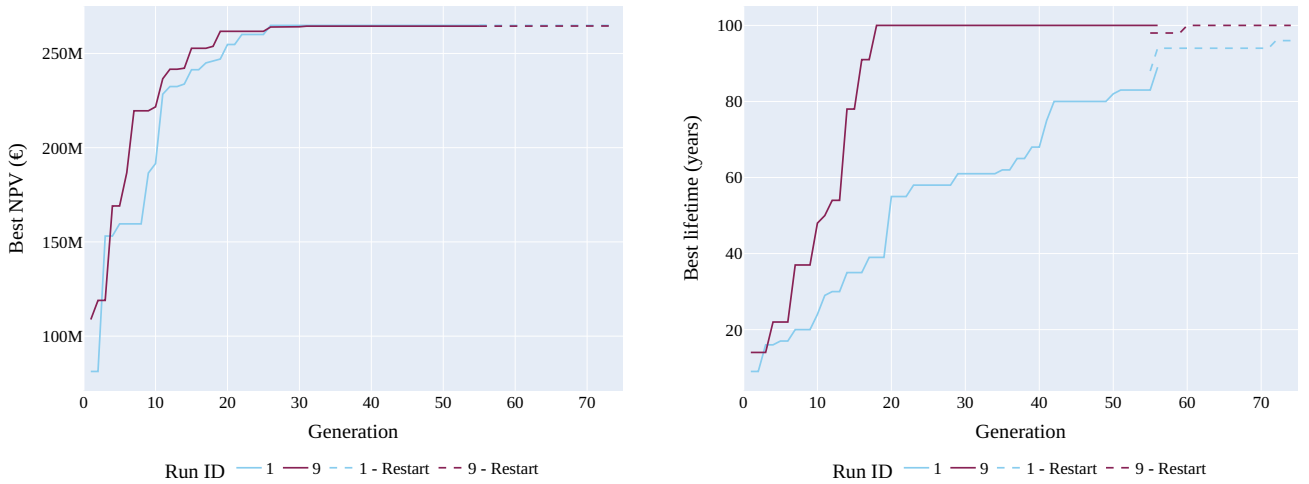


(a) Evolution of best NPV values across generations for nine independent optimization runs.

(b) Evolution of best system lifetime values across generations for nine independent optimization runs.

Figure 4.4: Convergence behavior of the MOO algorithm showing (a) NPV convergence and (b) system lifetime convergence across multiple independent runs.

To further validate convergence behavior, we conducted additional experiments by restarting two high-performing optimization runs (Run 1 and Run 9). For each case, the 55th generation population from the original run was used to initialize a continuation run for 20 additional generations. As shown in Figure 4.5, no improvement in NPV was observed during the continuation phase for both runs. For the system lifetime, there was no improvement in Run 9, given that it had already reached the maximum lifetime of 100 years. Run 1 did show a small increase in the lifetime of 7 years. These minimal improvements during continuation runs confirm that the original optimizations had indeed converged to stable solutions, validating the termination criteria and providing confidence in the final Pareto fronts.



(a) NPV evolution showing no improvement during continuation from generation 55 for both Run 1 and Run 9.

(b) System lifetime evolution confirming convergence plateau during continuation for both runs.

Figure 4.5: Convergence validation experiments demonstrating (a) NPV plateau and (b) system lifetime plateau when continuing optimization from the final populations of Run 1 and Run 9, confirming algorithm convergence.

Figure 4.6a presents the final Pareto fronts obtained from all nine independent runs, revealing the fundamental

trade-off between economic performance and system longevity. While higher NPV solutions can be achieved, they typically correspond to shorter system lifetimes, and conversely, configurations optimized for longevity may sacrifice some economic return, confirming the inherent tension between maximizing short-term economic returns and ensuring long-term resource sustainability.

Figure 4.6b visualizes the results of a comprehensive Pareto analysis across all nine runs, highlighting the Pareto-optimal frontier and key solution types. The color coding reveals how injection rates influence the objective trade-offs, with higher injection rates generally favoring NPV at the expense of system lifetime, indicating that aggressive operational strategies compromise reservoir longevity. Notable solution categories include the best NPV solution (emphasizing economic returns), the best lifetime solution (prioritizing longevity), and a compromise solution that balances both objectives.

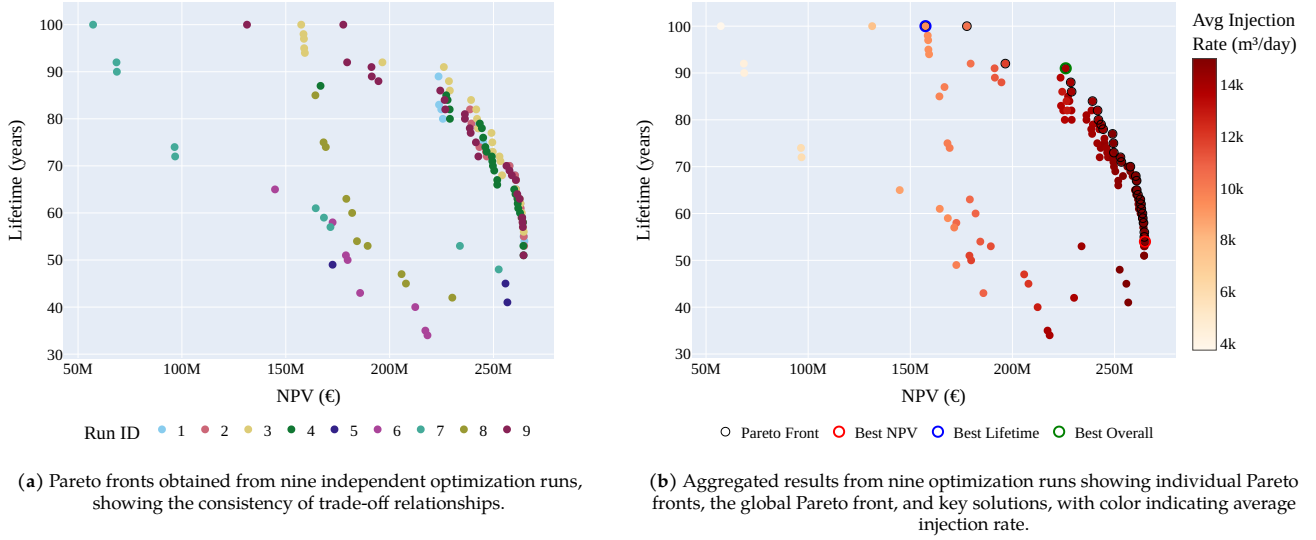


Figure 4.6: Visualization of Pareto front results from nine optimization runs: (a) illustrates the consistency of trade-off relationships across runs, and (b) presents the aggregated solution space with the final Pareto-optimal frontier, key solutions, and the influence of injection rate on objective trade-offs.

Figure 4.7 shows the spatial optimization patterns. Figure 4.7a shows the underlying heterogeneous permeability field, characterized by distinct high-permeability channels (shown in yellow) and lower-permeability background regions (shown in purple).

Figure 4.7b shows the frequency of injection and production locations of the overall Pareto front, revealing that the optimization consistently favors distinct zones: injectors are preferentially placed in the northeastern corner of the valid domain, while producers cluster in the southwest. This separation pattern suggests that optimal configurations maximize distance between injection and production wells while still positioning each in high-permeability regions that are geologically disconnected from each other. This spatial pattern reveals the fundamental physical trade-off: the optimization prioritizes high-permeability zones for good flow rates at each well, but deliberately avoids connected high-permeability pathways between wells to prevent premature thermal breakthrough, achieving an optimal balance between short-term productivity and long-term resource sustainability.

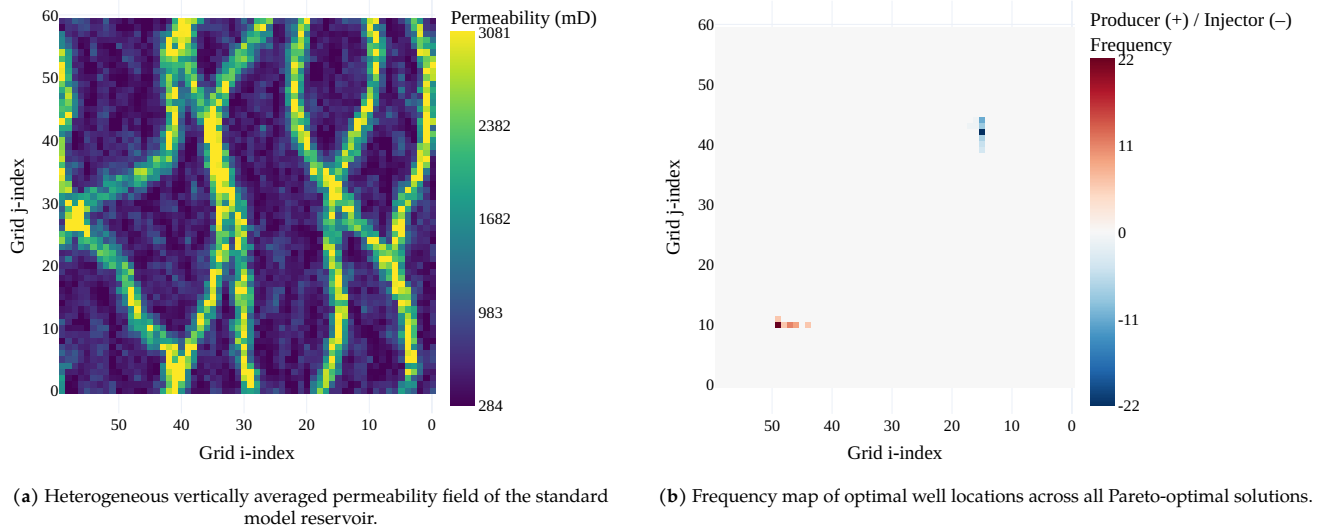


Figure 4.7: Spatial optimization analysis showing (a) the underlying geological constraints and (b) preferred well placement patterns identified by the optimization algorithm.

Table 4.1 presents a detailed comparison of three representative Pareto-optimal solutions, illustrating distinct operational strategies for balancing economic returns with system lifetime.

The solutions reveal three distinct strategies: an economically aggressive approach (*Best NPV*) employing symmetric maximum injection rates of 15,000 m³/day to achieve 264.9 M€ but limiting lifetime to 54 years; a resource preservation approach (*Best Lifetime*) using highly asymmetric injection rates (13,147 vs 5,525 m³/day) to extend operations to 100 years while generating 157.4 M€; and a balanced approach (*Best Overall*) capturing 85.4% of maximum NPV while achieving 91% of maximum lifetime through moderate injection asymmetry. This asymmetric strategy demonstrates that tailored flow allocation, rather than uniform distribution, is key to extending system lifetime.

All solutions exhibit boundary-constrained placement, with wells positioned at minimum allowable distances to the boundary (15 cells for injectors, 10 cells for producers). Perfect operational feasibility is confirmed through zero constraint violations and exact water balance maintenance across all solutions.

Performance Metric	Best NPV	Best Lifetime	Best Overall
<i>Objective Performance</i>			
NPV (M€)	264.9	157.4	226.1
System Lifetime (years)	54	100	91
<i>Well Configuration</i>			
Injector 1 Location	(15, 42)	(15, 44)	(15, 44)
Injector 2 Location	(15, 39)	(17, 43)	(15, 43)
Producer 1 Location	(47, 10)	(48, 10)	(48, 10)
Producer 2 Location	(44, 10)	(49, 10)	(49, 10)
Min. Injector-Producer Distance	41.0	45.3	46.7
<i>Operational Parameters</i>			
Injector 1 Rate (m ³ /day)	15,000	13,147	13,147
Injector 2 Rate (m ³ /day)	15,000	5,525	14,737
Producer 1 Rate (m ³ /day)	15,000	9,336	13,942
Producer 2 Rate (m ³ /day)	15,000	9,336	13,942
Total Injection (m ³ /day)	30,000	18,672	27,884
<i>Constraint Satisfaction</i>			
BHP Constraints Triggered	None	None	None
Water Balance Error (%)	0.00	0.00	0.00
Boundary Constraints Violated	0	0	0

Table 4.1: Comparison of representative Pareto-optimal solutions from standard model optimization

The results show that the MOO framework identifies spatially optimized well configurations that balance economic performance with system longevity under geological and engineering constraints, with consistent preferred well locations observed across multiple runs.

4.2. Enhanced Model Optimization Results

This section presents the optimization results obtained using the enhanced corner-point geometry model, which incorporates more detailed geological characteristics and active cell constraints compared to the standard model discussed previously. The enhanced model provides a more realistic representation of the WNB reservoir conditions, enabling more accurate evaluation of well placement and operational strategies. The results demonstrate the performance of the NSGA-II algorithm in identifying Pareto-optimal solutions that balance NPV maximization and system lifetime extension under the enhanced model's constraints. The following subsections analyze convergence behavior, Pareto front development, spatial optimization patterns, and sensitivity characteristics across multiple well configurations, providing comprehensive insights into optimal geothermal system configurations for practical implementation.

4.2.1. Single Configuration Analysis: 20 Doublet System

This subsection analyzes the optimization performance for a representative 20-injector, 20-producer configuration using the enhanced model, examining the Pareto front development, spatial well placement patterns, and solution feasibility characteristics to establish baseline performance metrics for subsequent multi-configuration comparisons.

Figure 4.8 demonstrates the multi-objective optimization performance for the 20-doublet configuration, showing both the trade-off relationship between NPV and system lifetime and the temporal evolution of the optimization process. The optimization process evaluated 8713 feasible solutions over 150 generations, with feasible solutions (those satisfying water balance constraints) colored by generation to illustrate algorithm improvement over time. The generational progression clearly shows that early generations (light orange, generations 1-50) predominantly produce solutions with poor performance in both objectives, clustering in the lower-left region with NPV values below 1.2 billion euros and lifetimes under 40 years. As the optimization progresses, later generations (darker orange/red, generations 50-150) successfully identify solutions across the full range of the

trade-off space, including high-NPV solutions approaching 1.6 billion euros and extended-lifetime solutions reaching 100 years.

The resulting Pareto front (black points) spans this full range, demonstrating that the algorithm effectively learns from poor initial solutions to discover a set of optimal trade-offs. Notably, the later generations exhibit dense clustering of solutions near the Pareto front, showing convergence behavior where the algorithm transitions from exploration and improvement to fine-tuning around optimal solutions. This temporal visualization illustrates the algorithm's learning capability and validates NSGA-II's effectiveness for geothermal optimization: the progression from poor-performing solutions in early generations to consistently identifying near-optimal solutions in later stages demonstrates that the algorithm can navigate the complex, multi-modal landscape of geothermal system design while maintaining solution diversity.

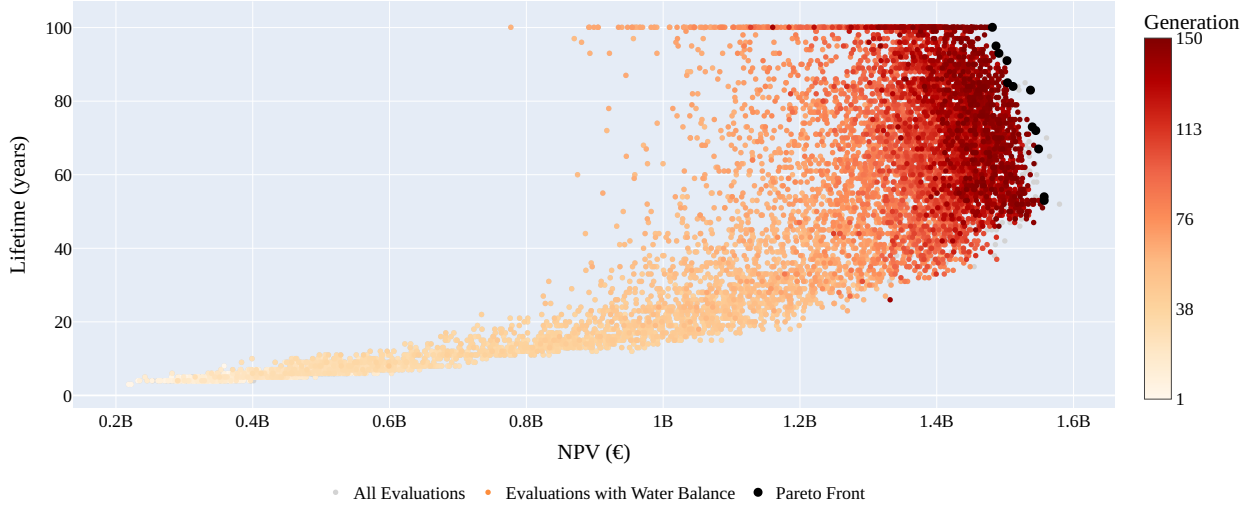
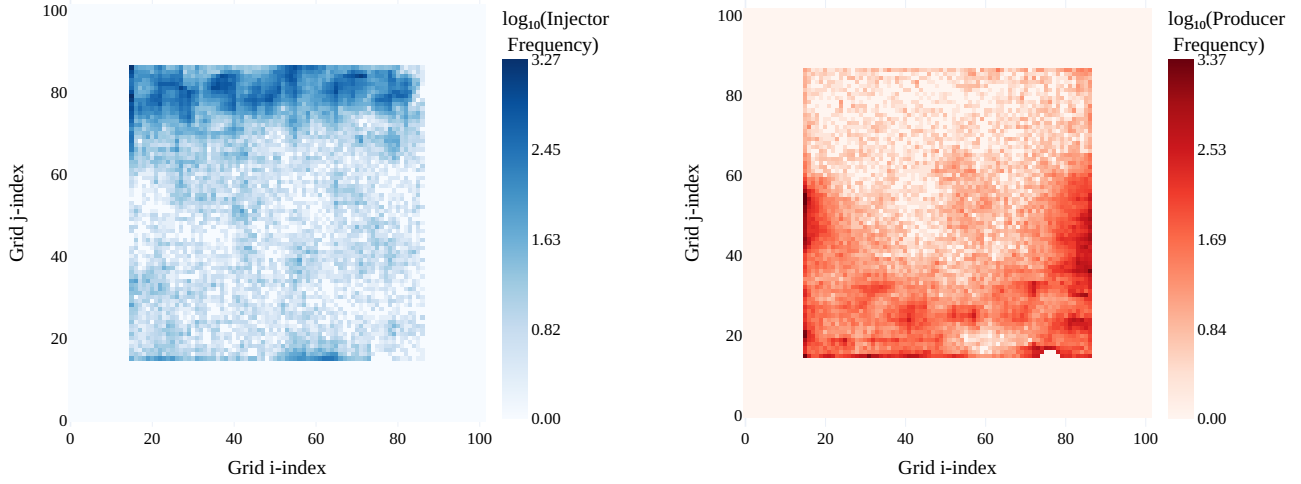


Figure 4.8: Pareto front analysis showing the trade-off between NPV and system lifetime for the 20-injector, 20-producer optimization run. Gray points represent all evaluations, colored points show feasible solutions meeting water balance constraints (colored by generation), and the black points indicate the final Pareto-optimal solutions.

The spatial well placement patterns across all evaluations throughout the optimization process are shown in Figure 4.9. The injector frequency heatmap (Figure 4.9a) shows concentrated placement preference along the northern boundary, with logarithmic frequency values reaching up to 3.27, indicating these locations were tested in over 1,800 evaluated solutions as the algorithm converged toward optimal configurations. The producer frequency distribution (Figure 4.9b) exhibits a U-shaped configuration along the southern, eastern, and western boundaries, with frequencies reaching up to 3.37, reflecting the algorithm's repeated exploration of these promising locations. The spatial separation between high-frequency injector and producer locations demonstrates the algorithm's learning behavior, increasingly focusing on configurations that maximize well spacing within the placement constraints. The logarithmic scaling indicates comprehensive exploration of the solution space, with even lower-activity areas evaluated multiple times throughout all generations.



(a) Injector placement frequency (\log_{10} scale) showing preferred locations for injection wells across all evaluated solutions. (b) Producer placement frequency (\log_{10} scale) showing preferred locations for production wells across all evaluated solutions.

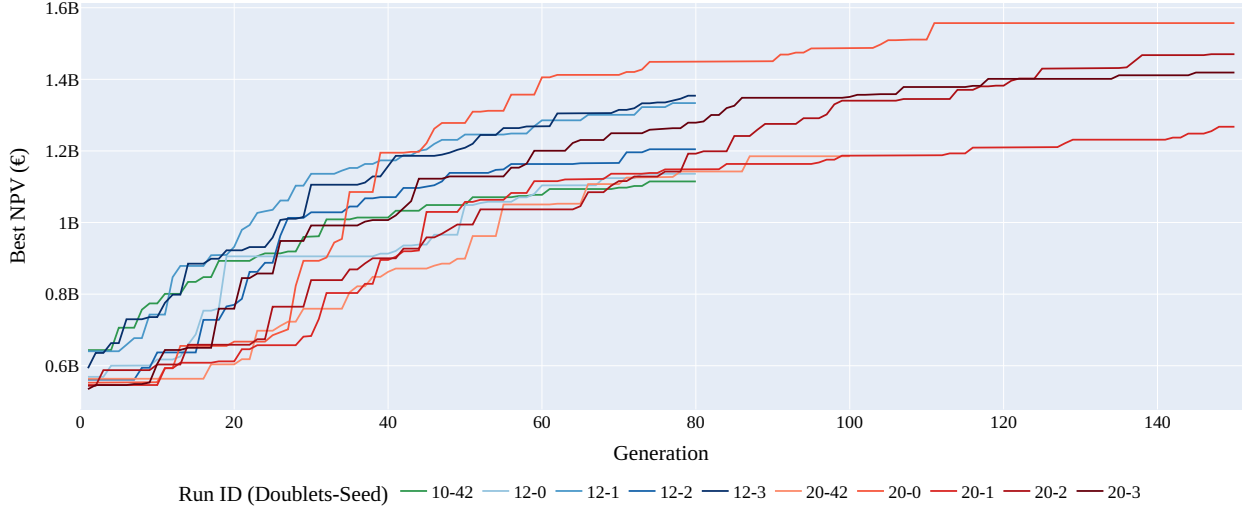
Figure 4.9: Well placement frequency heatmaps showing the spatial distribution of (a) injector and (b) producer locations across all optimization evaluations (\log_{10} scale).

4.2.2. Multi-Configuration Comparison and Optimal Well Placement Strategies

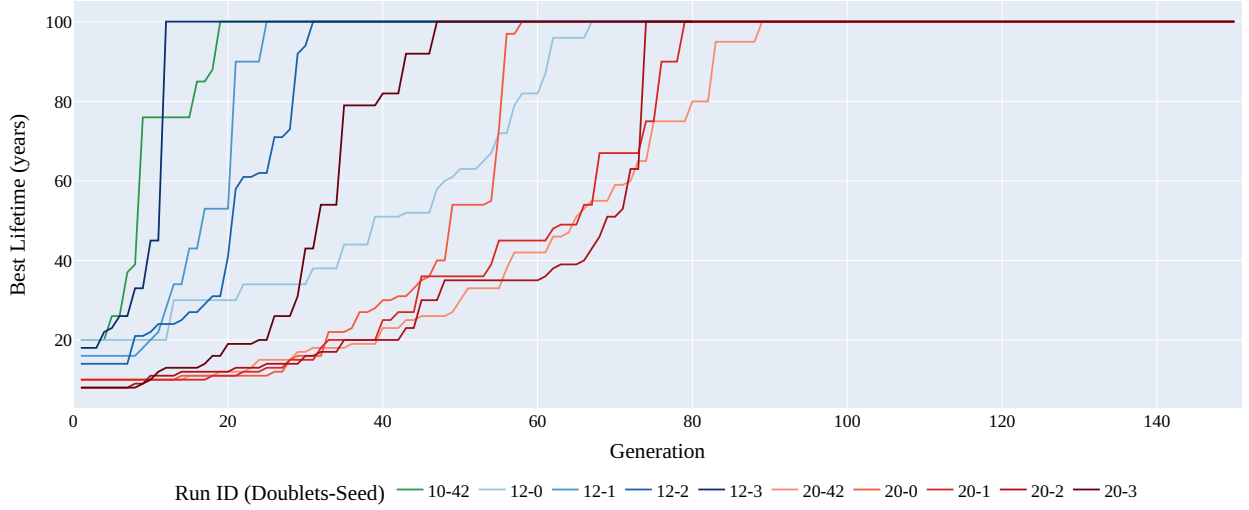
This subsection compares optimization results across different well configurations (10-doublet, 12-doublet, and 20-doublet) to evaluate convergence performance, analyze the impact of well count on trade-off relationships, and identify consistent spatial placement strategies that emerge across multiple optimization scenarios.

The optimization analysis presented in Figure 4.10 reveals distinct performance characteristics across the three well configurations based on 10 optimization runs (1 run with 10 doublets, 4 runs with 12 doublets, and 5 runs with 20 doublets). For NPV optimization (Figure 4.10a), the configurations show varying evolution patterns and final performance. The 20-doublet configuration demonstrates relatively slow initial improvement but generally achieves the highest economic performance, with most runs reaching 1.4-1.6 billion euros, though two runs achieve lower values around 1.2 billion euros. The 12-doublet runs show intermediate performance, typically reaching 1.2-1.4 billion euros, while the 10-doublet configuration achieves approximately 1.1 billion euros. For the 20-doublet runs, which were extended to 150 generations, NPV improvements appear to plateau around generation 70, with minimal further gains despite continued evolution.

The lifetime objective evolution (Figure 4.10b) reveals a clear relationship between well count and the speed of reaching maximum lifetime performance. One of the 12-doublet runs achieves the maximum lifetime of 100 years fastest, with the 10-doublet configuration following as a close second, both reaching this optimum before generation 20. The remaining 12-doublet runs demonstrate intermediate behavior, typically requiring 40-70 generations to attain maximum lifetime performance. The 20-doublet configuration shows the slowest progress, with all runs eventually reaching 100 years but the slowest requiring approximately 90 generations. This pattern reflects the increased spatial complexity introduced by higher well densities: while fewer wells provide greater spatial flexibility for achieving optimal injection-production spacing and delaying thermal breakthrough, higher well densities impose tighter spatial constraints that significantly complicate the search for optimal long-lifetime configurations, despite their superior economic potential through increased heat extraction capacity.



(a) Best NPV convergence



(b) Best lifetime convergence

Figure 4.10: Convergence comparison of all optimization runs with different injector configurations. Evolution of the Best (a) NPV and (b) lifetime objectives over generations, comparing 10 optimization runs across three well configurations: 1 run with 10 doublets, 4 runs with 12 doublets, and 5 runs with 20 doublets. Run labels indicate the number of doublets followed by the random seed

To investigate the potential for further optimization beyond standard termination criteria, a restart experiment was conducted using one of the 20-doublet runs, extending the optimization from 100 to 250 generations. Figure 4.11 presents the complete solution space exploration colored by generation, while Figure 4.12 shows the evolution of both objectives throughout the extended run.

The restart analysis reveals clear evidence of diminishing returns in extended optimization. The objective evolution (Figure 4.12) demonstrates that while the best NPV continues to improve during the additional 150 generations, achieving approximately 0.1B€ improvement, this represents a substantially reduced rate of progress compared to the initial 100 generations, which achieved nearly 1.0B€ improvement (from 0.25B€ to 1.2B€). The best lifetime objective shows no improvement during the restart phase, having already reached the maximum value of 100 years before generation 100.

The Pareto front analysis (Figure 4.11) confirms this pattern, showing that while the front advances slightly in terms of NPV, the majority of new feasible solutions cluster near the previously established front rather than

significantly extending it. This demonstrates that continued optimization beyond 100 generations yields only marginal improvements relative to the computational investment required, with the additional 150 generations producing limited gains compared to the rapid progress achieved in the initial optimization phase.

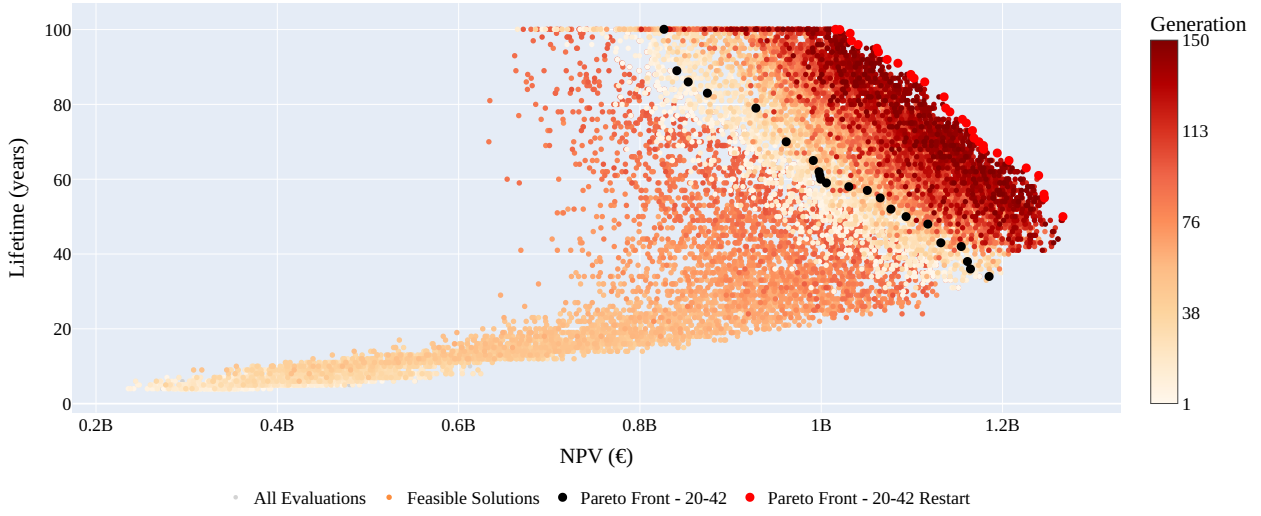
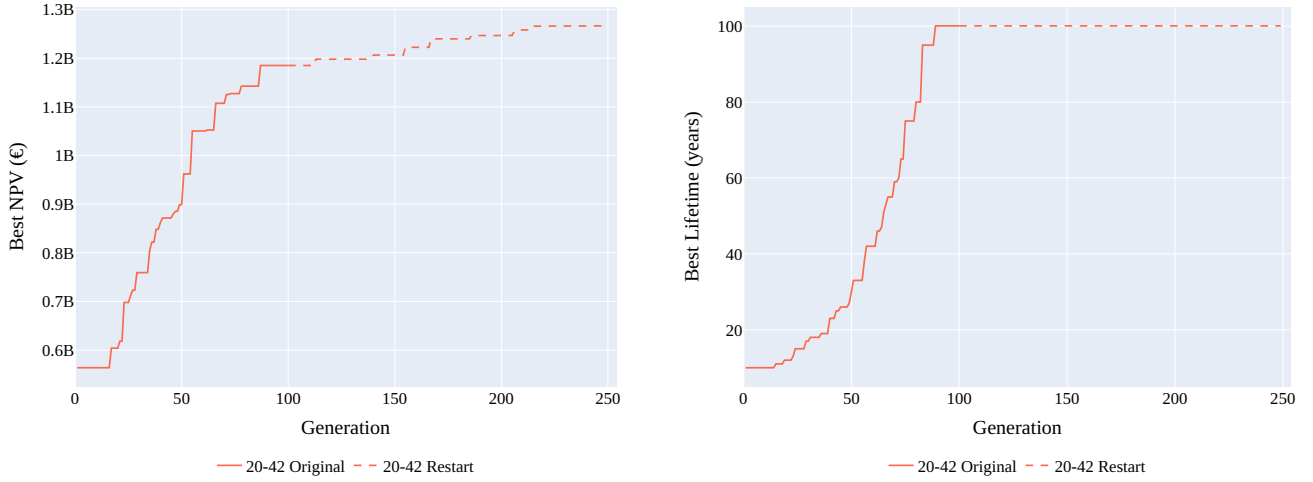


Figure 4.11: Solution space exploration for the 20-doublet restart experiment showing all evaluations and feasible solutions colored by generation, with Pareto fronts for the original run (generations 1-100) and restart continuation (colored from generation 1 to clearly indicate the restart location).



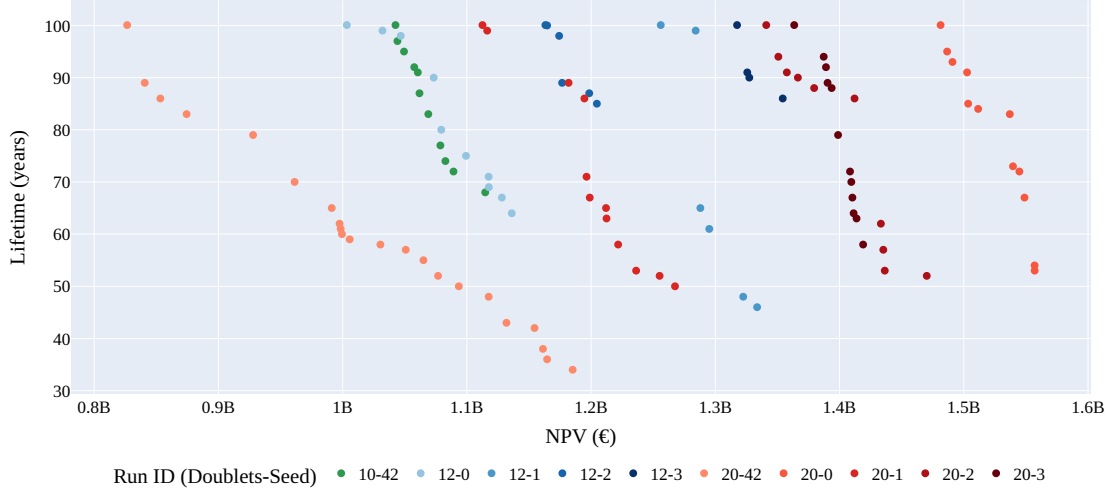
(a) NPV evolution showing convergence during continuation from generation 100.

(b) System lifetime evolution confirming convergence plateau during continuation.

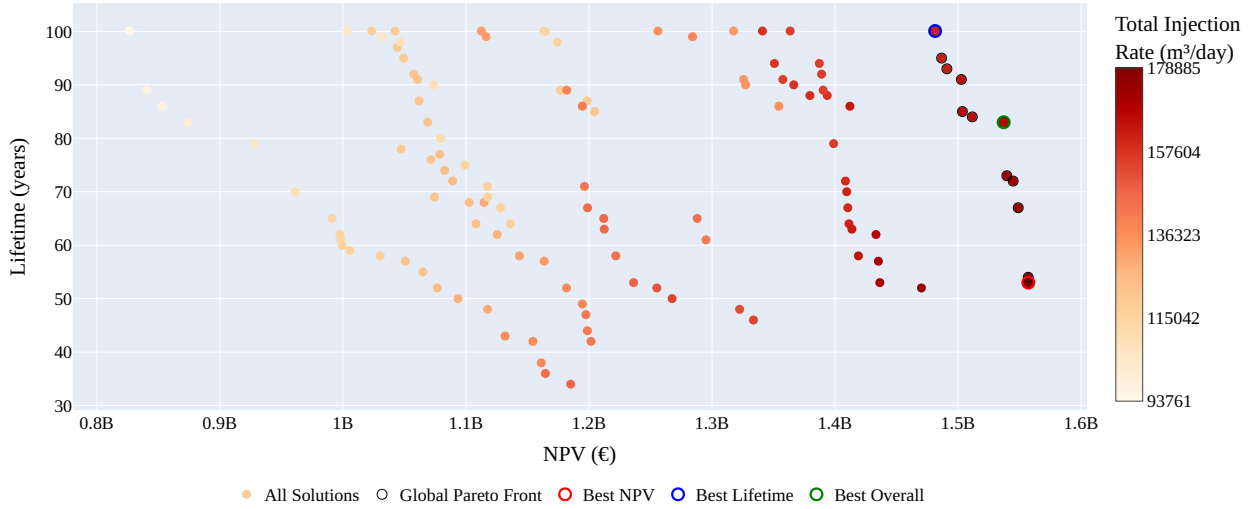
Figure 4.12: Convergence validation experiments for the 20-doublet configuration demonstrating (a) NPV plateau and (b) system lifetime plateau when continuing optimization from generation 100, confirming algorithm convergence.

Figure 4.13 provides a comprehensive comparison of the Pareto fronts and solution characteristics across all 10 optimization runs. The individual Pareto fronts (Figure 4.13a) demonstrate clear performance differences between well configurations, with most 20-doublet runs achieving the highest NPV values, followed by the 12-doublet runs, and the 10-doublet run showing the lowest economic performance. However, one 20-doublet run exhibits a notably wide Pareto front positioned toward the left of the plot, though its best NPV still slightly exceeds that of the 10-doublet run and one of the 12-doublet runs. Figure 4.13b shows the combined solution space colored by total injection rate, revealing a strong correlation between injection capacity and economic performance.

The injection rate analysis clearly demonstrates that the highest NPV solutions are achieved by runs with the greatest total injection (and production) rates. This relationship reflects the direct link between heat extraction capacity and economic return. The varying shapes of the Pareto fronts across runs reflect the interaction between NPV potential and the 100-year lifetime constraint. Runs achieving lower maximum NPV values exhibit wider Pareto fronts because they can explore a broader range of the NPV-lifetime trade-off space. In contrast, runs achieving higher NPV values show narrower, more vertical Pareto fronts that appear to be truncated by the 100-year lifetime ceiling. This pattern suggests that if the lifetime constraint were higher, these high-performing runs would likely exhibit wider Pareto fronts as well. The global Pareto front is comprised entirely of solutions from a single high-performing 20-doublet run, indicating that this particular optimization achieved complete dominance across the entire trade-off spectrum, while other configurations and runs contribute to different portions of the overall solution space.



(a) Pareto fronts from 10 optimization runs across three well configurations (1 run with 10 doublets, 4 runs with 12 doublets, and 5 runs with 20 doublets), showing the impact of well count on trade-off relationships.



(b) Aggregated results from 10 runs, showing individual Pareto fronts, the global Pareto front, and key solution types colored by total injection rate.

Figure 4.13: Visualization of Pareto front results from 10 enhance model optimization runs: (a) illustrates the impact of well count on trade-off relationships, and (b) presents the aggregated solution space with the final Pareto-optimal frontier, key solutions, and the influence of total injection rate on objective trade-offs.

Figure 4.14 presents three optimized well configurations corresponding to the Best NPV, Best Lifetime, and

Best Overall solutions, all derived from the same optimization run. Marker size in each panel reflects the flow rate of individual wells, which is key to interpreting spatial performance patterns.

All three configurations exhibit a consistent spatial placement strategy that aligns with the optimization process preferences identified in the frequency analysis: injectors are positioned along the northern boundary of the domain, while producers follow a distinctive pattern along the southern, eastern, and western boundaries. Notably, the eastern and western producer placements extend only to approximately 60% of the edge length, maintaining strategic distance from the northern injector locations to maximize spacing between injection and production wells. A slightly higher density of producers is observed along the eastern boundary, likely reflecting the deeper and warmer reservoir conditions in that region (as shown in Figure 3.4), which enhance production efficiency.

This spatial arrangement leverages the high-permeability fluvial channels and greater reservoir thickness in the northern region, where injectors can achieve higher flow rate capacities. The positioning of high-capacity wells in areas where vertically averaged horizontal permeabilities exceed 500–600mD optimizes both injection efficiency and thermal management. The U-shaped producer configuration ensures maximum separation between injection and production points within the placement constraints, thereby delaying thermal breakthrough and extending system lifetime.

Across all three configurations, a notable clustering pattern emerges where multiple wells are positioned in close spatial proximity. The consistent appearance of such clusters indicates that similar system performance could potentially be achieved through fewer wells operating at higher injection or production rates, which would reduce capital expenditure and operational complexity while maintaining comparable NPV and lifetime objectives. This clustering is induced by the imposed maximum rate constraint of 15,000 m³/day per well, which prevents the optimization from achieving higher total rates through fewer, higher-capacity wells.

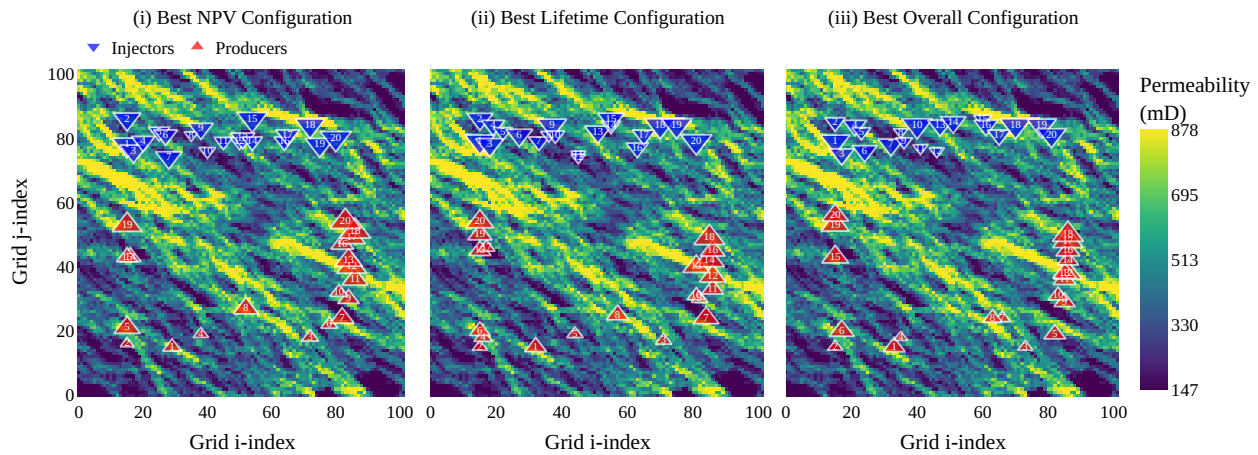


Figure 4.14: Optimal well configurations for three key solutions overlaid on the vertically averaged horizontal reservoir permeability field. (i) Best NPV configuration, (ii) Best Lifetime configuration, and (iii) Best Overall configuration. Injectors (blue inverted triangles) and producers (red triangles) are numbered and sized proportionally to their flow rates, showing how well placement and operational strategies vary based on optimization objectives.

Table 4.2 provides a quantitative comparison of the three optimal configurations highlighted in Figure 4.14. It confirms that the Best NPV solution achieves the highest economic return (1.557 B€) but at the cost of a shorter system lifetime (53 years). Conversely, the Best Lifetime solution sustains operations for the full 100-year duration but yields the lowest NPV (1.481 B€). The Best Overall solution offers a balanced performance across both objectives with an NPV of 1.537 B€ and a lifetime of 83 years.

Operational metrics such as flow rate ranges and injector-producer distances further elucidate differences in system design and efficiency. All configurations satisfy operational constraints, including BHP limits and water balance. All three solutions utilize the same 20-doublet well configuration, demonstrating that operational strategies rather than well count drive performance differences. The Best NPV solution achieves higher average flow rates (8,855.15 m³/day) compared to the Best Lifetime solution (8,063.45 m³/day), indicating that higher

injection rates maximize economic return but potentially accelerate reservoir depletion. The Best Lifetime solution operates at lower intensity to extend system longevity while maintaining competitive NPV values.

The Best Overall solution represents a balanced approach, capturing 98.7% of maximum NPV while achieving 83% of maximum lifetime through optimized well placement and moderate flow rate management (8,369.1 m³/day average).

Performance Metric	Best NPV	Best Lifetime	Best Overall
<i>Objective Performance</i>			
NPV (B€)	1.557	1.481	1.537
System Lifetime (years)	53	100	83
<i>Well Configuration</i>			
Configuration	20-douplet	20-douplet	20-douplet
Min. Injector-Producer Distance	23.1	24.2	19.1
<i>Operational Parameters</i>			
Average Injector Rate (m ³ /day)	8,855.15	8,063.45	8,369.1
Average Producer Rate (m ³ /day)	8,855.15	8,063.45	8,369.1
Injector Rate Range (m ³ /day)	2,678 - 13,213	1,738 - 12,840	3,203 - 12,868
Producer Rate Range (m ³ /day)	1,551 - 15,001	2,706 - 15,000	1,720 - 15,000
Total Injection (m ³ /day)	177,103	161,269	167,382
<i>Constraint Satisfaction</i>			
BHP Constraints Triggered	None	None	None
Water Balance Error (%)	0.00	0.00	0.00
Boundary Constraints Violated	0	0	0

Table 4.2: Comparison of representative Pareto-optimal solutions from enhanced model optimization

The final Pareto solution analysis in Figure 4.15 identifies the most consistently selected well placement locations across multiple trade-off scenarios. Unlike the broader exploration patterns presented earlier, these frequency maps include only the final Pareto-optimal solutions, revealing more focused spatial preferences. The injector frequency distribution (Figure 4.15a) reaches a maximum of 8, indicating repeated selection of specific locations in 8 out of the 12 Pareto-optimal solutions analyzed. Preferred injector zones are concentrated along the northern boundary, consistent with the spatial strategy observed in the optimal configurations. The producer frequency distribution (Figure 4.15b) shows peak frequencies of 8, with favored positions along the eastern and western edges of the placement area, consistent with the U-shaped producer arrangement that maximizes injection-production separation. These recurring frequency patterns confirm that the identified spatial placement strategy—with northern injectors and peripherally distributed producers—consistently emerges as optimal across different trade-off scenarios.

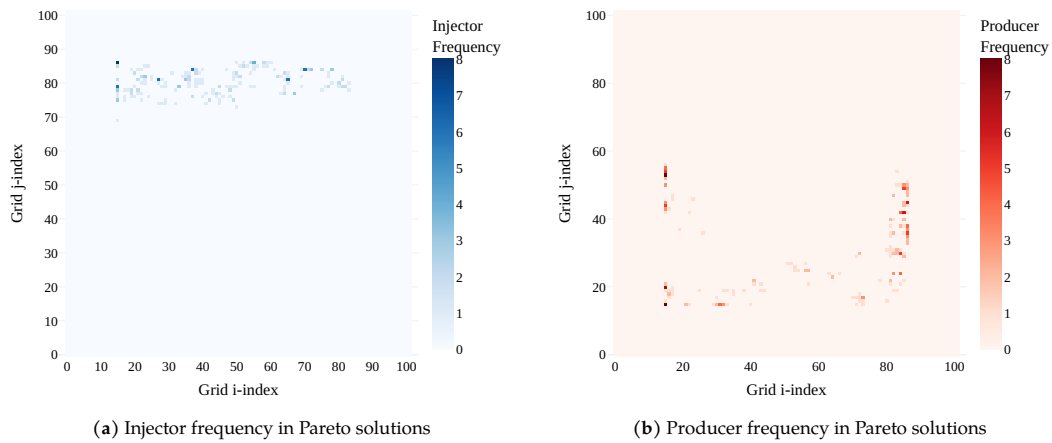


Figure 4.15: Spatial distribution of well placement frequency among final Pareto-optimal solutions for the enhanced model. (a) Injector frequency and (b) producer frequency show preferred optimal locations, with higher frequencies indicating more consistent placement across multiple Pareto solutions.

4.2.3. Detailed Analysis of Best Lifetime Solution

This subsection provides a detailed analysis of one of the key Pareto-optimal solutions, specifically the Best Lifetime solution.

Figure 4.16 presents the production temperature evolution of all production wells over the 100-year operational period, illustrating the thermal performance of the system. The red line indicates the production temperature for the well with the highest average production temperature, while the blue line represents the well with the lowest average production temperature.

It is evident that achieving a long system lifetime requires a strategic balance between wells that maintain high, stable production temperatures without thermal breakthrough and a limited number of wells that do experience breakthrough. Examining the locations of these producers reveals an optimal spatial configuration within the reservoir that considers both distance and subsurface connectivity patterns. The lowest performer (PRD20) (labelled in Figure 4.17) is situated in a shallower part of the reservoir (as shown in Figure 3.4a) and positioned in a zone of higher permeability that facilitates cold plume propagation, allowing the thermal front to reach this producer despite not being directly connected by discrete channels. In contrast, the highest performer (PRD11) is located in a deeper section of the reservoir with naturally higher temperatures and benefits from a strategic positioning where other producers act as protective barriers, intercepting and diverting the advancing cold front before it reaches PRD11, effectively shielding this well from early thermal breakthrough.

This optimized well placement strategy creates a sustainable production profile where the majority of wells maintain temperatures above the economic threshold for extended periods, while a few strategically positioned wells are allowed to experience breakthrough as an acceptable trade-off that actually enhances overall system economics. The wells experiencing breakthrough are operated at higher flow rates to maximize NPV during their productive period, recognizing that increased production intensity can yield significantly higher economic returns despite reduced longevity. The visualizations of the cold plume development at 10, 50, and 100 years (Figure 4.17a, 4.17b, and 4.17c) further confirm this interpretation, showing how the thermal front propagates through zones of enhanced permeability and how the strategic arrangement of producers creates protective buffers that intercept the advancing cold front, demonstrating the importance of both permeability architecture and well positioning in determining thermal breakthrough timing.

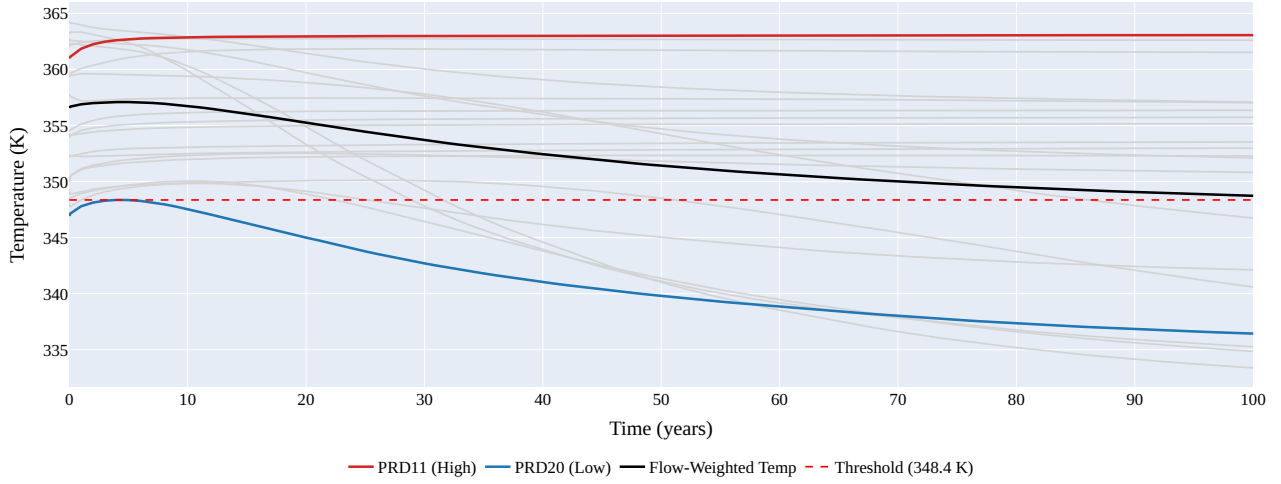


Figure 4.16: Temperature evolution of production wells over the 100-year operational period for the Best Lifetime solution. Individual well temperatures (gray), highest-temperature well (red), lowest-temperature well (blue), flow-weighted average temperature (black), and breakthrough threshold (dashed) are shown. The optimal solution maintains the flow-weighted average above the threshold throughout the 100-year period despite some individual wells experiencing breakthrough.

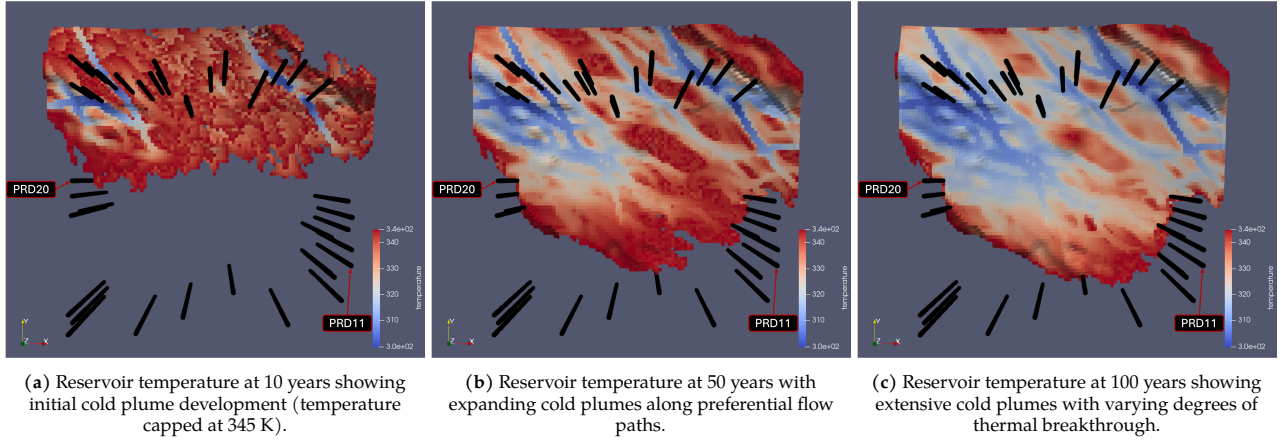


Figure 4.17: Temporal evolution of reservoir temperature distribution for the Best Lifetime solution, showing cold plume development at (a) 10 years, (b) 50 years, and (c) 100 years. PRD20 and PRD11 are labeled to identify the lowest and highest temperature production wells, respectively. Temperature scale is capped at 345 K to highlight the progression of injection cooling effects through preferential flow paths.

4.2.4. Effect of Temperature Threshold Fraction

This subsection investigates the impact of reducing the temperature threshold fraction from 15% to 5% on the optimization results, examining how this change affects optimization evolution, the Pareto front characteristics and well placement strategies.

Figure 4.18 shows that the 5% threshold produces a Pareto front positioned lower in the objective space compared to the 15% threshold, with most solutions falling well below the 100-year maximum simulation time. This downward shift occurs because the stricter 5% threshold causes thermal breakthrough at a smaller temperature decline, effectively reducing system lifetime and subsequently NPV. However, the 5% threshold demonstrates a wider NPV range across the Pareto front, suggesting greater diversity in economic performance under stricter thermal constraints.

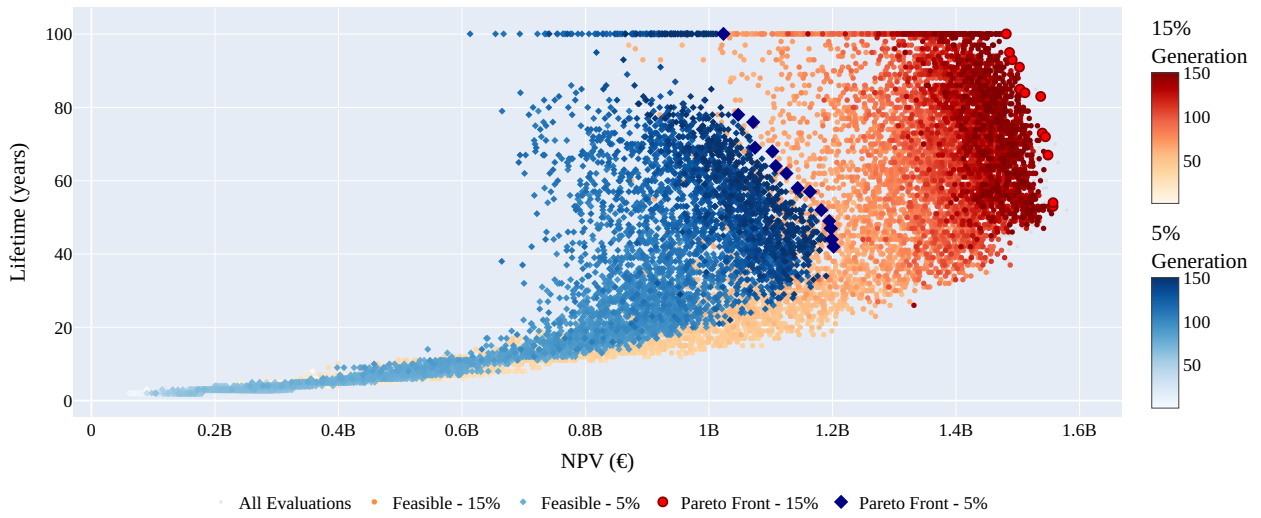


Figure 4.18: Comparison of Pareto fronts for 15% and 5% temperature threshold fractions. Gray points represent all evaluated solutions, colored points show feasible solutions (colored by generation), and the red and blue points indicate the final Pareto-optimal solutions of both configurations.

Figure 4.19 illustrates that the 15% threshold consistently enables higher total injection rates across the Pareto front. This enhanced injection capacity is a key driver of the superior NPV performance observed with the 15% threshold, as higher injection rates facilitate greater energy extraction and increased revenue generation. With the stricter 5% threshold, lower injection rates are required to avoid early breakthrough, which reduces energy production and economic returns.

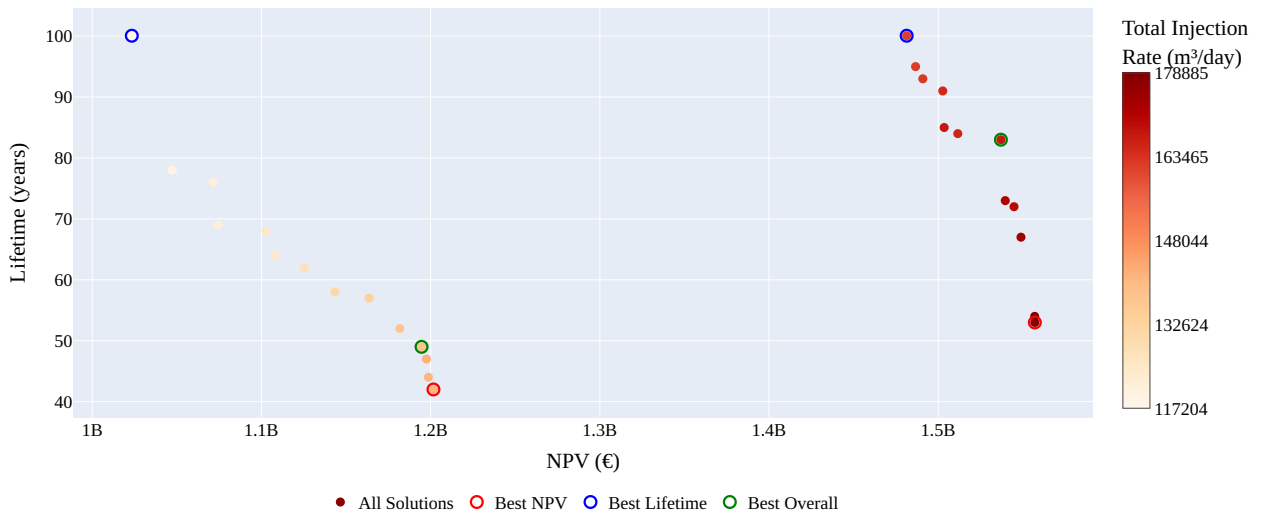


Figure 4.19: Comparison of Pareto fronts for different temperature threshold fractions (15% and 5%), with solutions colored by total injection rate. Key solutions (Best NPV, Best Lifetime, and Best Overall) are highlighted for each threshold configuration.

Figure 4.20 demonstrates consistency in optimal well placement patterns between the two threshold configurations. The spatial distribution of injectors and producers remains largely similar across different optimization objectives, indicating that fundamental well placement principles are relatively insensitive to the specific threshold value. The most notable difference is a shift in producer distribution, with the 5% threshold showing an increase in producer concentration along the western edge compared to the eastern edge.

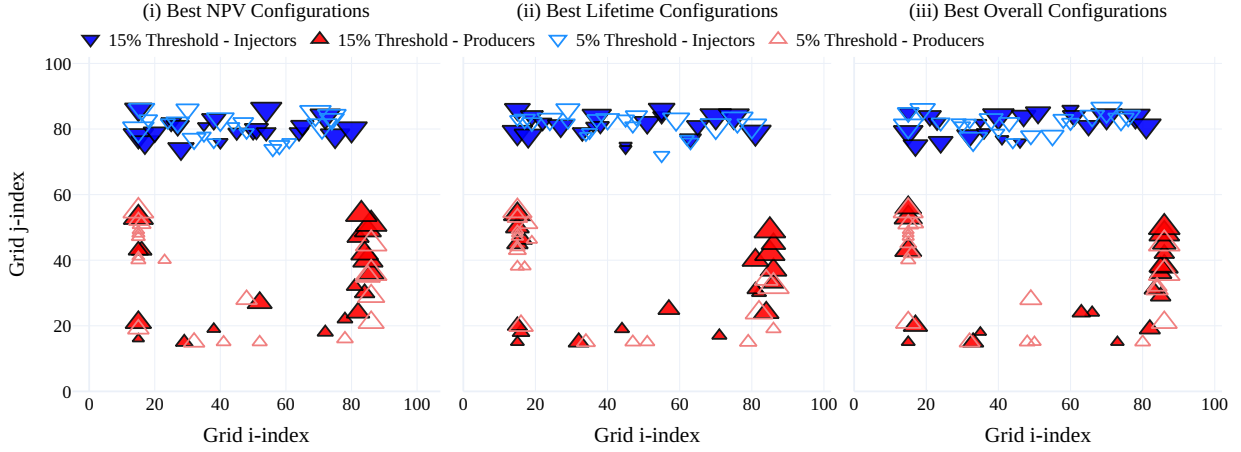


Figure 4.20: Comparison of optimal well placement strategies under different temperature threshold criteria.

4.2.5. Sensitivity to Geological Realizations

To assess the robustness of the optimization framework across geological uncertainty, identical experimental parameters and random seed (seed 0) were applied to three different geological realizations of the enhanced WNB model. This sensitivity analysis examines how geological structure variations influence Pareto fronts and optimal well placement strategies.

Figure 4.21 presents the Pareto fronts from three different stochastic realizations of the enhanced WNB model. Realization 1 represents the best-performing case from the previous analysis (configuration 20-0 from Figure 4.13a), while realizations 2 and 3 provide different random realizations of the same geological model with identical parameters but different stochastic positioning of geological features. The resulting Pareto fronts are similar and closely intertwined across the NPV-lifetime trade-off space. Although realization 3 achieves the highest NPV solution, all realizations produce solutions within comparable ranges, indicating that the optimization framework successfully adapts to stochastic geological variability while maintaining consistent performance characteristics.

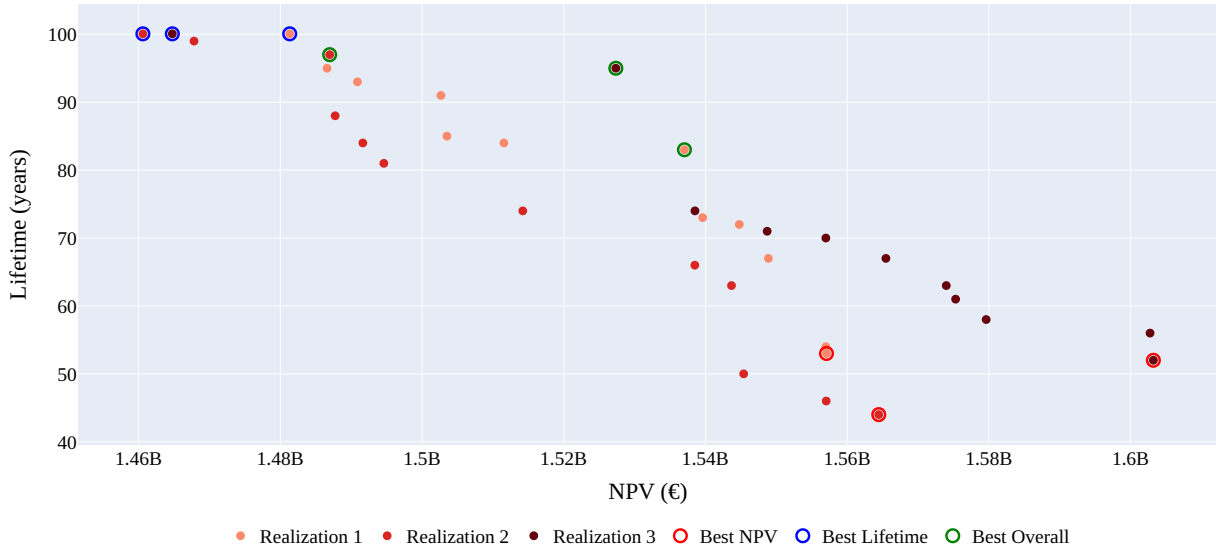


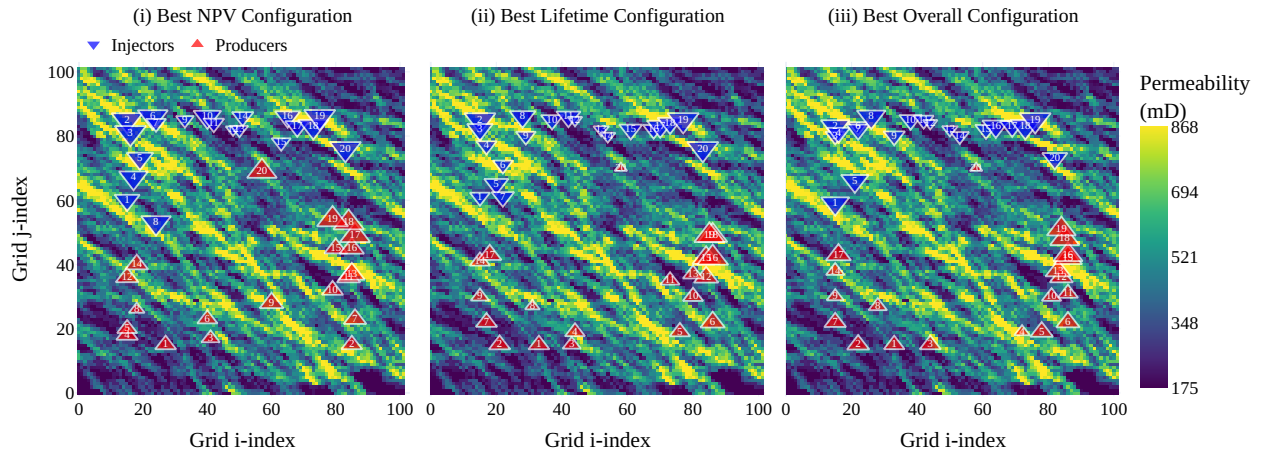
Figure 4.21: Comparison of Pareto fronts obtained from optimizations using three different geological realizations. Each realization's Pareto front is shown with a distinct color, with the Best NPV, Best Lifetime, and Best Overall solutions highlighted for each.

Figure 4.22 compares optimal well placement patterns for realizations 2 and 3, complementing the realization

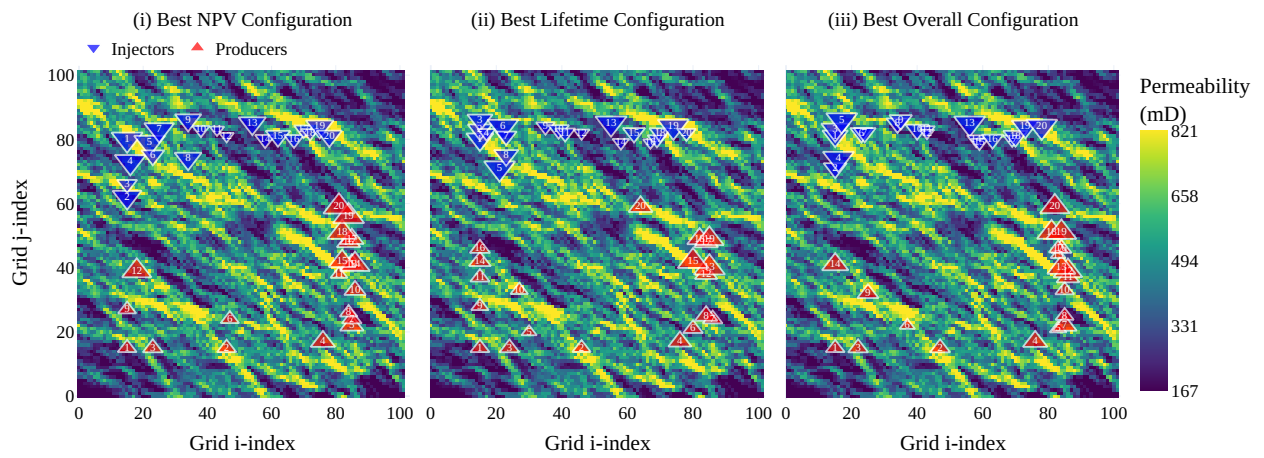
1 configurations from Figure 4.14. All realizations maintain the fundamental spatial strategy established in the previous analysis: injectors positioned along the northern boundary to exploit both the greatest reservoir thickness and high-permeability fluvial channels, while producers follow a U-shaped pattern along the southern, eastern, and western boundaries. The eastern and western producer placements extend only to approximately 60% of the edge length, balancing two competing objectives: maximizing distance from injectors to delay thermal breakthrough while positioning wells in the deeper, warmer eastern regions that enhance production efficiency.

The main difference between geological realizations appears in the Best NPV configurations for realizations 2 and 3, where some injectors move toward the western boundary compared to realization 1. This westward shift shows the framework can find and use local high-permeability zones specific to each geological realization while staying within the thick northern reservoir section. However, these are small adjustments rather than major strategy changes, as the overall approach of using reservoir thickness for injection capacity and balancing producer placement between thermal protection and reservoir temperature stays the same.

The small differences in optimal configurations across geological realizations show that sensitivity to geological uncertainty is manageable. This stability comes from the consistent reservoir structure across all realizations—identical thickness and depth patterns mean that the northern boundary remains best for injection regardless of specific permeability patterns, while the trade-off between distance and temperature continues to favor the U-shaped producer arrangement. The observed changes demonstrate the framework's ability to adapt to local permeability differences while maintaining a consistent overall strategy, supporting its practical use under realistic geological uncertainty.



(a) Optimal well configurations for key solutions in geological realization 2. (a) Best NPV configuration, (b) Best Lifetime configuration, and (c) Best Overall configuration. Injectors (blue inverted triangles) and producers (red triangles) are numbered and sized proportionally to their flow rates.



(b) Optimal well configurations for key solutions in geological realization 3. (a) Best NPV configuration, (b) Best Lifetime configuration, and (c) Best Overall configuration. Injectors (blue inverted triangles) and producers (red triangles) are numbered and sized proportionally to their flow rates.

Figure 4.22: Comparison of optimal well placement strategies across different geological realizations, demonstrating how the optimization framework adapts to geological uncertainty while pursuing consistent economic and lifetime objectives.

5

Discussion & Limitations

This chapter interprets the key findings of the MOO framework applied to geothermal system design in the WNB. It examines the implications of optimized well placement and operational strategies, discusses how constraints influenced performance outcomes, and evaluates the capabilities of NSGA-II in resolving competing objectives. The discussion also compares the results to relevant literature, highlights methodological contributions, and outlines the limitations and assumptions that frame the scope and transferability of the findings. Finally, it identifies promising directions for future research that could extend and enhance the optimization framework.

5.1. Interpretation of Key Findings

What makes well placement and operational controls critical decision variables in optimizing multi-well geothermal systems in the WNB?

Well placement and operational control parameters are critical decision variables because they directly control thermal breakthrough timing and heat extraction efficiency, as demonstrated by the substantial performance differences observed across optimization runs. The spatial positioning of wells determines thermal front propagation paths, while injection rates control the velocity of thermal breakthrough and the balance between economic return and system longevity.

The optimization consistently identified optimal spatial placement patterns that maximize injection-production separation while exploiting high-permeability zones, favorable reservoir thickness, and optimal temperature conditions. Flow rate allocation proved equally critical. The 20-doublet Best Lifetime solution achieved 100-year lifetime with 1.481 B€ NPV, while the Best NPV solution generated 1.557 B€ over 53 years through higher average injection rates (8,855 vs 8,063 m³/day). This demonstrates that uniform flow distributions severely limit optimization outcomes.

Together, these findings emphasize the necessity of treating well placement and flow management as interdependent decision variables. Ignoring their spatial and operational interplay risks both economic inefficiency and premature reservoir degradation.

What constraints are necessary for balancing economic and operational performance in geothermal system optimization?

The optimization results demonstrate that geological, hydraulic, and operational constraints are essential for achieving realistic trade-offs. Boundary distance constraints maintained simulation integrity by preventing artificial enhancement from model edges. Pressure constraints limited bottom-hole pressures to avoid overpressurization, ensuring thermal and hydraulic realism while contributing to asymmetric injection strategies. Water balance constraints guaranteed conservation of volume and improved realism by disallowing solutions that violated recirculation principles.

Together, these constraints provided essential structural guidance, ensuring that optimization outputs remained physically interpretable, operationally feasible, and aligned with the geological characteristics of the reservoir model.

How can NSGA-II be applied to balance the competing objectives of maximizing NPV and system lifetime in geothermal systems?

NSGA-II proved effective across multiple well configurations, consistently identifying broad Pareto fronts spanning from high-NPV solutions (up to 1.6 B€) to extended-lifetime solutions (100 years). Early generations (1-25) produced poor-performing solutions, while later generations (50-150) successfully identified optimal trade-offs across the full solution space (Figure 4.8).

The choice of well count significantly influences optimization complexity. While 20-doublet configurations achieved highest economic performance (1.4-1.6 B€ NPV), they required more generations to achieve maximum lifetime performance. The 10-doublet configurations demonstrated faster convergence to 100-year lifetimes due to increased spatial flexibility, while the 20-doublet configurations, despite achieving higher economic performance, imposed tighter spatial constraints that slowed optimization convergence.

Convergence analysis confirmed rapid discovery of viable solutions within 20-30 generations for the standard model (Figure 4.4) and varying patterns for different well configurations in the enhanced model (Figure 4.10), with restart experiments validating robustness (Figure 4.12).

Importantly, NSGA-II's diverse solution sets allow decision-makers to explore multiple designs rather than being restricted to single outcomes—essential flexibility given varying policy priorities and risk tolerances in geothermal development.

How can trade-offs between NPV and system lifetime be quantified and analyzed using the Pareto front generated by NSGA-II?

The Pareto front provides quantitative analysis of trade-offs, with enhanced model results showing NPV values ranging from 0.8 to 1.6 B€ and lifetimes spanning 35 to 100 years (Figure 4.13). The front's shape reveals the cost of improving each objective: steep slopes indicate that gaining additional NPV requires sacrificing significant system lifetime, while flatter regions show where economic improvements can be achieved with minimal impact on longevity.

Solution density analysis offers insight into optimization sensitivity—dense regions suggest many alternatives with similar trade-offs, while sparse regions indicate sensitive zones where small parameter changes significantly shift outcomes.

Injection rate analysis reveals strong correlation between total injection capacity and economic performance. Representative solutions serve as decision-making anchors: Best NPV (1.557 B€ over 53 years), Best Lifetime (1.481 B€ over 100 years), and Best Overall (1.537 B€ over 83 years) demonstrate different operational strategies while maintaining perfect constraint satisfaction.

What practical design and operational insights can be derived from the optimized solutions, and how can these insights inform improvements to the current "first-come, first-served" deployment strategies in large reservoirs like the WNB?

Optimized solutions reveal key insights challenging current deployment strategies. An important finding is that higher total injection capacity directly correlates with superior economic performance, as demonstrated by the 20-doublet configurations achieving the highest NPV values (1.4-1.6 B€) compared to 12-doublet (1.2-1.4 B€) and 10-doublet (1.1 B€) systems. This suggests that coordinated development strategies maximizing total system capacity could substantially outperform individual doublet deployments.

For this specific model, high-performing configurations consistently placed injection wells along the northern boundary and producers in the U-shaped pattern, as illustrated in the three key optimal configurations (Figure 4.14). While these specific spatial patterns are model-dependent, the optimization reveals a consistent underlying strategy: injection wells are positioned in the thickest reservoir regions with high-permeability zones, while producers balance maximizing distance from injectors with targeting high-temperature, high-permeability areas. The temperature evolution analysis demonstrates how this strategic spatial arrangement can prevent thermal breakthrough, with the Best Lifetime solution maintaining flow-weighted average temperature above the threshold throughout the 100-year period (Figure 4.16).

The lifetime optimization strategy reveals that maximum longevity involves strategic sacrifice of some wells to breakthrough while protecting others. This finding suggests significant potential for adaptive control strategies

where breakthrough wells could be shut down and flow redistributed in real-time.

Implementation requires shifting from "first-come, first-served" approaches to frameworks that systematically optimize well placement and controls for maximum system-wide capacity while managing thermal interference. The optimization methodology provides a systematic approach for identifying trade-offs between economic performance and system longevity, supporting evidence-based planning regardless of the specific reservoir characteristics.

Main Research Question

How can MOO with NSGA-II be applied to determine the optimal placement and control of multi-well geothermal systems to maximize both NPV and system lifetime?

NSGA-II, integrated with high-fidelity reservoir simulation and operational constraints, effectively identifies optimal trade-offs between NPV and system lifetime in geothermal systems. The algorithm consistently produced Pareto fronts capturing spectra of viable configurations from economically aggressive (up to 1.6 B€ NPV) to longevity-focused designs (100-year lifetimes) across multiple well configurations ranging from 10 to 20 doublets.

Multi-configuration analysis confirmed the framework's effectiveness across different well counts and initialization conditions, though performance varied with random seed initialization, demonstrating both the algorithm's exploration capability and the importance of multiple optimization runs. The results demonstrate that the framework adapts to varying geological conditions and well densities while consistently identifying optimization principles that maximize injection-production separation in high-permeability zones.

This study validates NSGA-II as a foundation for multi-objective geothermal optimization, offering a principled approach for balancing economic and sustainability goals in complex energy systems. The comprehensive solution sets provide stakeholders with actionable insights beyond objective values, enabling informed decision-making for sustainable geothermal development across diverse reservoir conditions.

5.2. Comparison to Literature and Existing Strategies

The findings of this study align with and expand upon previous research on the optimization of geothermal systems, especially in the context of large-scale deployment in the WNB. Notably, Kane et al. (2025) introduced a flexible well density framework that adapts well spacing to large-scale geological heterogeneity patterns (specifically linear and Gaussian trends in porosity and permeability) using synthetic models representing fluvial channel systems and transitional geological formations. Their work emphasized cashflow optimization and demonstrated that tailoring well patterns to subsurface variability can improve both thermal sweep and economic return. However, Kane et al.'s optimization focused solely on spatial configuration, employing fixed volumetric flow rates (3000 m³/day for the linear model and 2000 m³/day for the Gaussian model) imposed due to numerical convergence limitations when higher flow rates were applied to low-transmissivity reservoir zones. Operational controls were not subject to optimization, creating a significant limitation that distinguishes the present study, which integrates multi-objective optimization (NSGA-II) that simultaneously addresses spatial well placement and system-level performance trade-offs.

Daniilidis, Khait, et al. (2020) focused on optimizing operational controls, specifically yearly flow rates of geothermal doublets in a fixed two-doublet configuration over a 30-year period, using the DARTS simulator coupled with the Sequential Least Squares Programming (SLSQP) method. Their framework emphasized high computational performance and confirmed that optimizing NPV yields better long-term outcomes compared to maximizing energy output alone. While their optimization was confined to a fixed spatial configuration (two doublets with 780 m well spacing in a structured 3D heterogeneous reservoir), our approach integrates both spatial (well placement) and temporal (control strategies), offering a more comprehensive strategy for system-wide performance improvement.

Willems and M. Nick (2019) highlighted the shortcomings of the prevailing "first-come, first-serve" strategy in the WNB, particularly in terms of thermal interference and suboptimal resource utilization. They advocated for a coordinated approach to field development that considers regional-scale optimization and estimated that coordinated "masterplan" deployment could increase heat recovery efficiency by tens of percentages compared to current practices. Our findings directly respond to these concerns by demonstrating that Pareto-optimal

well configurations can significantly delay thermal breakthrough and enhance overall system resilience. Unlike their primarily conceptual analysis, our model quantitatively evaluates trade-offs using simulation-based optimization, contributing practical tools for coordinated geothermal planning.

In summary, this work bridges the methodological gap between spatially adaptive well placement (Kane et al. (2025)), operational control optimization (Daniilidis, Khait, et al. (2020)), and strategic basin-wide planning (Willems and M. Nick (2019)), thereby offering a unified and computationally efficient framework that leverages NSGA-II's population-based search capabilities to handle the complex, multi-modal optimization landscape inherent in multi-well geothermal systems in heterogeneous reservoirs.

5.3. Methodological Contributions and Advancements

- **Integrated economic and thermal-hydraulic objectives:** Simultaneously optimized NPV and system lifetime using a unified multi-objective framework, enabling explicit trade-off analysis relevant to both public and private sector stakeholders.
- **Constraint-aware optimization:** Developed a repair operator that enforces physical constraints (e.g., boundary distance, water balance, and pressure limits) during solution generation, improving simulation feasibility and reducing wasted evaluations.
- **Operational realism in objective evaluation:** Incorporated bottom-hole pressure constraints and asymmetric flow allocation into the optimization, enhancing alignment with real-world operational feasibility and regulatory standards.
- **Coupled spatial-operational optimization:** Unlike conventional approaches that fix well locations while optimizing rates or vice versa, this framework enables simultaneous optimization of both variables by making flow rates capacity-dependent on well locations through pre-simulation-based rate allocation. This coupled approach captures the interdependency between spatial configuration and operational performance more effectively than sequential optimization strategies.
- **Restart-based convergence validation:** Performed restart experiments to confirm convergence behavior of NSGA-II, improving confidence in Pareto front stability.
- **Enhanced geological realism:** Used corner-point grid geometry and heterogeneous permeability fields to better capture subsurface variability typical of the WNB.

5.4. Limitations and Uncertainties

While this study provides valuable insights into MOO of geothermal systems, several limitations and uncertainties must be acknowledged that could influence the applicability and robustness of the results.

5.4.1. Geological and Model Uncertainties

Limited geological uncertainty quantification: While this study tested three geological realizations to assess sensitivity to subsurface variability, this represents a limited sample for comprehensive geological uncertainty quantification. Although the results demonstrated consistent spatial optimization patterns across the three realizations, a more extensive ensemble analysis (e.g., 50-100 realizations) would be required to fully capture the range of possible subsurface configurations and quantify the robustness of optimization outcomes.

Grid resolution limitations: Computational costs limit the spatial resolution achievable in reservoir models, particularly for CPG simulations. Higher resolution grids would provide more detailed geological representation but are currently computationally prohibitive for population-based optimization.

Limited systematic geological parameter analysis: The study transitioned from a simplified synthetic model to a complex enhanced model without systematically evaluating individual geological parameter effects (depth/initial temperature, thickness, heterogeneity). This makes it difficult to isolate which factors most strongly influence optimization outcomes and limits transferability to other geological settings.

5.4.2. Optimization and Algorithmic Constraints

Algorithm limitations: While NSGA-II is designed to find diverse Pareto-optimal solutions, there is no guarantee that global optima have been identified in the complex, multi-modal optimization landscape characteristic of geothermal systems.

Temporal constraint limitations: The 100-year simulation horizon creates a fundamental constraint that significantly influences Pareto front characteristics, particularly for sparse well configurations. When optimization is constrained to a maximum 100-year operational period, this temporal cutoff becomes binding for configurations that do not fully saturate the available reservoir space. In such cases, maximum NPV solutions coincide with maximum allowable lifetime, causing the traditional trade-off between economics and longevity to become constrained and the Pareto front to degenerate toward a single dominant solution.

Framework computational inefficiencies: The current repair operator performs unnecessary pre-simulation for rate allocation in maximize mode, where flow rates are not decision variables. In maximize mode, the pre-simulation could be performed during solution evaluation instead of in the repair operator, which would eliminate redundant computations and remove the need for rate caching mechanisms. This architectural change would streamline the optimization process and reduce computational overhead per generation.

5.4.3. Economic and Operational Assumptions

Static economic parameters: The economic evaluation relies on fixed assumptions for heat prices, discount rates, and costs that may not reflect future market conditions. Sensitivity to these parameters has not been systematically evaluated, and energy market changes could significantly alter economic viability rankings.

Regulatory assumptions: The study implements current SodM pressure regulations, but future regulatory changes or operational flexibility in practice could alter the feasible design space.

Fixed operational strategies: Flow rates were optimized as constant values over the entire project lifetime, without incorporating temporal adaptation or feedback mechanisms that could respond to changing reservoir conditions.

These limitations highlight important constraints on the current study's scope and applicability, while identifying critical areas for future research that could enhance the framework's robustness and practical utility.

5.5. Future Work Directions

The limitations and scope of the current study point toward several promising research directions that could significantly enhance the optimization framework's capabilities and practical applicability.

5.5.1. Alternative Optimization Formulations

Single-objective approaches with constraints: Implement ϵ -constraint methods with fixed lifetime constraints (e.g., minimum 40 years) while maximizing NPV as a single objective. This approach would reduce computational costs, focus optimization on economically relevant timeframes, and avoid the inherent limitations of the current dual-maximization approach that may force solutions toward unrealistically long operational periods.

Alternative objective functions: Test different optimization objectives such as Heat In Place (HIP) recovery percentage to assess reservoir efficiency metrics beyond economic and temporal performance. This would evaluate sweep efficiency - how effectively the well configuration contacts and extracts thermal energy from the reservoir - providing insights into resource utilization effectiveness and supporting more comprehensive sustainability assessments.

Regulatory sensitivity analysis: Investigate the impact of removing or relaxing regulatory pressure constraints on optimization outcomes to understand the trade-offs between operational flexibility and regulatory compliance. This analysis could inform policy discussions about optimal regulatory frameworks for geothermal development.

5.5.2. Enhanced Optimization Strategies

Variable well configurations: Develop optimization frameworks where the number of wells becomes a decision variable rather than a fixed constraint, allowing the optimizer to determine optimal well density for given geological and economic conditions. This could involve mixed-integer optimization approaches that handle discrete decisions alongside continuous variables.

Expanded operational ranges: Test higher maximum flow rates and wider well spacing constraints to investigate whether fewer wells operating at higher injection rates can achieve comparable performance while avoiding the spatial clustering observed in current solutions. This approach would also enable exploration of more intensive development scenarios within realistic operational limits.

Brownfield development scenarios: Implement optimization frameworks that incorporate existing well locations as fixed constraints, representing realistic development scenarios where new wells must be optimized around existing infrastructure. This addresses the practical reality that most geothermal development occurs in areas with some existing activity.

5.5.3. Dynamic and Adaptive Control

Time-varying operational strategies: Develop dynamic operational frameworks with time-varying flow rates and adaptive control mechanisms that respond to thermal breakthrough, seasonal demand variations, and changing economic conditions. This could include automated shutdown and restart protocols for thermal breakthrough management.

Real-time optimization integration: Investigate frameworks that incorporate real-time monitoring data for adaptive optimization during operations, allowing continuous refinement of strategies based on actual reservoir response.

5.5.4. Uncertainty Quantification and Robustness

Ensemble-based optimization: Extend the framework to handle multiple geological realizations simultaneously, providing robust solutions that account for geological uncertainty. This ensemble approach could quantify solution sensitivity to geological assumptions and identify designs that perform well across multiple scenarios.

Economic sensitivity analysis: Conduct systematic sensitivity analysis of key economic parameters (heat prices, discount rates, capital costs) to understand their impact on optimization outcomes and develop robust strategies that perform well under varying economic conditions.

5.5.5. Systematic Geological Parameter Sensitivity

Individual parameter impact assessment: Conduct systematic sensitivity analysis of key geological parameters (reservoir depth/initial temperature, thickness, heterogeneity levels) by varying single parameters while keeping others constant. This would identify which geological factors most strongly influence optimal placement strategies and support broader framework application.

5.5.6. Computational and Algorithmic Improvements

Alternative optimization algorithms: Test alternative multi-objective algorithms (MOEA/D, SPEA2) and hybrid approaches to compare performance with NSGA-II and potentially identify more efficient optimization strategies for the specific characteristics of geothermal systems.

Framework architecture optimization: Address the framework architecture inefficiencies identified in the current implementation, particularly the presimulation process for rate allocation. Streamlined architectures could reduce computational overhead and improve solution quality.

High-resolution modeling: Leverage advancing computational resources to implement higher grid resolution and more detailed geological representations, potentially through adaptive mesh refinement and parallel computing strategies.

5.5.7. Basin-Scale and Multi-Field Applications

Regional optimization: Extend the framework to basin-scale optimization incorporating multiple geothermal fields and inter-field interactions. This could support coordinated development planning across multiple operators and reservoir systems.

Priority research directions include ensemble-based optimization for uncertainty quantification, alternative optimization formulations using ϵ -constraint methods, and development of dynamic operational frameworks that can enhance practical applicability of optimization-informed geothermal development.

6

Conclusion & Recommendations

This study successfully developed and validated a MOO framework for geothermal well placement and control in the WNB, demonstrating significant potential for improving upon current "first-come, first-served" deployment strategies.

6.1. Main Conclusions

This research answers the main research question: *How can MOO with NSGA-II be applied to determine the optimal placement and control of multi-well geothermal systems to maximize both NPV and system lifetime?*

NSGA-II, integrated with high-fidelity reservoir simulation and constraint-aware optimization, effectively identifies optimal trade-offs between NPV and system lifetime in geothermal systems. Applied to the enhanced WNB model, the framework consistently produced Pareto-optimal solutions spanning NPV ranges of 0.8-1.6 billion euros and system lifetimes of 35-100 years across multiple well configurations (10-20 doublets) and geological realizations.

Key optimization insights reveal both case-specific results and transferable principles. For the WNB model, the optimization consistently positioned injectors along the northern boundary (thickest reservoir with high-permeability channels) and producers in a U-shaped configuration balancing separation with access to warmer zones.

These results demonstrate three generalizable principles: (1) injectors should target zones combining maximum thickness and permeability for optimal injection capacity, (2) producers should balance high-temperature access with sufficient injector separation, and (3) flow rates must be location-dependent, determined by well interference effects and pressure constraints rather than uniform allocation across all wells.

The optimization reveals critical operational insights about configuration-aware rate management. The Best Overall solution achieved 98.7% of maximum NPV (1.537 billion euros) while maintaining 83% of maximum lifetime (83 years) through rate allocation that accounts for well interference and pressure limitations. Importantly, maximum system longevity is achieved not by uniformly protecting all wells, but through strategic sacrifice of some producers to thermal breakthrough while maintaining others at stable temperatures—a finding that suggests significant potential for adaptive control strategies where breakthrough wells could be shut down and flow redistributed in real-time.

6.2. Contributions and Impact

Methodological Innovation: This work presents an integrated framework combining NSGA-II MOO with geothermal reservoir simulation (DARTS) and constraint-aware solution generation. A key innovation is the simultaneous optimization of both well locations and operational rates—rather than the conventional approach of fixing one while optimizing the other, the framework makes flow rates capacity-dependent on well locations, enabling true coupled spatial-operational optimization. The constraint-aware repair operators and this integrated rate optimization strategy represent significant advances in handling the complex, multi-modal optimization landscape of geothermal systems.

Quantified Benefits of Coordination: The study provides quantitative evidence that coordinated development strategies can achieve superior performance compared to independent optimization. The consistent spatial

patterns identified across multiple runs and geological realizations demonstrate that strategic planning can overcome the limitations of current "first-come, first-served" approaches.

Practical Design Guidelines: The research delivers actionable spatial design principles and operational strategies directly applicable to heterogeneous reservoirs. The identified clustering patterns suggest that similar system performance could be achieved through fewer, strategically placed wells, potentially reducing capital expenditure while maintaining performance.

6.3. Recommendations

For Industry: Implement pre-development multi-objective optimization studies, adopt configuration-aware rate allocation that respects well interference and pressure constraints, and develop collaborative planning mechanisms for basin-wide resource utilization.

For Regulators: Establish spatial zoning guidelines informed by optimization studies, transition from "first-come, first-served" to coordinated development frameworks, and develop incentive structures that reward long-term sustainability over short-term gains.

For Future Research: Priority directions include ϵ -constraint methods with fixed lifetime constraints, dynamic operational frameworks with adaptive control systems, and ensemble-based optimization for uncertainty quantification.

6.4. Final Remarks

This research demonstrates that optimization-informed geothermal development can significantly enhance both economic performance and resource sustainability. The framework provides essential tools for strategic resource management during the expansion phase of geothermal energy deployment.

The constraint-aware multi-objective optimization approach is applicable beyond geothermal to other subsurface energy systems requiring spatial-operational trade-offs. By providing quantitative methods for evaluating NPV-lifetime trade-offs, this framework supports the evidence-based decision-making needed to maximize geothermal energy's contribution to renewable energy transition while ensuring long-term resource sustainability.

Declaration of Generative AI Use

AI tools, including ChatGPT (OpenAI) and Claude (Anthropic), were used to support both writing and coding tasks during the development of this thesis. All AI-generated content was reviewed, verified, and modified as needed to ensure accuracy and alignment with the research objectives. The author assumes full responsibility for the content and conclusions presented.

References

- Akin, T. (2025). GTEcon: Python library for techno-economic assessment of high-temperature geothermal ates, btes, and mtes systems. Retrieved February 2025, from <https://github.com/taylan-akin/GTEcon>
- Bäck, T. (1996). *Evolutionary Algorithms in Theory and Practice: Evolution Strategies, Evolutionary Programming, Genetic Algorithms*. Oxford University Press.
- Chen, Y., Rongier, G., Mullins, J. R., Voskov, D., & Daniilidis, A. (2025). Coupled Numerical and Analytical Simulation on the Delft Campus Geothermal Well. <https://pangea.stanford.edu/ERE/pdf/IGAstandard/SGW/2025/Chen1.pdf>
- Coello Coello, C. A., Lamont, G. B., & Van Veldhuizen, D. A. (2007). *Evolutionary algorithms for solving multi-objective problems* (2nd ed). Springer.
- Compennolle, T., Eswaran, A., Welkenhuysen, K., Hermans, T., Walraevens, K., van Camp, M., Buyle, M., Audenaert, A., Bleys, B., van Schoubroeck, S., Bergmans, A., Goderniaux, P., Baele, J.-M., Kaufmann, O., Vardon, P. J., Daniilidis, A., Orban, P., Dassargues, A., Serge, B., & Piessens, K. (2023). Towards a dynamic and sustainable management of geological resources [Publisher: The Geological Society of London]. *Geological Society, London, Special Publications*, 528(1), 101–121. <https://doi.org/10.1144/SP528-2022-75>
- Daniilidis, A. (2024). Towards Comprehensive Uncertainty Quantification in Direct-Use Geothermal Systems [ISSN: 2214-4609 Issue: 1], 2024, 1–5. <https://doi.org/10.3997/2214-4609.2024101678>
- Daniilidis, A., Khait, M., Saeid, S., Bruhn, D. F., & Voskov, D. (2020). A high performance framework for the optimization of geothermal systems, comparing energy production and economic output. *Proceedings world geothermal congress. 2020a*, 491–515.
- Daniilidis, A., Nick, H. M., & Bruhn, D. F. (2020). Interdependencies between physical, design and operational parameters for direct use geothermal heat in faulted hydrothermal reservoirs. *Geothermics*, 86, 101806. <https://doi.org/10.1016/j.geothermics.2020.101806>
- Daniilidis, A., Nick, H. M., & Bruhn, D. F. (2021). Interference between geothermal doublets across a fault under subsurface uncertainty; implications for field development and regulation. *Geothermics*, 91, 102041. <https://doi.org/10.1016/j.geothermics.2021.102041>
- Daniilidis, A., Saeid, S., & Doonechaly, N. G. (2021). The fault plane as the main fluid pathway: Geothermal field development options under subsurface and operational uncertainty. *Renewable Energy*, 171, 927–946. <https://doi.org/10.1016/j.renene.2021.02.148>
- Deb, K., Pratap, A., Agarwal, S., & Meyarivan, T. (2002). A fast and elitist multiobjective genetic algorithm: NSGA-II [Conference Name: IEEE Transactions on Evolutionary Computation]. *IEEE Transactions on Evolutionary Computation*, 6(2), 182–197. <https://doi.org/10.1109/4235.996017>
- Deb, K., & Agrawal, R. B. (1995). Simulated Binary Crossover for Continuous Search Space. *Complex Systems*, 9(2). Retrieved July 11, 2025, from https://www.complex-systems.com/abstracts/v09_i02_a02/
- Deutsch, C. V., & Journel, A. G. (1997). *Gslib: Geostatistical software library and user's guide* (2nd ed.). Oxford University Press.
- Deutsch, C. V., & Wang, L. (1996). Hierarchical object-based stochastic modeling of fluvial reservoirs. *Mathematical Geology*, 28(7), 857–880. <https://doi.org/10.1007/BF02066005>
- Dey, N. (Ed.). (2024). *Applied Multi-objective Optimization*. Springer Nature. <https://doi.org/10.1007/978-981-97-0353-1>

- Donselaar, M. E. (2016). Reservoir Architecture Modelling for Geothermal Energy Production - Case Study of the Delft Sandstone Member, West Netherlands [ISSN: 2214-4609 Issue: 1], 2016, 1–5. <https://doi.org/10.3997/2214-4609.201600596>
- Emmerich, M. T. M., & Deutz, A. H. (2018). A tutorial on multiobjective optimization: Fundamentals and evolutionary methods [Publisher: Springer Science and Business Media LLC]. *Natural Computing*, 17(3), 585–609. <https://doi.org/10.1007/s11047-018-9685-y>
- Islam, J., Vasant, P. M., Negash, B. M., Laruccia, M. B., Myint, M., & Watada, J. (2020). A holistic review on artificial intelligence techniques for well placement optimization problem. *Advances in Engineering Software*, 141, 102767. <https://doi.org/10.1016/j.advengsoft.2019.102767>
- Kane, E., Leeuwenburgh, O., Joosten, G., Daniilidis, A., & Bruhn, D. (2025). Flexible well patterns and cashflow optimisation on large-scale geothermal field development. *Renewable Energy*, 122494. <https://doi.org/10.1016/j.renene.2025.122494>
- Kong, Y., Pang, Z., Shao, H., & Kolditz, O. (2017). Optimization of well-doublet placement in geothermal reservoirs using numerical simulation and economic analysis. *Environmental Earth Sciences*, 76(3), 118. <https://doi.org/10.1007/s12665-017-6404-4>
- Limberger, J., Boxem, T., Pluymaekers, M., Bruhn, D., Manzella, A., Calcagno, P., Beekman, F., Cloetingh, S., & van Wees, J.-D. (2018). Geothermal energy in deep aquifers: A global assessment of the resource base for direct heat utilization. *Renewable and Sustainable Energy Reviews*, 82, 961–975. <https://doi.org/10.1016/j.rser.2017.09.084>
- Luke, S. (2013). *Essentials of metaheuristics: A set of undergraduate lecture notes; Online Version 2.0* (2. ed). Lulu.
- Mijnlieff, H. F. (2020). Introduction to the geothermal play and reservoir geology of the Netherlands. *Netherlands Journal of Geosciences*. <https://doi.org/10.1017/njg.2020.2>
- Moeck, I. S. (2014). Catalog of geothermal play types based on geologic controls. *Renewable and Sustainable Energy Reviews*, 37, 867–882. <https://doi.org/10.1016/j.rser.2014.05.032>
- Scholten, M., Bossennec, C., Ryder, S., Holečková, P., Pham, H., Sass, I., Peach-Gibson, A., Kranz, S., Bloemendal, M., & Soutar, I. (2023). *Detailed dissemination, exploitation and communication plan* (Project Deliverable No. D4.1). PUSH-IT Consortium. https://www.push-it-thermalstorage.eu/wp-content/uploads/2024/10/PUSH-IT-D4.1-Detailed-dissemination-exploitation-and-communication-plan_Final.pdf
- Schulte, D. O., Arnold, D., Geiger, S., Demyanov, V., & Sass, I. (2020). Multi-objective optimization under uncertainty of geothermal reservoirs using experimental design-based proxy models. *Geothermics*, 86, 101792. <https://doi.org/10.1016/j.geothermics.2019.101792>
- SodM. (2024). Protocol bepaling maximale injectiedrukken bij aardwarmtewinning - Publicatie - Staatstoezicht op de Mijnen. Retrieved May 14, 2025, from <https://www.sodm.nl/documenten/publicaties/2013/11/23/protocol-bepaling-maximale-injectiedrukken-bij-aardwarmtewinning>
- Song, G., Song, X., Li, G., Shi, Y., Wang, G., Ji, J., Xu, F., & Song, Z. (2021). An integrated multi-objective optimization method to improve the performance of multilateral-well geothermal system. *Renewable Energy*, 172, 1233–1249. <https://doi.org/10.1016/j.renene.2021.03.073>
- TNO. (n.d.). Economic model | Thermogis. Retrieved May 15, 2025, from <https://www.thermogis.nl/en/economic-model>
- Vardon, P. J., Abels, H. A., Barnhoorn, A., Daniilidis, A., Bruhn, D., Drijkoningen, G., van Esser, B., Laumann, S., van Paassen, P., Meleza, L. V., & Vondrak, A. G. (2024). A Research And Energy Production Geothermal Project On The TU Delft Campus: Project Implementation And Initial Data Collection. <https://pangea.stanford.edu/ERE/db/GeoConf/papers/SGW/2024/Vardon.pdf>
- Voskov, D., Abels, H., Barnhoorn, A., Chen, Y., Daniilidis, A., Bruhn, D., Drijkoningen, G., Geiger, S., Laumann, S., Song, G., Vardon, P. J., Vargas Meleza, L., Verschuur, E., & Vondrak, A. (2024). A research and produc-

- tion geothermal project on the TU Delft campus: 49th Workshop on Geothermal Reservoir Engineering [Publisher: Stanford University]. *PROCEEDINGS, 49th Workshop on Geothermal Reservoir Engineering*.
- Wagner, W., & Kretzschmar, H.-J. (2008). *International Steam Tables: Properties of Water and Steam Based on the Industrial Formulation IAPWS-IF97*. Springer Berlin Heidelberg. <https://doi.org/10.1007/978-3-540-74234-0>
- Wallmeier, C. (2024). Afterlife - Thermal Recharge of an Optimized Geothermal System [ISSN: 2214-4609 Issue: 1], 2024, 1–5. <https://doi.org/10.3997/2214-4609.202421263>
- Wang, J., Zhao, Z., Liu, G., & Xu, H. (2022). A robust optimization approach of well placement for doublet in heterogeneous geothermal reservoirs using random forest technique and genetic algorithm. *Energy*, 254, 124427. <https://doi.org/10.1016/j.energy.2022.124427>
- Wang, Y., Voskov, D., Daniilidis, A., Khait, M., Saeid, S., & Bruhn, D. (2023). Uncertainty quantification in a heterogeneous fluvial sandstone reservoir using GPU-based Monte Carlo simulation. *Geothermics*, 114, 102773. <https://doi.org/10.1016/j.geothermics.2023.102773>
- Wang, Y., Voskov, D., Khait, M., & Bruhn, D. (2020). An efficient numerical simulator for geothermal simulation: A benchmark study. *Applied Energy*, 264, 114693. <https://doi.org/10.1016/j.apenergy.2020.114693>
- Wang, Y., Voskov, D., Khait, M., Saeid, S., & Bruhn, D. (2021). Influential factors on the development of a low-enthalpy geothermal reservoir: A sensitivity study of a realistic field. *Renewable Energy*, 179, 641–651. <https://doi.org/10.1016/j.renene.2021.07.017>
- Willems, C. J. L., & M. Nick, H. (2019). Towards optimisation of geothermal heat recovery: An example from the West Netherlands Basin. *Applied Energy*, 247, 582–593. <https://doi.org/10.1016/j.apenergy.2019.04.083>
- Willems, C. J. L., Nick, H. M., Weltje, G. J., & Bruhn, D. F. (2017). An evaluation of interferences in heat production from low enthalpy geothermal doublets systems. *Energy*, 135, 500–512. <https://doi.org/10.1016/j.energy.2017.06.129>
- Willems, C. J. L., Vondrak, A., Mijnlief, H. F., Donselaar, M. E., & Kempen, B. M. M. v. (2020). Geology of the Upper Jurassic to Lower Cretaceous geothermal aquifers in the West Netherlands Basin – an overview. *Netherlands Journal of Geosciences*, 99, e1. <https://doi.org/10.1017/njg.2020.1>
- Zhang, L., Dieudonné, A.-C., Daniilidis, A., Dong, L., Cao, W., Thibaut, R., Tas, L., & Hermans, T. (2025). Thermo-hydro-mechanical modeling of geothermal energy systems in deep mines: Uncertainty quantification and design optimization. *Applied Energy*, 377, 124531. <https://doi.org/10.1016/j.apenergy.2024.124531>
- Zhang, Q., & Li, H. (2007). MOEA/D: A Multiobjective Evolutionary Algorithm Based on Decomposition. *IEEE Transactions on Evolutionary Computation*, 11(6), 712–731. <https://doi.org/10.1109/TEVC.2007.892759>
- Zhang, S., Jiang, Z., Zhang, S., Zhang, Q., & Feng, G. (2021). Well placement optimization for large-scale geothermal energy exploitation considering nature hydro-thermal processes in the Gonghe Basin, China. *Journal of Cleaner Production*, 317, 128391. <https://doi.org/10.1016/j.jclepro.2021.128391>
- Zitzler, E., Laumanns, M., & Thiele, L. (2001). *SPEA2: Improving the strength pareto evolutionary algorithm* (Report) [Accepted: 2022-08-12T12:06:45Z Publication Title: TIK Report Volume: 103]. ETH Zurich. <https://doi.org/10.3929/ethz-a-004284029>